NTNU – Trondheim
Norwegian University of
Science and Technology

Shear resistance for concrete dams

Laboratory tests

Manuel Colio Gutiérrez

Hydropower Development
Submission date: June 2013
Supervisor: Leif Lia, IVM
Co-supervisor: Olav Jørstad, Norconsult AS

Norwegian University of Science and Technology
Department of Hydraulic and Environmental Engineering

TABLE OF CONTENTS

TABLE OF CONTENTS I

ACKNOWLEDGMENTS V

SUMMARY VI

1. INTRODUCTION 1

1.1 Background 1

1.2 Purpose 1

1.3 Objectives 1

1.4 Methodology 2

1.5 Limitations 2

1.6 Disposition of the thesis 2

2. LITERATURE STUDY: SLIDING STABILITY OF CONCRETE DAMS. 4

2.1 Methods to calculate sliding stability of concrete dams 4
2.1.1 Sliding resistance method 4
2.1.2 Shear friction factor 5
2.1.3 Limit equilibrium method 8

2.2 Regulations for sliding stability safety 9
2.2.1 Norway 9
2.2.2 Other countries 11
2.2.2.1 Canada 11
2.2.2.2 USA 15
2.2.2.2.1 FERC guidelines 15
2.2.2.1.2 USBR guidelines 16
2.2.2.3 Sweden 17
2.2.2.3.1 RIDAS guidelines 17
2.2.2.3.2 New guidelines proposed by Johansson et. Al (2012): 18

2.3 Summary 20

3. LITERATURE STUDY: SHEAR RESISTANCE OF ROUGH ROCK JOINTS. 21

3.1 Introduction 21

3.2 Rock joint shear strength failure criteria 22
3.2.1 Mohr-Coulomb model 22
3.2.2 Dilantancy models 22

3.2.3 JRC models 34

3.3 Previous results 37
3.3.1 Ruggeri G. (2004) ICOLD 37
3.3.1.1 Rocha M. (1964) 37
3.3.2.2 Lo et. Al (1991-1990) 38
3.3.2.3 EPRI (1992) 39
3.3.3 Ghosh, A.K. (2010) 39
3.3.4 Xue F. Gu et. Al (2003) 40
3.3.5 Reena Negi (2012) 44
3.3.6 Kodikara and Johnston (1993) 46
3.3.7 Indraratna et Al (1997) 48

13.4 Summary 50

4. DIRECT SHEAR TESTS AT LTU. 52

4.1 Introduction 52

4.2 Review of 2012 direct shear tests at LTU 52
4.2.1 Introduction 52
4.2.2 Test description 52
4.2.3 Results 54
4.2.4 Discussion of laboratory results 58
4.2.5 Testing results into shear strength failure criterions 66
4.2.6 Comparison of test results with NVE guidelines 70
4.2.7 Proposed model to estimate shear strength 73
4.2.7 Summary 77

4.3 Apparatus description 79

4.4 Samples preparation 80
4.4.1 Rock samples 80
4.4.2 Mechanical properties of rock samples 82
4.4.3 Casting of concrete 82
4.4.4 Mechanical properties of concrete samples 84

4.5 Test description 84

4.6 Results 85

4.7 Analsysis of the laboratory test results. 86
4.7.1 Discussion of the test results 86
4.7.2 Testing results into shear strength failure criterions 94
4.7.3 Comparison between tests 2012 and 2013 96
4.7.4 Comparison with NVE guidelines 99
4.7.5 Validation of the proposed model 100

4.8 Summary 102

5. CONCLUSIONS AND FURTHER RESEARCH 104

6. REFERENCES 105

LIST OF FIGURES 107

LIST OF TABLES 113

APPENDIX A 114

APPENDIX B 116

APPENDIX C 118

APPENDIX D 141

ACKNOWLEDGMENTS

This thesis has been written as a part of the 2-year`s program M.Sc. in Hydropower Development at the Institute for Water and Environmental Engineering at the Norwegian University of Sciences and Technology (NTNU) at Trondheim, Norway.

This study period in Norway has represent a tough challenge for me because all that mean to live away in a new country and in a new culture, therefore and first of all , I would like to truly thank my family in Spain who always supported me, even in the bad moments.

I would like to thank Energi Norge for financing the project because without their financial support, this thesis would not have been possible. Special gratitude to my supervisors Leif Lia (NTNU) and Olav Anders Jørstad (Norconsult) for their patience, wise advises and feedback through my thesis.

I want also to express my gratitude to Gabriel Sas and Thomas Forsberg for their help during the laboratory tests at Luleå University of Technology.

Trondheim 10th June, 2013

_____

Manuel Colio Gutiérrez

SUMMARY

The Mohr-Coulomb shear strength failure criterion is used nowadays by most of the countries in their guidelines to estimate the shear capacity between the dam and the foundation. However, the Mohr-Coulomb model does not take into consideration the roughness of the concrete-to-rock interface. The fact the roughness the influence of the roughness is ignored by the guidelines leads to an overestimation of the shear capacity between the dam and the rock. Therefore, there is a need to increase the understanding of the roughness influence on the shear capacity between the dam and the foundation, in order to be able to incorporate the roughness effect into the formulas to estimate the sliding stability of concrete dams founded on rock.

This thesis aims to investigate the influence of the roughness in the shear capacity between the dam and the rock.

The methodology followed to achieve this goal is the following:

- Literature study in stability analysis of concrete dams and the methods to calculate the shear resistance between the dam and the rock at concrete dam foundations.
- Literature study on shear strength of rough rock joints, the parameters affecting the shear capacity and the different models to estimate it.
- Carry out direct shear tests at Lulea University of Technology (LTU).

To investigate the effect of the roughness in the shear resistance of concrete-to-rock joints a series of direct shear tests was decided to be implemented in this thesis at Luleå University of Technology (LTU) in Sweden. In total 12 tests were conducted on concrete-rock specimens with a size of $240x240\ mm^2$. The surface of the rock specimens was artificially manipulated shaping them with triangular asperities of equal angles and lengths over the whole surface. Four different asperity angle profiles were tested; 40, 20, 10 and 0 degrees. The concrete specimens were obtained by casting concrete against the rock specimens. The concrete type used was B45/40. In order to study the effect of the bonding between the concrete and the rock in the shear resistance, four specimens were casted directly on the rock surface, while for the rest a plastic wrap was placed on the rock surface to avoid adhesion. The rock type used in the tests is gneiss and had a compressive strength of 159 MPa. The normal stress levels selected were 1.2 MPa, 2.2 MPa and 3.2 MPa. The results from the direct shear tests are shown in Table 1. The Table shows the normal load applied, N, the horizontal load applied, H, the normal stress, $\boldsymbol{\sigma_n}$, peak shear stress, $\boldsymbol{\tau_{max}}$, shear displacement at peak, $\delta_{h,peak}$, the maximum shear displacement, $\delta_{h,max}$, peak friction angle, ϕ_{max}.

The results show that an increase on the asperity angle, the roughness, leads to a significant increase of the shear resistance of the concrete-to-rock joint. For the test carried out for a normal stress of 2.2 MPa, the peak shear stress obtained for an asperity angle of 40, 20 and 10 degrees was 4.73 MPa, 3.54 MPa and 1.97 MPa, respectively. It can be seen that the shear capacity for the 40 degrees asperity angle is over twice the shear capacity of the 10 degrees

asperity angle. Both the normal load and the bonding between the concrete and the rock greatly influenced the shear resistance. For the specimens tested with bonding the shear capacity reached was a lot higher than for the ones tested without bonding. The failure mode of the concrete asperities was also depending on the roughness, for the lowest roughness (10 degrees), sliding was the governing failure mode occuring, while for 20 and 40 degrees the asperities were sheared off.

The results from the direct shear tests have been tested into several shear strength failure criterion in order to check which one gave the best fit with the test results. The models that have been tested are the following:

- Mohr-Coulomb model
- Patton model
- Barton & Choubey model
- Maksimovic model

Out of the comparison between the predicted shear capacity from each model and the actual shear capacity observed from the tests, the model that gave the best fit was the model proposed by Barton and Choubey.

A comparison of the results obtained from the tests with the Norwegian guidelines (NVE) has been also conducted. By comparing the shear capacity obtained from the tests with the Mohr-Coulomb model one realizes how conservative the actual NVE guidelines are due to the fact that the influence of the roughness in the shear capacity between the concrete and the rock is ignored. Moreover the basic friction angle estimated from the direct shear tests was found to be approximetaly 30 degrees and the reccommended basic friction angle by NVE to use when assessing the shear capacity between the dam and the rock is 45 degrees. This is another prove that the actual criterion used by NVE guidelines to estimate the sliding stability of concret dams does not capture in realistic way the nature of the shear phenomenon at the dam-rock interface.

Finally, an attempt to develop an equation to estimate the peak shear stress of concrete-to-rock joint with surfaces shaped with triangular asperities is proposed based on the test results carried out by Liahagen (2012). The failure criterion proposed is based on the Mohr-Coulomb model but introducing a factor which incorporates the effect of the roughness into the shear capacity. The proposed model is tested into the test results carried out in this thesis, and the correlation seemed to be fairly good for 10 and 20 degrees asperity angle but not that good for the highest roughness tested, 40 degrees.

The following topics shall be considered to take to further research:

- Shear tests on concrete-to-rock under *in-situ* conditions
- Further investigate the effect of bonding in the shear capacity
- Direct shear tests on different rock types
- Direct shear tests with specimens with irregular triangular asperity profiles

Test	i [°]	N [kN]	H [kN]	$\delta_{h,peak}$ [mm]	σ_n [MPa]	τ_{max} [MPa]	ϕ_{max} [°]	δ_{Hmax} [mm]	Comments
1.1	40	69.12	325.76	3.16	1.2	5.65	77.72	27.89	bonded
1.2	40	126.72	418.75	3.71	2.2	7.27	73.19	27.90	bonded
1.3	40	126.72	272.45	1.93	2.2	4.73	65.2	25.38	
1.4	40	184.32	433.07	2.92	3.2	7.52	66.80	33.42	
2.1	20	69.12	272.45	2.34	1.2	4.73	75.93	33.18	bonded
2.2	20	126.72	203.90	1.96	2.2	3.54	59.08	28.14	
2.3	20	184.32	293.22	3.44	3.2	5.09	57.71	33.18	
3.1	10	69.12	89.10	3.27	1.2	1.54	51.90	30.4	
3.2	10	126.72	113.47	2.23	2.2	1.97	41.52	33.18	
3.3	10	184.32	145.15	1.60	3.2	2.52	38.34	33.18	
4.1	0	69.12	215.42	2.07	1.2	3.74	74.3	33.18	bonded
4.2	0	184.32	92.73	0.53	3.2	1.61	26.78	33.18	

Table 1. Results from the direct shear tests at LTU.

1. INTRODUCTION

1.1 Background

The Mohr-Coulomb linear criterion is the model used nowadays by most of the countries in their guidelines to estimate the shear capacity between the dam and the foundation. However, numerous investigations done during the last fifty years have revealed that there several factors that have a relevant influence on the shear strength and that Mohr-Coulomb does not take into consideration. Therefore, by using the Mohr-Coulomb criterion to estimate the shear capacity of the interface dam-foundation leads to a design loads way too conservative and therefore a too conservative dam design. One of these factors that influence the shear resistance is the roughness of the concrete-to-rock interface, which effect on shear strength has been reported by many authors that it increases the shear resistance.

Therefore, there is a need to increase the understanding of the roughness influence on the shear capacity between the dam and the foundation, in order to be able to incorporate the roughness effect into the formulas to estimate the sliding stability of concrete dams founded on rock.

1.2 Purpose

The main purpose of this thesis is to investigate the influence that the roughness, in the form of triangle asperities, has on the shear capacity between the concrete and the rock.

1.3 Objectives

a. Increase the knowledge on the methods used in different countries to assess the stability against sliding.
b. Gain knowledge of the parameters affecting the shear resistance of rough rock-rock and concrete-to-rock joints and learn about the methodology to carry our direct shear tests as well.
c. Study the influence of interface asperities on the shear capacity by conducting direct shear tests.

1.4 Methodology

The following methodology will be used in order to accomplish the goal and the objectives of this thesis:

- Literature study in stability analysis of concrete dams and the methods to calculate the shear resistance between the dam and the rock at concrete dam foundations.
- Literature study on shear strength of rough rock joints, the parameters affecting the shear capacity and the different models to estimate it.
- Review and evaluation of the tests carried out in 2012.
- Conduction of direct shear tests at Lulea University of Technology (LTU).

1.5 Limitations

There are several limitations within this Master Thesis. First of all, the time limitation due to the fact that this thesis comprised only one semester therefore the author did not have the necessary time to investigate many other things related to the topic.

The number of tests carried out at the laboratory is the other main limitation of this thesis; only twelve direct shear tests were conducted due to the budget limitation.

1.6 Disposition of the thesis

In order to give to the lecturer an overview of the structure of the thesis, a brief description of the content of each chapter is given.

The thesis starts with a literature study on the stability of the sliding analysis of light-weight concrete dams in chapter 2, through this chapter three different methods are presented to calculate the sliding stability of the concrete dams and also the regulations regarding sliding stability in Norway and in other countries (Canada, USA, Sweden) are presented.

Literature study on shear resistance is described during chapter 3. Firstly, the most important models that been developed to represent the shear behavior of rough rock joints. After the presentation of those theoretical models, a literature study on previous results obtained during lab tests by different authors in order to have provided the author inspiration for the test program developed at LTU in Sweden and the necessary knowledge of the parameters that affect the shear behavior in rock-concrete joints.

Through the chapter 4, the direct shear tests carried out at Lulea University of Technology is presented. First of all, it contains a review of the tests in which Simen Liahagen participated in 2012; the results are both presented and analyzed. Based on those tests, a model to estimate

the peak shear strength of a concrete-to-rock interface is proposed. The results from the 2012 tests are testing into commonly used models to estimate the shear resistance and are also compared to NVE guidelines. After the review of the laboratory tests from 2012, the test series conducted in 2013 are introduced and the results are presented.

An analysis of the test results is carried out through chapter 4 and the test results are testing into commonly used method to estimate shear resistance and finally the equation proposed to estimate the peak shear strength of based on the Mohr-Coulomb model is validated.

Finally, the conclusions of this thesis are drawn and the suggestions for further research in future M.Sc. thesis within this field are described.

2. LITERATURE STUDY: SLIDING STABILITY OF CONCRETE DAMS.

The following chapter describes the different methods to assess the sliding stability of concrete dams. It contains the three methods to calculate the sliding stability of concrete dams mentioned by Johansson F. (2009), the sliding resistance method, the shear friction factor and the limit equilibrium method. The regulation regarding stability of concrete dams in Norway is presented and also the regulation in other countries with a large tradition in the dam engineering field as USA, Canada and Sweden.

2.1 Methods to calculate sliding stability of concrete dams

Resistance to sliding along any plane above the base of a dam is a function of the shearing strength of the concrete, or of the construction lift joint, at the base it depends on the shearing strength of the concrete, foundation or interface (R.B. Jansen, 1988).

According to Johansson F. (2009) we can find two types of sliding failure in rock joints, plane sliding and wedge sliding. Wedge sliding and plane sliding are similar but the wedge sliding is more difficult to solve analytically due to the fact that its geometry makes it a three-dimensional problem. Within this section, 3 methods to evaluate the plane sliding will be presented.

2.1.1 Sliding resistance method

This criterion was the first criterion used to evaluate the safety against sliding (Johansson 2009). This method is based on the calculation a coefficient of friction, μ. This coefficient is calculated by dividing the sum of horizontal forces or the forces which are parallel to the sliding plane, $\sum H$, by the sum of the effective vertical forces normal to the sliding plane, $\sum V$. In order to avoid the sliding, the coefficient of friction shall be not larger than a maximum coefficient of friction, as shown in the equation (1).

$$\mu = \frac{\sum H}{\sum V} \leq \mu_{max} \qquad (2.1)$$

2.1.2 Shear friction factor

The shear friction factor method is currently used in the Norwegian regulations for sliding stability of concrete dams (NVE 2005). It is based on the calculation of a safety factor against sliding; this safety factor will be found by dividing the horizontal force available to resist the horizontal loads (the horizontal shear capacity) by the actual horizontal forces that are causing the displacement (Energi Norge 2012). Note that the Mohr-Coulomb equation is used to estimate the shear resistance of the sliding plane. The safety factor is estimated as follows:

$$FS = \frac{c \cdot A + \sum V \cdot \tan \phi}{\sum H} \qquad (2.2)$$

Where FS is the safety factor, c is the cohesion of the sliding surface considered; A is the contact area of the sliding plane, ϕ is the friction angle of the sliding plane, $\sum V$ are the sum of the vertical forces acting and $\sum H$ is the sum of the horizontal forces acting.

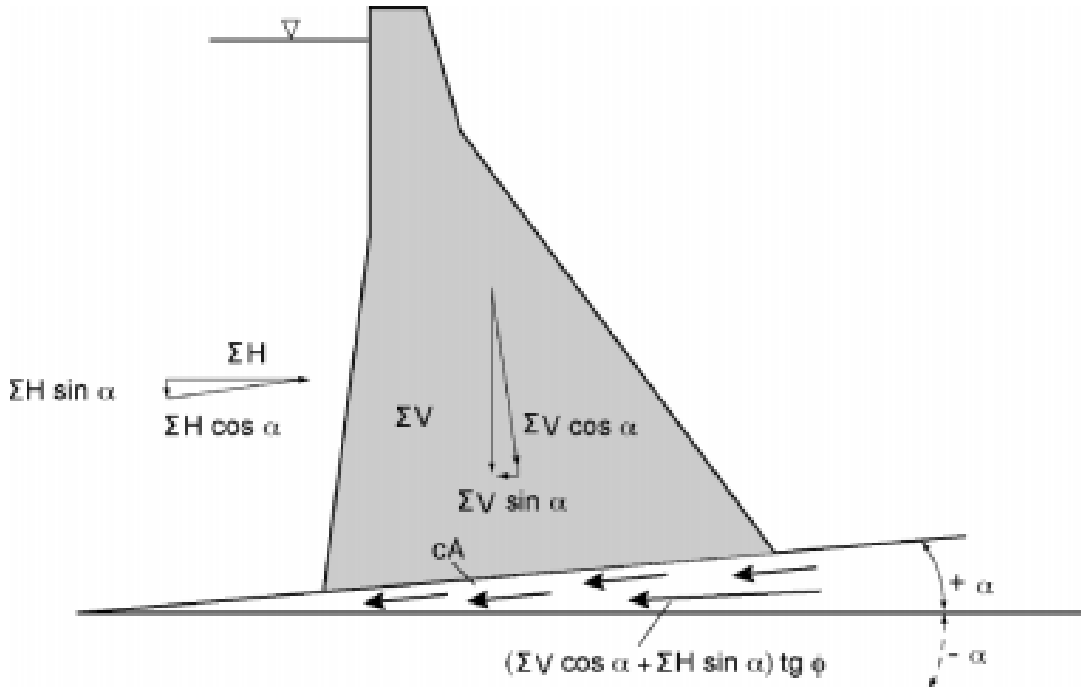

Figure 1. Sliding resistance of a sliding plane with an inclination angle of α (taken from (NVE,2005))

It must be noted that if the surface of sliding considered is inclined as shown in figure 1, then the inclination angle of the plane (α) shall be taken into account in the formula, the equation will be now as follows, to see the derivation go to appendix A.

$$FS = \frac{\frac{c \cdot A}{cos\alpha \cdot (1 - tan\alpha \cdot tan\phi)} + \sum V \cdot tan(\alpha + \phi)}{\sum H} \quad (2.3)$$

Where:

∑V = summation of vertical forces
∑H = summation of horizontal forces
A = area of potential failure plane developing cohesion (c)
c = cohesion (unit shearing strength at zero normal stress)
α = angle between inclined sliding plane developing and the horizontal (positive for upwards sliding)
ϕ = angle of internal friction

In the case where the potential sliding is located below the terrain, a passive resistance may be utilize as a contribution for sliding resistance. The magnitude of the downstream resistance is defined by the plane that represents the weakest path to daylight (R.B. Jansen, 1988). The equation for the safety factor will be as follows:

$$FS = \frac{R + P_p}{\sum H} \quad (2.4)$$

Where;

R = summation of vertical forces
∑H = summation of horizontal forces
P_p = maximum passive horizontal resistance by the rock wedge

The equation will be different whether the sliding planes are horizontal or, as normally occurs in natural rock joints, if the potential sliding planes have an inclination. The parameters *R* and P_p will have to be derived to taken into consideration this inclination. Johansson F. (2009) gives examples of this. The following figure shows a horizontal joint ending in the rock mass

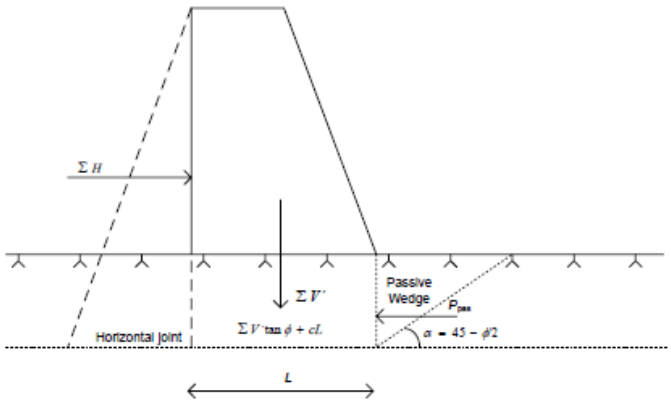

Figure 2. Plane sliding along a horizontal joint ending in the rock mass plus passive wedge resistance (taken from (Johansson,2009))

The equation for the calculation of the safety factor will be as follows:

$$FS = \frac{\sum V` \cdot tan\phi + c \cdot L + P_p}{\sum H} \quad (2.5)$$

The following figure shows an example of a situation where the sliding plane is inclined. The inclination of the potential sliding plane must be taken into consideration and the safety factor equation will change. Nicholson (1983) derived the equations to determine the summation of vertical forces and the maximum passive horizontal resistance by the rock wedge (R and P_P respectively) for an up-hill sliding plane. The formulation is shown below:

$$R = \sum V \cdot \tan(\phi + \alpha_{dam}) + \frac{c_{dam} + A_{dam}}{cos\alpha_{dam} \cdot (1 - tan\phi \cdot tan\alpha)} \quad (2.6) \quad ; \text{For up-hill sliding planes}$$

$$R = \sum V \cdot \tan(\phi + \alpha_{dam}) + \frac{c_{dam} + A_{dam}}{cos\alpha_{dam} \cdot (1 - tan\phi \cdot tan\alpha)} \quad (2.7) \quad ; \text{For down-hill sliding planes}$$

$$P_P = W \cdot \tan(\phi + \alpha_{pas}) + \frac{c_{pas} + A_{pas}}{cos\alpha_{pas} \cdot (1 - tan\phi \cdot tan\alpha_{pas})} \quad (2.8)$$

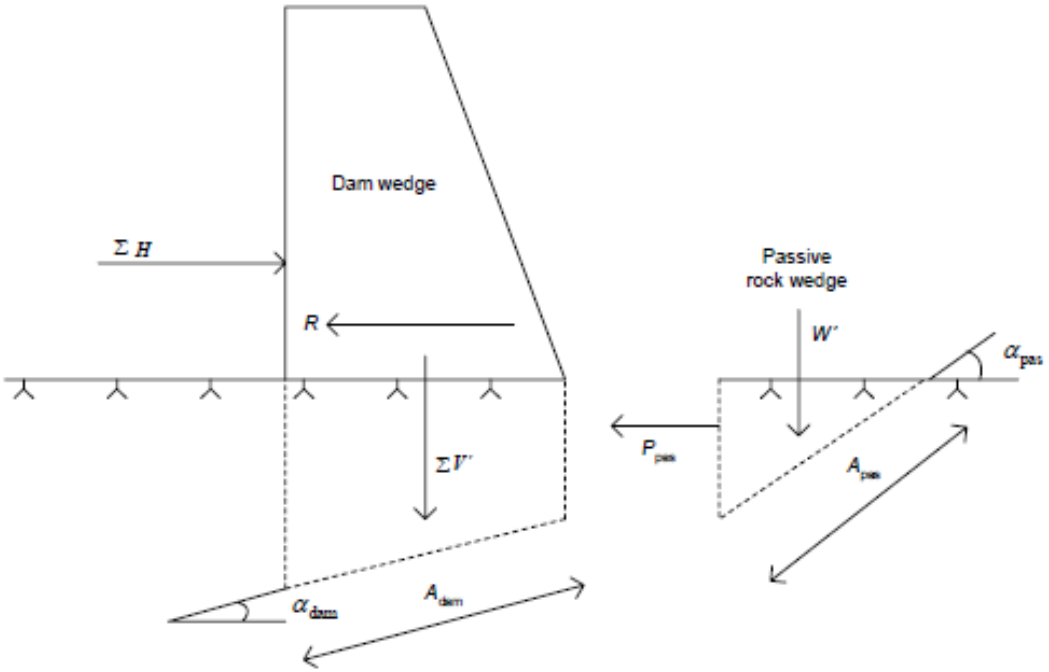

Figure 3. Forces acting on a hypothetical dam with inclined sliding planes according to the shear friction method (taken from (Johansson, 2009))

Where $\Sigma V'$ is the sum of vertical forces including the reduction from uplift forces, ϕ is the friction angle for the sliding plane, α is the for the inclined failure plane against the

horizontal, *c* is the cohesion for the sliding plane, *A* is the area of the potential failure plane, and *W´* is the effective weight of the passive rock wedge, plus any superimposed loads. Subscripts *dam* and *pas* stands for dam wedge and passive wedge respectively.

The shear friction method has some limitations that were pointed out by Nicholson (1983). One of limitations is related to the mathemathics needed to solve the equations R and Pp, because if the expresion φ±α reaches the value of 90º the safety factor would be infinity. Another limitation is related to the fact that the passive wedge force is independent from the forces acting on the dam, this means that if we consider the dam and the passive wedge as a single block it will not be in static equilibrium unless the safety factor becomes one. Finally, the shear friction factor methos is only applicable to failure modes along one or more planes.

The table below shows the recommended shear friction safety factor in the USBR guidelines (from Novak 2007).

Sliding plane	Normal Load combination	Unusual load combination	Extreme load combination
Dam concrete/base interface	3.0	2.0	≥1
Foundation rock	4	2.7	1.3

Table 2. Recommended shear friction safety factors in USBR guidelines (taken from (Novak,2007))

2.1.3 Limit equilibrium method

The limit equilibrium method defines the safety factor as the shear strength of the sliding plane divided by the shear stress applied along that plane, the equation of the safety is shown below:

$$FS = {}^{\tau_F}/_{\tau} \tag{2.9}$$

Where:

τ_F = shear stenght available

τ = shear stress applied

If the Mohr-Coulomb shear stenght failure criterion is used to express the shear strength available, the equation will be rewritten as follows (Novak, 2007):

$$FS = \frac{c + \sigma \cdot tan\varphi}{\tau} \tag{2.10}$$

Where σ is the normal stress acting on the sliding plane, c is the cohesion and φ is the basic friction angle.

When the sliding plane considered has an inclination as it is shown in the figure x, the formula will be as follows:

$$F_s = \frac{c \cdot A + [\Sigma V \cdot \cos\alpha + \Sigma H \cdot \sin\alpha] \cdot \tan\phi}{\Sigma H \cdot \cos\alpha - \Sigma V \cdot \sin\alpha} \quad (2.11)$$

Where;

∑V = summation of vertical forces
∑H = summation of horizontal forces
A = area of potential failure plane developing cohesion (c)
c = cohesion (unit shearing strength at zero normal stress)
α = angle between inclined sliding plane developing and the horizontal (positive for upwards sliding)
ϕ = angle of internal friction

2.2 Regulations for sliding stability safety

In this section the current guidelines to assess the safety sliding stability of concrete dams in Norway and in different countries is presented.

2.2.1 Norway

The Norwegian Water Resources and Energy Directorate (NVE) is responsible for the guidelines and regulation regarding the safety of sliding stability in concrete dams. These guidelines are covered in *Retningslinjer for betongdammer* (2005).

Factor of safety:

NVE uses the shear friction factor method to estimate the factor of safety against sliding (Energi Norge 2012), which has been described on last sections. The factor of safety is computed by comparing the maximum horizontal resistance force with the actual horizontal load acting on the potential failure plane considered. The Mohr-Coulomb criterion is used to estimate the maximum horizontal resistance and then the factor of safety will be defined by the equation 2. Note that equation 2 is applicable to any inclination of the sliding plane considered.

$$S = \frac{F}{\sum H} = \frac{\frac{c \cdot A}{cos\alpha \cdot (1 - tan\phi \cdot tan\alpha)} + \sum V \cdot \tan(\phi + \alpha)}{\sum H}$$

When the sliding plane is horizontal the formula is as follows:

$$S = \frac{c \cdot A + \sum V \cdot \tan(\phi)}{\sum H} \tag{2.13}$$

Where;

∑V = summation of vertical forces
∑H = summation of horizontal forces
A = area of potential failure plane developing cohesion (c)
c = cohesion (unit shearing strength at zero normal stress)
α = angle between inclined sliding plane developing and the horizontal (positive for upwards sliding)
ϕ = angle of internal friction

Friction angle and cohesion:

According to NVE "*Guidelines for concrete dams*" (2005) the contribution of the cohesion of the rock-concrete interface at the dam foundation must not be taken into account in the calculation of the total resistance to slide unless that contribution can be confirmed through laboratory experiments.

As Energi Norge (2012) points out NVE does not describe clearly on the guidelines how those cohesion values should be documented by the experiment. Energi Norge (2012) states that "*The direct origin of the claim is not known, but it seems to conform to international practice both in dam safety and other areas. Possibly due to claim one or more of the following reasons:*
• *Conservative approach (internal security)*
• *The cohesive ties the sensitivity to strain (broken at low strains)*
• *Possible presence of tensile stress (not captured by the simplified 2D analysis)*
• *Unsafe pore pressure and poretrykksvariasjon*
• *Possible presence of erosion, corrosion and wear (leaching, kalkutfellinger more)*
• *Unknown foundation preparation*

The NVE "*Guidelines for concrete dams*" (2005) sets that for badly groomed construction joints (like for example cement slurry) the cohesion from concrete should not normally be considered. On the other hand, the guideline says that for well-groomed construction joints, a contribution from cohesion can be included in the calculation of the factor of safety against sliding. The contribution of the cohesion to the sliding resistance will be calculated as a $0.085\sqrt{f_{cd}}$ or simply as f_{cd} if there is a lack of confirmation from laboratory experiments, being the f_{cd} the design compressive strength of concrete.

Regarding the selection of the friction angle values to be included in the factor of safety formula, NVE "*Guidelines for concrete dams*" (2005) says that, unless the friction angle of the sliding plane considered is well-documented by laboratory tests, the following values shall be used:

- 50 ° for hard rocks, rough surface and favorable cleavability in transition rock / concrete.
- 45 ° for hard rocks, small roughness with apparent cleavability and loose rocks without cleavability.
- 40 ° for loose rocks with clear cleavability.
- 45 ° for sliding planes in concrete.

Safety factors against sliding:

NVE "*Guidelines for concrete dams*" (2005) sets the following requirements for the factor of safety to fulfill the safety against sliding.

Contribution from cohesion	**Minimum safety factors for sliding stability (S)**	
	Design load	**Accidental load**
No cohesion	S ≥1.5 (*S ≥1.4)	S ≥1.1
Cohesion obtained from tests	S ≥2.5	S ≥1.5
Cohesion from literature	**S ≥3	**S ≥2

Table 3. Minimum safety factors against sliding stability (taken from (NVE. 2005))

* For ponds where cracks will increase the pore pressure (mainly buttress dams).
** It is not allowed to incorporate cohesion contribution to the safety factor calculation.

Energi Norge (2012) states that the origin of the minimum requirements of the safety factors is unknown and it suggests that the values are taken from the "Dam Safety Guidelines", developed by CDSA in 1995.

2.2.2 Other countries

This chapter presents the guidelines to evaluate the sliding stability of concrete dams in other countries to compare with the NVE regulations. The countries selected are Canada, USA and Sweden and Spain.

2.2.2.1 Canada

The Canadian Dam Association (CDA) published in 2007 a *"Dam Safety Guidelines"* which contains the guidelines that are used in Canada to evaluate the sliding stability of concrete dams. These guidelines were developed by the members of the CDA. In addition to the these document, the CDA also published 9 technical bulletins which contains "*methodologies and procedures for use by qualified professionals as they carry out dam analyses and safety assessments"*(CDA website). The guidelines that deal with the sliding stability are found within the Technical Bulletin 9 : "Structural considerations for dam safety".

It must be noted that Canada does not any law or federal regulation which states the requirements regarding the dam safety issues (CDA, 2010). The Canadian Dam association (CDA) is a *"a volunteer organization was formed in the 1980s to provide dam owners, operators, consultants, suppliers and government agencies with a national forum to discuss issues of dam safety in Canada*" (CDA, 2010).

Load combinations:

According to CDA (2007) the load combinations are classified in three groups depending on the likelihood of occurrence as it can be seen in Table 4:

Load combination	*Return period (T_R)*	*Annual exceedance probability (AEP)*
Usual (normal)	$T_r \leq 50\ years$	$AEP \geq 0.02$
Unusual	$50 < T_r \geq 1000\ years$	$0.02 > AEP \geq 0.001$
Extreme	$T_r \geq 1000\ years$	$AEP < 0.001$

Table 4. Classification of the load combinations (taken from (CDA,2010))

CDA (2007) points out that the structural performance and the risk of failure not only depends on the probability of occurrence of the loading condition but it is also dependent on the safety factors used, the degree of conservatism when selecting the shear strength parameters of the foundation (cohesion and friction angle) and the hydrological data.

The normal or usual load conditions are those to which the dam will be subjected to during normal operations, it has a recurrence up to 50 years and it includes self-weight, ice, silt, earth pressure, and HRWL (highest regulated water level) and also the tailwater water pressure and the uplift pressure (CDA, 2007). The normal load condition is similar to the design loads that are described on the Norwegian guidelines (Energi Norge, 2012).

The unusual loadings are between the usual loading and the extreme loadings. According to CDA (2007) it refers to the loads that occur infrequently and can damage the structure more than the normal loads but in a way that the dam can keep working safely and satisfactorily and the period of occurrence is between 50 years and 1000 years.

CDA (2007) says that the structure shall be assessed for two different situations in conjunction with the permanent and operating loads from the normal loading case:

- Unusual loading - Flood discharge loading
- Unusual loading – Plugged drains

The extreme loadings conditions refer to those which are highly unlikely to occur and they would be considered as emergencies if they occur, the dam must be able to withstand the extreme loads without failing (CDA, 2007). The return period for these type of loads is higher than 1000 years. There are three cases that shall be assessed within the extreme loading:

1. *Extreme loading – Earthquake :* The usual loading case must be checked together with the loads produced by the earthquake. CDA (2007) says that due to the fact that the ice cover would either break up or would not contribute favorably, there is no need to include the ice loads when assessing the extreme earthquake event.

2. *Extreme loading – Flood:* Normal loads from the usual loading case, except for the ice, must be assessed together with the loads produced by the passage of the extreme flood.

3. *Post-Earthquake condition:* When cracking produced by the seismic event have been identified at any weak section of the structure, a stability analysis must be done in order to check if the dam is still able to withstand the usual loads (CDA, 2007). According to CDA (2007), when analyzing the state of the structure after the earthquake ,the following should be considered:

    a. Loss of cohesive bonds in regions of seismically induced tensile stress
    b. Degradation of the friction angle die to earthquake
    c. Appropiate upliddt conditions
    d. Increase in silt pressure due to liquefaction of reservoir silt
    e. Effect of seismic excitation on dam appurtenant structures, especially on the operation of flow control equipment, after the earthquake event

Safety factor calculation:

CDA (2007) allows using 4 different methods of analysis to evaluate the safety of a dam but it recommends using a simple approach using conservative assumptions to start the evaluation of the dam. Afterwards, a more detailed analysis can be carried out if there is a need of a better understanding of the dam structural behavior. The methods mentioned by CDA (2007) are the following:

- Rigid body method
- Cracked base analysis
- Parametric analysis
- Finite element analysis
- Dynamic analysis

The limit equilibrium method is the method used by the CDA (2007) in order to assess the sliding stability; this method has been described in the section 5.1.3:

$$S = \frac{c \cdot A + (\sum V \cdot cos\alpha + \sum H \cdot sin\alpha) \cdot tan\phi}{(\sum H \cdot cos\alpha - \sum V \cdot sin\alpha)} \quad (2.14)$$

Where:

$\sum$V = summation of vertical forces
$\sum$H = summation of horizontal forces

A = area of potential failure plane developing cohesion (c)
c = cohesion (unit shearing strength at zero normal stress)
α = angle between inclined sliding plane developing and the horizontal (positive for upwards sliding)
ϕ = angle of internal friction

Cohesion and friction angle:

Intact concrete: CDA (2007) states that the shear strength parameters can be found in the report "Sliding resistance of concrete gravity dams" written by CEATI in 1998.

Lift joints: According to CDA (2007) if information from laboratory tests is not available then the lift joint must be considered as an unbonded joint without cohesive strength. CDA (2007) provides two different sources to determine the shear strength parameters:

- EPRI (1992) and CEATI (1998): $\varphi = 45º \; and \; c = 0$
- Donelly and Rigbey (2006): $\varphi = 35º - 48º \; and \; c = 0$

CDA (2007) argues that in the case that the selection of this shear strength parameters leads to uneconomical designs, then the shear strength parameters (friction angle and cohesion) can be estimated by laboratory tests or from the historical data from dams which were constructed at the same time, on sites with the same geology and built by the same company. In these cases, CDA (2007) allows to use a conservative estimate of the cohesion strength.

CDA (2007) indicates that in the cases where the lift joint is good condition without available test data, shear strength values can be used to determine the shear strength of the joint. It is mentioned by CDA (2007) to use the values given by CEATI (1998), $c = 0.085 \cdot f_{cd} \; and \; \varphi = 57º$.

Concrete-foundation contact zone: It is pointed out by CDA (2007) that to evaluate the shear strength one must take into consideration both the type of foundation material and the geological and geometric characteristics of the interface concrete-rock. CDA (2007) indicates that when shear strength parameters cannot be obtained from testing, one can obtained them by using documentation. However if the contact surface presents evidence of leakage or relevant pore pressures, the rock-concrete interface shall be treated as unbounded and no cohesion strenght must be considered, unless testing data available can confirm the existence of bonding along the contact surface.

Safety factors against sliding:

According to CDA (2007) the function of the safety factors is to ensure that the dam will have enough resistance to sliding. CDA (2007) stated that the safety factors make possible to compare the sliding resistance between different dams and they are not represent an absolute indicator of safety. The following table shows the minimum acceptable safety factors based on rigid body analysis:

Load combination	*Minimum acceptable safety factors*		
	without cohesive strength	*with cohesive strength from tests*	*with cohesive strength from literature*
Usual	$\geq \mathbf{1.5}$	$\geq \mathbf{2}$	$\geq \mathbf{1.5}$
Unusual	$\geq \mathbf{1.3}$	$\geq \mathbf{1.5}$	$\geq \mathbf{2}$
Extreme-Flood	$\geq \mathbf{1.1}$	$\geq \mathbf{1.1}$	$\geq \mathbf{1.3}$
Extreme-Earthquake	The earthquake load case is used to establish post-earthquake condition of the dam		
Post-earthquake	$\geq \mathbf{1.5}$	Shear resistance based on friction and cohesion needs to be considered carefully since the analysis surface may not remain in compression throughout the earthquake and results in cracking which will change the resistance parameters	

Table 5. Minimum acceptable safety factors against sliding (taken from (CDA, 2007))

2.2.2.2 USA

Several guidelines are used in the United States to evaluate the sliding stability of concrete dams. It has been decided to present in this section two of them. Firstly, the guidelines described by the Federal Energy Regulation Commission (FERC, 2002) are presented and secondly the regulation proposed by the US Bureau of Reclamation in the document "*Design Criteria for Concrete Arch and Gravity Dams", Engineering Monograph n. 19, 1974*".

2.2.2.2.1 FERC guidelines

The loading combinations that are provided by FERC (2002) are the following:

- Usual loading combination-Normal operating condition
- Unusual loading combination-Flooding Discharge loading
- Unusual loading combination-Ice
- Extreme loading combination-Usual loading + Earthquake

In the FERC guidelines the safety factor against sliding is calculated by using the shear friction method. Regarding the contribution of cohesive strength at the contact rock-concrete at the foundation, it is pointed out by FERC (2002) that even though it is recognized the presence of the cohesive bond, it is also hard to know exactly the contribution of this cohesion to the shear strength. That is why FERC (2002) provides an alternative table with safety factors for the cases when the cohesion is not account for. In these guidelines, the dams are classified in two groups; Dams with high risk and dams with low risk.

The following tables show the minimum acceptable factors of safety that are used in the FERC guidelines for both cases (considering the cohesion and without considering it):

Load combination	Dams with high risk	Dams with low risk
Usual	$S = 3$	$S = 3$
Unusual	$S = 2.0$	$S = 3$
Post-earthquake	$S = 1.3$	$S > 1.0$

Table 6. Minimum recommended safety factors for high and low risk dams (taken from (FERC,2002))

Load combination	Normal load
Usual	$S = 1.5$
Unusual	$S = 1.3$
Post-earthquake	$S = 1.3$

Table 7. Minimum recommended safety factors against sliding if cohesion is not considered.

2.2.2.1.2 USBR guidelines

The Bureau of Reclamation developed a guidelines for assessing the sliding stability of concrete dams in the document *"Design Criteria for Concrete Arch and Gravity Dams", Engineering Monograph n. 19, 1974.*

The loading combinations provided by USBR (1974) are the following:

- Usual loading combination: Normal design reservoir elevation with appropriate dead loads, uplift, silt, ice and tailwater.
- Unusual loading combination: Maximum design reservoir elevation with appropriate dead loads, silt, tailwater and uplift.
- Extreme loading combination: Usual loading combination plus of the effects of the maximum credible earthquake.

The sliding stability is assessed by the calculation of a factor of safety by using the shear friction factor, which has been explained more in detail in the section 5.1.2.

The table 2 shows the minimum requirements regarding the factors of safety against sliding given by USBR (1974):

Sliding plane	***Usual***	***Unusual***	***Extreme***
within the dam	3	2	1
concrete-to-rock contact	3	2	1
foundation	4	2.7	1.3

Table 8. Minimum requirements for safety factors against sliding for different loading cases (taken from (USBR, 1974))

2.2.2.3 Sweden

The guidelines for the design of concrete dams (both gravity and buttress dams) are described by "*RIDAS 2012 - Kraftföretagens Guideline for dammsäkerhet*" and instructions "*Tillämpningsvägledning for concrete dams Section 7.3*", prepared by the Svensk Energi. (Liahagen , 2012).

The Swedish guidelines recommend to assess the safety against sliding at the interface concrete-to-rock and also at any weakest joints within the foundation.

2.2.2.3.1 RIDAS guidelines

Load combinations:

The following loading combinations shall be checked when evaluating the stability of concrete dams:

- Normal loading combination
- Exceptional loading combination
- Accidental loading combination

Calculation of factor of safety:

To assess the sliding stability of concrete dams founded on rock the guidelines recommend to use the sliding resistance method described in section 5.1.1.

Cohesion and friction angle:

The RIDAS guidelines recommend not to use the contribution of cohesion in the shear resistance. In dams constructed on good quality rock RIDAS recommend to use the following, shown in table 2, as allowable coefficients of friction, where the failure value corresponds to a friction angle of 45º (Johansson, 2009).

Foundation type	*Normal load case*	*Exceptional load case*	*Accidental load case*	*Failure value for tan(ϕ)*
Rock	0.75	0.90	0.95	1

Table 9. Recommended coefficients of friction according to RIDAS for dams founded on rock of good quality (Johansson, 2009).

Requirements for safety factor:

When the dam is not founded in good quality rock, the value $tan\varphi$ shall be evaluate it through investigations of the rock mass and then those values should be reduced with a factor of safety to calculate the allowable coefficient of friction (Johansson, 2009). The following table shows the recommended safety factor values to fulfill the safety against sliding:

Foundation	*Normal case*	*Exceptional case*	*Accidental case*
Rock	$S \geq 1.35$	$S \geq 1.10$	$S \geq 1.05$

Table 10. Factors of safety according to RIDAS for reduction of the failure value of tan(ϕ) (taken from (Johansson,2009))

2.2.2.3.2 New guidelines proposed by Johansson et. Al (2012):

Johansson et Al (2012) proposed new guidelines to assess the sliding stability of concrete dams in Sweden. According to the authors, three different sliding failure modes of the concrete dam were described (See figure 7) and to evaluate the sliding stability the shear resistance of the following potential failure planes must be calculated:

- Type A: Failure in the concrete-to-rock interface, without cohesion:

  $$T = N \cdot tan(\phi_b + i) \quad (2.15)$$

  Where T is the peak shear strength along the failure plane, N is the effective normal force perpendicular to the failure plane, ϕ_b is the dilation corrected (basic) friction angle and i is the dilation angle from surface roughness.

  Johansson et Al (2012) indicates that the dilation angle can be estimated by measuring the exposed large asperities on the concrete-to-rock surface for new dams and for existing dams it shall be estimate by measuring the rock surface or from pictures during the construction of the dam.

- Type A2: Failure in the concrete-to-rock interface with cohesion:

  $$T = c \cdot A_c + N \cdot R \cdot tan(\phi_i) \quad (2.16)$$

  Where T is the peak shear strength along the failure plane, c is the cohesion, A_c is the area with compressive stresses and cohesion, N is the effective normal force perpendicular to the failure plane, R is the reduction factor that represents the part of the normal force acting on the area and ϕ_i is the internal friction angle for the intact interface.

  As Johansson et Al (2012) suggest the broken and the intact part of the concrete-to-rock interfaces should not be added together because of the different degree of stiffness. According to Eltervaag (2012), different degree of stiffness on the interface will lead to a concentration of the stresses in the stiffest areas, therefore if the area with bonding is small compared to the total area, the shear stress could exceed the shear capacity and that area would crack. If the area with bonding is relatively large, these areas will not crack and the contribution from bond will govern the shear behavior of the whole concrete-to-rock interface (Eltervaag, 2012).

- Type B: Failure along existing joint in the rock foundation:

$$T = N \cdot tan(\varphi_r + i) \quad (2.17)$$

Where T is the peak shear strength along the failure plane, N is the effective normal force perpendicular to the failure plane, ϕ_r is the residual friction angle according to Barton and Choubey (1977) and i is the contribution of roughness.

- Type C: Failure in the rock mass:

$$T = c_m + N \cdot tan(\phi_m) \quad (2.18)$$

Where T is the peak shear strength along the failure plane, N is the effective normal force perpendicular to the failure plane, c_m is the cohesion in rock mass and ϕ_m is the friction angle for the rock mass. Johansson et Al (2012) indicates that the strength parameters of the rock mass can be estimated by using rock mass classification systems and empirical failure criterion.

The following table shows the acceptable safety factor proposed in the new guidelines proposed by Johansson et Al (2012):

Type of sliding failure	***Load case***		
	Normal	***Exceptional***	***Accidental***
A1. Concrete-to-rock interface. Without bonding.	1.5	1.3	1.1
A2. Concrete-to-rock interface. With bonding.	2.0	1.5	1.1
B. Persistent joint in foundation.	1.5 (-1.1)*	1.3 (-1.05)*	1.1 (-1.0)*
C. Rock mass.	3.0	2.0	1.3

Table 11. Minimum requirements for safety factors against sliding for each type of failure (taken from (Johansson et Al, 2012))

2.3 Summary

The objective of this chapter is to introduce the methods used nowadays to assess the sliding stability of concrete dams. Moreover, an overview of the guidelines and regulations used in countries with a large tradition in the dam engineering field, such as Norway, Sweden, and Canada are presented. A summary of these sections is presented below.

The methods to calculate the sliding stability of concrete dams that have been presented through this chapter are three; The sliding resistance method, the shear friction method and the limit equilibrium method. The differences between these methods are the formulas used to estimate the safety factor against sliding. The sliding resistance method describes the safety factor as the relation between the parallel and perpendicular forces to the sliding plane considered. The shear friction factor estimates the safety factor against sliding by dividing the maximum available force to resist the sliding of the plane considered (the shear resistance) by the horizontal load acting on that plane. Finally, the limit equilibrium method is described, which defines the factor of safety as the shear strength of the sliding plane divided by the shear stress applied along that plane.

The regulations and guidelines used in Norway and in other countries like Canada, USA and Sweden have been also presented. Most of the regulations make use of the Mohr-Coulomb criterion to estimate the shear strength of the sliding plane, and since there are many uncertainties regarding the contribution of the cohesion to the shear resistance of the dam-rock interface at the foundation, this is not taken into consideration unless it can be confirm through laboratory experiments. Since the Mohr-Coulomb model does not take into consideration the influence of the roughness in the shear strength, which increases strongly the shear capacity of the plane considered (as it will be showed through next chapter), the currently guidelines worldwide underestimates the shear capacity of the concrete-to-rock interface at dam foundations and thus the design of the dams will be too conservative. In order to account the influence of roughness on shear resistance Johansson et Al (2012) proposed a new set of guidelines in Sweden regarding the safety against sliding stability, they proposed that the effect of the surface roughness can be included when estimating the shear resistance of the concrete-rock interface.

In Norway, the guidelines to assess the safety against sliding stability are described by the Norwegian Water Resources and Energy Directorate (NVE), The method used by the Norwegian guidelines is the shear friction factor and the shear resistance of the sliding plane considered is calculates by using the Mohr-Coulomb equation.

NVE regulations imposes restrictions on when the contribution of the cohesion can be used when estimating the shear resistance but according to Energi Norge (2012) it is not clearly stated how the cohesion should be obtained in laboratory experiments. Regarding the friction angle to be considered, NVE states that should be used is 45º, which can be considered as too conservative.

3. LITERATURE STUDY: SHEAR RESISTANCE OF ROUGH ROCK JOINTS.

3.1 Introduction

The key factor that governs the safety against sliding stability of concrete dams is the shear strength (both of the rock joints within the foundation of the dam and of the concrete-to-rock interface) and it is influenced by parameters which makes difficult and uncertain the prediction of the shear strength. These parameters are, according to Johansson (2009), the normal stress, the uniaxial compressive strength of the joint surfaces, the surface roughness, the weathering of the surfaces and the infilling material.

Since the 1960's, many empirical shear strength models have been developed by rock mechanics researches which attempt to estimate the shear strength of a rough rock joint

The aim of this thesis is to investigate the effect of roughness in the shear behavior on concrete-to-rock interface which is a specific case of the general problem of rough rock joints. In order to increase the knowledge of the frictional behavior of rough rock joints a literature study on the existing shear strength empirical models for rough rock joints is presented in this chapter.

Furthermore, this literature study also contains a review of direct-shear test results obtained by different authors regarding the investigation of the influence of roughness on shear strength both in rock joints and concrete-to-rock joints. This was done to increase the knowledge of the parameters that influence the shear strength of both rough rock-to-rock and concrete-to-rock joints and also in order to gain knowledge on the techniques of the direct shear tests and to inspire the author for the test program at Lulea University of Technology.

3.2 Rock joint shear strength failure criteria

The following review of the different proposed models to estimate the shear strength of rock joints is based on the literature study presented by Johansson F. (2009) and by Graselli (2001).

3.2.1 Mohr-Coulomb model

The Mohr-Coulomb is the first known shear strength failure criterion. It is the result of the investigations about friction between two flat surfaces carried out by Coulomb 1776 and Mohr 1882, this model indicates that the shear behavior of a joint is only function of the parameter so-called basic friction angle. The equation that defines the shear resistance by Mohr-Coulomb is best known as:

$$\tau = c + \sigma_n \cdot \tan(\varphi_b) \quad (3.1)$$

Where τ is the shear stress at failure, σ_n ia the effective normal stress acting on the failure plane c is the cohesion and φ_b is the basic friction angle. The friction angle can be defined as the maximum inclination angle that a considered sliding plane can have before it starts to slide.

This shear resistance criterion is widely used nowadays due to its simplicity and it is the method that is used in most of the sliding stability guidelines for concrete dams to estimate the shear resistance.

3.2.2 Dilantancy models

The Mohr-Coulomb model is only valid to represent the friction behavior of two materials along a flat surface and it does not capture the discontinuous character of natural rock joints. It does not take into account the fact that natural rock joints have a roughness that contributes to the shear resistance. In order to incorporate the effect of roughness of the natural rock joints into the shear strength, many rock mechanics researches started to investigate about this topic.

Failure envelope was recognized to be curve in the 1960s and one of the most important contributions was made by Patton (1966). Patton conducted a series of direct shear tests on specimens with regular saw-teeth artificial joint and from those experiments a bi-linear failure criterion was established.

Patton (1966) found that the shear behavior of the joints was different depending on the magnitude of the normal stress applied. Under low normal stress the sliding overriding the

asperities was the mechanism governing the shear behavior. Therefore, with low normal stresses, the asperities contribute to the shear resistance and the expression to estimate the shear strength had the form:

$$\tau = \sigma_n \cdot \tan(\varphi_b + i) \tag{3.2}$$

Where τ is the shear stress at failure, σ_n is the effective normal stress acting on the failure plane c is the cohesion and φ_b is the basic friction angle and i is the inclination of each tooth of the saw-teeth profile.

At higher levels of normal stress, the contribution of the saw-teeth in the shear resistance disappeared due to the fact that the asperities are sheared off. In this case, the failure criterion has the form:

$$\tau = \sigma_n \cdot \tan(\varphi_r) \tag{3.3}$$

where φ_r is the residual shearing resistance of an initially intact material and c the cohesion when the teeth are sheared of at their base. The equations and the principle that defines the Patton`s model are shown in Figure 4.

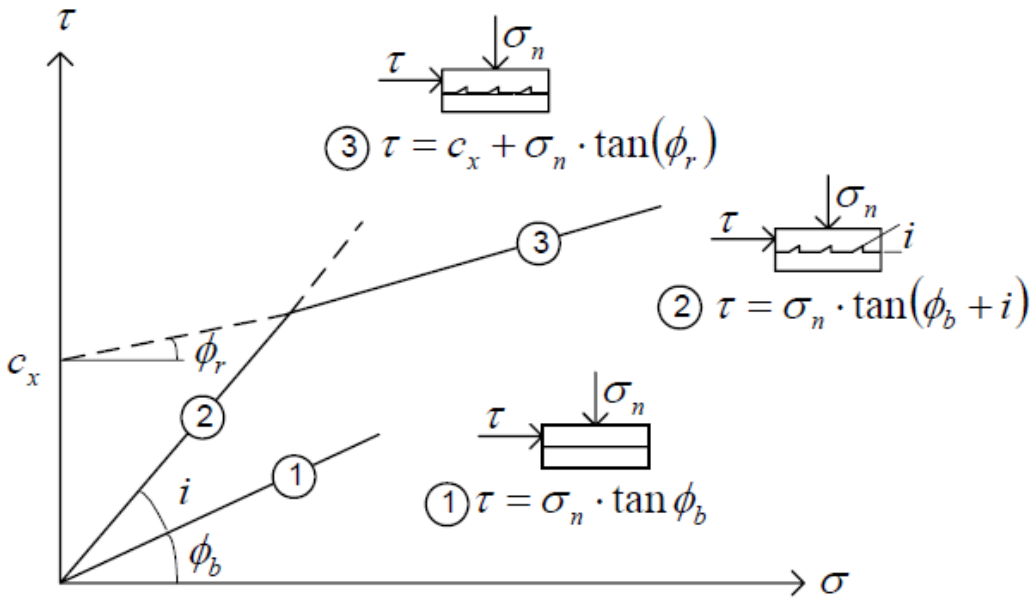

Figure 4. Bilinear failure envelop proposed by Patton (taken from (Johansson, 2009))

The Patton`s model describes fairly well the shear strength along surfaces with an equal number of teeth regularly spaced but according to Graselli (2001) this model does not describe that well the shear behavior of irregular rock joints. Regarding this discrepancy with real rock joints, Patton (1966) argued that abrupt changes in the failure envelope for rock surfaces does not reflect just a change of the failure mode but reflects changes in the intensities of different failure modes occurring simultaneously.

According to B. Indraratna (1997), Patton`s model is suitable for low asperity angles but if the angle of asperities is high it overestimates the shear strength in the low to medium normal stress range. Another important limitation of Patton`s failure criteria is the difficulty to determine the parameter i on natural rough rock joint because in the nature the geometry of the asperities presented on the joints are not constant and present a great variety of asperities with regard to the geometry.

As H. J. Schneider (1975) states *"With this method only the peak or initial friction can be considered and no statement can be made about the development of the frictional forces and the dilatation of the joint with increasing shear movement".*

In order to taken into account the dilation, Patton`s empirical shear strength model was extended to natural profiles by Maksimovic (1995). He proposed a bilinear criterion of hyperbolic type, where the frictional resistance component is based on three components (basic friction angle, roughness angle and median angle pressure). The following equation to estimate the peak shear strength of rough rock joints is proposed:

$$\tau = \sigma_n \cdot tan\left(\phi_b + \frac{\Delta\phi}{1 + \frac{\sigma_n}{p_n}}\right) \tag{3.4}$$

Where; ϕ_b is the basic friction angle, $\Delta\phi$ is the "joint roughness angle" which represents the surface roughness of the joint and the associated dilatancy effects at zero normal stresses, it can be described and the angle of maximum dilatancy (Maksimovic, 1995), p_n is the median angle pressure which is equal to $(\Delta\phi/2)$ and represents the strength and rigidity of asperities that make the joint surface rough, τ is the peak shear stress, is the normal stress σ_n.

Ladanyi and Archambault (1970) identified several problems in the Patton`s bilinear model. They argued that since the stress distribution is not uniform over the contact surface of the teeth, some of the teeth are partially broken before reaching the peak shear stress. Also they indicated that the average inclination angle i and the cohesion intercept are difficult to estimate on natural irregular rock joints. In order to solve these drawbacks they stated that *"it may be of interest if a more general failure model could be developed, which would be valid for any irregular rock surface and would contain a limited number of relevant parameters".*

The model proposed by Ladanyi and Archambault (1970) has two different shear resistance components. The first one is the shear strength when sliding is the shear mechanism and the second one is when the asperities are sheared off and only shearing is the governing shear mechanism. In there is no shearing of the asperities, the maximum shear strength before sliding occurs over the asperities can be considered as a sum of three components:

$$S_{sliding} = S_1 + S_2 + S_3 \tag{3.5}$$

Where; S_1 is the component due to external work in dilating against the external force, S_2 is the component due to additional internal work in friction due to dilatancy, and S_3 is the component due to work done in internal friction if sample did not change volume in shear.
The component S_1 due to external work done in dilation is defined as follows:

$$S_1 = N \cdot \frac{dy}{dx} = N \cdot v \tag{3.6}$$

In the equation 3.6, N is the normal force on the surface, dy and dx are the increment in normal and shear displacement respectively, and v is the rate of dilation at failure.

The component S_2 due to additional internal work in friction due to dilation, and it is expressed as:

$$S_2 = S \cdot v \cdot tan\phi_r \tag{3.7}$$

where v is the rate of dilation at failure and ϕ_r is the statistical average value of friction angle that is assesses when sliding occurs along the irregularities of different orientations.

Component S_3 of friction for a flat rough surface and it can be expressed as:

$$S_3 = N \cdot tan\phi_u \tag{3.8}$$

Where N is the normal stress applied and ϕ_u is the frictional resistance along the contact surfaces of the teeth.

When all the asperities have been sheared off, the shear strength will be defined by the equation 3.9:

$$S_{shearing} = A \cdot s_o + N \cdot tan\phi_o \tag{3.9}$$

As Patton mentioned, the shearing along an rough rock joint is governed by two failure modes simultaneously, and each failure mode will take place in different portions of the total area. For example, if the asperities are sheared off only over an area $A_{shearing}$ of the total area , then the sliding will take place over an area $A_{sliding} = A_{total} - A_{shearing}$. Therefore, the equation that defines the shear strength can be written as follows:

$$S = (S_1 + S_2 + S_3) \cdot (1 - a_s) + S_4 \cdot a_s \tag{3.10}$$

The parameter a_s is called the shear area ratio and can be defined by equation 3.11:

$$a_s = \frac{A_{shearing}}{A_{total}} \tag{3.11}$$

Substituting in equation 3.5 for S_1 to $S_{shearing}$ and dividing all the forces by A and taking into account the degree of interlocking, η, the following equation to determine the shear strength will be obtained:

$$\tau = \frac{\sigma \cdot (1 - a_s) \cdot (\upsilon + tan\phi_u) + a_s \cdot (\sigma \cdot tan\phi_i + \eta \cdot c_i)}{1 - (1 - a_s) \cdot \upsilon \cdot tan\phi_f} \tag{3.12}$$

The degree of interlocking can be defined by equation 3.13:

$$\eta = 1 - \frac{\Delta x}{\Delta L} \tag{3.13}$$

Where; $\Delta x$is the horizontal displacement and ΔL represents the length of the asperities in the shear direction. The figure 6 shows the definition of the interlocking concept and also the results from the bilinear model and the Ladanyi & Archabault model.

From equation 3.12 one can see that the shear area ratio a_s and υ are function of the normal stress applied. In the cases of low normal stress, $\sigma \approx 0$ and therefore the parameters $a_s \sim 0$ and $\upsilon \sim \tan(i)$. If the normal stresses is high (shearing of the asperities) then $a_s \sim 1$ and $\upsilon \sim 0$.

According to Ladanyi and Archambault (1970) from the test results it was conclude that as increases with linearly at the beginning and reaches the value of one at the transition pressure of rock substance (σ_T). The value of υ decreases rapidly at low normal stress and reached zero value at a very small rate. The rate of variation of both a_s and υ with normal stress can be seen on figure 5.

The transition pressure of rock substance, σ_T, was selected by Layandy & Arch (1970) to be the normal stress at which the shearing of asperities is taking place all over the area of the joint surface. They proposed the following equations to determine the parameters a_s and υ, in the range of normal stress $0 < \sigma_n < \sigma_T$.

$$a_s \approx 1 - \left(1 - \frac{\sigma_n}{\eta \cdot \sigma_T}\right)^{k_1} \tag{3.14}$$

$$\upsilon \approx -\left(1 - \frac{\sigma_n}{\eta \cdot \sigma_T}\right)^{k_2} \cdot \tan(i) \tag{3.15}$$

The exponent k_1 and k_2 have a value of approximately $k_1 \approx 1.5$ and $k_2 \approx 4$. Ladanyi & Archa (1970) points out that the estimations of the paramaters a_s and υ must be seen only as a help to visualize how these parameters vary with the normal pressure.

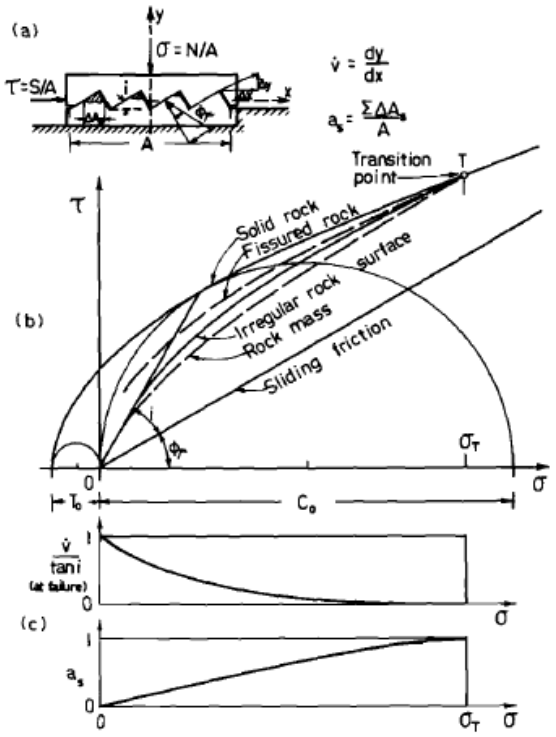

Figure 5. (a) Definition of the degree of interlocking. (b) Results according to the bilinear model. (c) Results according to the proposed model. (taken from (Johansson, 2009))

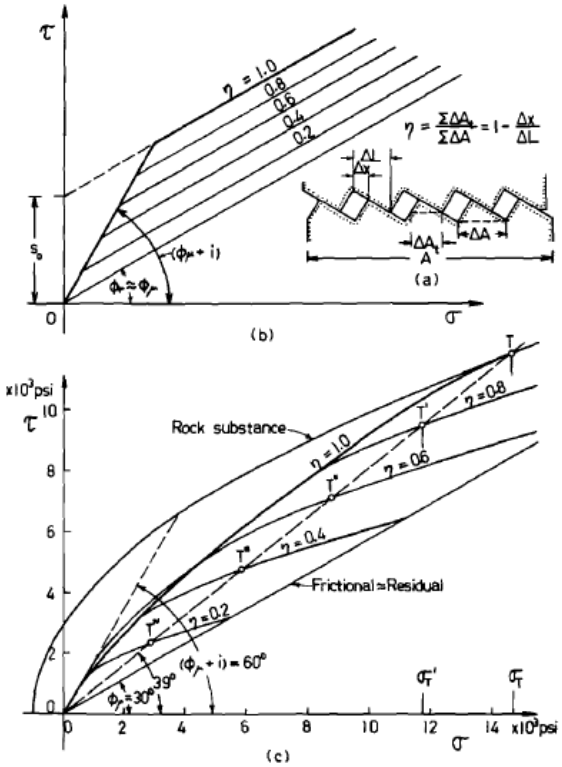

Figure 6. (a) Definition of the dilation rate and the shear area ratio. (b) expected failure enveloped for irregular rock surfaces, and rock mass, respectively. (c) Anticipated variation of dilation rate and shear area ratio with normal pressure. (taken from (Johansson, 2009))

Some peak shear strength models have been developed during the last years by using technology that allows to measure and characterize rock joint surface in three dimensions. One of them was developed by Graselli (2001), who established a failure criterion for rough unfilled joints which is able to incorporate the three dimensional joint morphology. Graselli used three-dimensional scanner to map the joint surface after shearing. The reconstruction of the rough surface was done by using a triangulation algorithm on measured point clouds. This resulted in a discretization of the surface in triangles and only those triangles that are facing the shear direction present resistance to shear. The total contact area (A_c) can be estimated by summing the areas of those triangles facing the shear direction. A parameter called the apparent dip angle, θ^* , determine the shear resistance contribution from each triangles, which is described in Figure 7. According to Graselli (2001) the following equation can be used to define the relation between A_c and θ^*:

$$A_c = A_o \cdot \left(\frac{\theta^*_{max} - \theta^*}{\theta^*_{max}}\right)^C \tag{3.16}$$

Where A_c is the total contact area, θ^*_{max} is the maximum apparent dip angle, C is a roughness parameter and θ^* is the apparent dip angle.

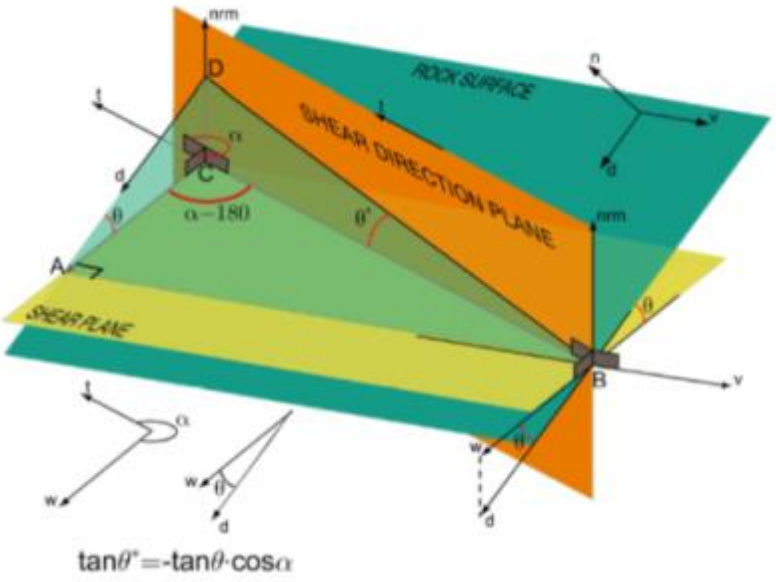

Figure 7. Geometrical identification of the apparent dip angles, as function of the shear direction.

Graselli indicates that only the zones that were facing the shear direction and are steeper than a threshold value of inclination, which is defined as $\theta`_{cr}$ , are involved in the shear resistance. And the zones which an inclination equal to the threshold inclination $\theta`_{cr}$ only will be in contact and will not contribute to the shear resistance and the areas which their inclination is larger than $\theta`_{cr}$ will be sheared or even crushed if the normal stress applied is very high.

The equation was proposed by Graselli (2001) to estimate the peak shear strength based on the extensive laboratory tests is defined as:

$$\tau_p = \sigma_n \cdot \tan(\phi_r) \cdot \left[1 + e^{\frac{-\theta_{max} \cdot \sigma_n}{9 \cdot A_o \cdot C \cdot \sigma_t}}\right] \quad (3.17)$$

Where τ_p is the peak shear strength of the joint, σ_n is the applied average normal stress, σ_t is the tensile strength of the intact material obtained with standard Brazilian test, ϕ_r is the residual friction angle (after a standard displacement of 5 mm), A_o is the maximum potential contact area for the specified shear direction, θ_{max} is the maximum apparent dip angle with respect to the shear direction, C is the roughness parameter.

According to Cai-Chu Xia et. Al (2013) the model developed by Graselli (2001) presents the following limitations: The model does not estimate properly the shear strength on smooth rock joints, because for a smooth joint θ_{max} is equal to zero and equation 3 will be rewrite as $\tau = 2 \cdot \sigma_n \cdot \tan(\varphi_b)$ which is not consistent with equation for shear strength $\tau = \sigma_n \cdot \tan(\varphi_b)$ for smooth horizontal joints. Another limitation pointed out by Cai-Chu Xia et. Al (2013) is that the ratio (θ^*_{max}/C) does not have a clear physical meaning. They argued that the equation proposed by Graselli does not follow the standard formula of Mohr-Coulomb friction law and it does not consider the peak dilatancy angle caused by roughness. Finally, the last limitation found is that Graselli`s equation is difficult to understand from an engineering point of view.

In order to overcome these limitations and improve the Graselli`s equation, Cai-Chu Xia et. Al (2013) proposed the following equation to estimate the peak shear strength of a rock joint:

$$\tau_p = \sigma_n \cdot tan\left\{\varphi_b + \frac{4 \cdot A_o \cdot \theta^*_{max}}{C+1} \cdot \left[1 + e^{\left(-\frac{1}{9 \cdot A_o} \cdot \frac{\theta^*_{max}}{C+1} \cdot \frac{\sigma_n}{\sigma_t}\right)}\right]\right\} \quad (3.18)$$

The model is based on Graselli`s equation and thus the parameters used in equation 3 applied for the equation developed by Cai-Chu Xia et. Al (2013).

Johansson F, (2009) in his PhD thesis developed a conceptual model to estimate the peak shear strength of unfilled rough rock joints. The objective is study was to study the influence of the scale effect of unfilled rough rock joints in the peak shear resistance. The model is based on the adhesion theory which indicates that all surfaces present a level of roughness at a microscopic level. The contact points between two surfaces will be where the asperities of the surfaces touch each other, thus the total contact area will only be a part of the total nominal contact area and as it is pointed out by Johansson (2009) the normal stress at the contacting points can be so high that the plastic yield strength of the material can be reach, at the asperity level.

The true contact area A_c can be calculated as:

$$A_c = \frac{N}{q_u} \tag{3.19}$$

Where N is the normal load and q_u represents the plastic yield strength. Since the q_u is a constant value, A_c is proportional to the normal load (Johansson, 2009). Therefore the shear resistance of each contact point will be defined a parameter called the adhesive strength of the contact point s, the shear strength T will be then:

$$T = A_c \cdot s \tag{3.20}$$

By combining the equations 3.19 and 3.20, the shear resistance can be expressed as follows:

$$T = N \cdot \frac{s}{q_u} \tag{3.21}$$

As it is pointed out by Johansson F. (2009) the relation s/q_u is the tangent of a friction angle.

The asperities can fail by three different failure modes, as it is mentioned by Johansson F. (2009). Failure can occur by sliding, shear or crushing of asperities, and tensile failure, at steeper angles of the asperity the tensile failure is more likely occur and at less inclined degree of asperities, sliding is the most probable failure mode to occur. The mechanical behavior behind each failure mode is also described by Johansson F. (2009) as *"Sliding over inclined asperities requires displacement increment along the contact interface between asperities at contact in order to shear off the adhesive bonds that exists at the contact points. On the other hand, prior to shear, prior to shear or tensile failure of interlocked asperities, the displacement increment along he contact interface between asperities in contact decreases".*

To study how a single asperity fail at different angles of the asperity inclination, i, Johansson carried out an analysis of a two dimensional idealized asperity, the idealized asperity can be seen in figure 8.

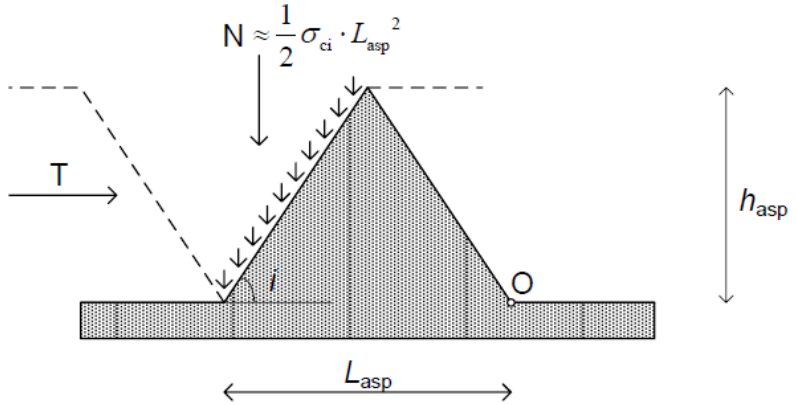

Figure 8. Two dimensional idealized asperity used in the calculation (taken from (Johansson, 2009))

Johansson (2009) provided three expressions of resistance associated to the three different failure modes mentioned. The sliding resistance along the side of the asperity facing the shear direction can be estimated by using the Patton`s equation:

$$T = N \cdot tan(\phi_b + i) \tag{3.22}$$

The resistance to shear through the intact rock at the base of the idealized asperity is calculated as:

$$T = c_i \cdot L_{asp}^2 + N \cdot tan(\phi_i + i) \tag{3.23}$$

Finally, the resistance to tensile failure at the base of the asperity is described. Johansson (2009) indicates that the tensile failure will take place when the average tensile stress at the asperity reaches a value higher than the tensile strength of the intact rock. The moment is calculated at point O in the figure 2 and gives:

$$T = \frac{(3 \cdot \sigma_{ci} + 4 \cdot \sigma_{ti}) \cdot L_{asp}^2}{2 \cdot tan(i)} \tag{3.24}$$

In order to illustrate how the resistance values of each failure mode vary with the asperity angle inclination, an example was done by Johansson (2009). Typical values from intact granite were assumed in the example. The uniaxial compressive strength, σ_{ci} is assumed to be 150 MPa, the tensile strength, σ_{ti}, to be 10 MPa, cohesion, c_i, to be 20 MPa, and friction angle, ϕ_i, to be 60º and the basic friction angle, ϕ_b, to be 30º. The base width of the asperity has been assumed to be 10 mm. The results of this calculation are shown in Figure 9.

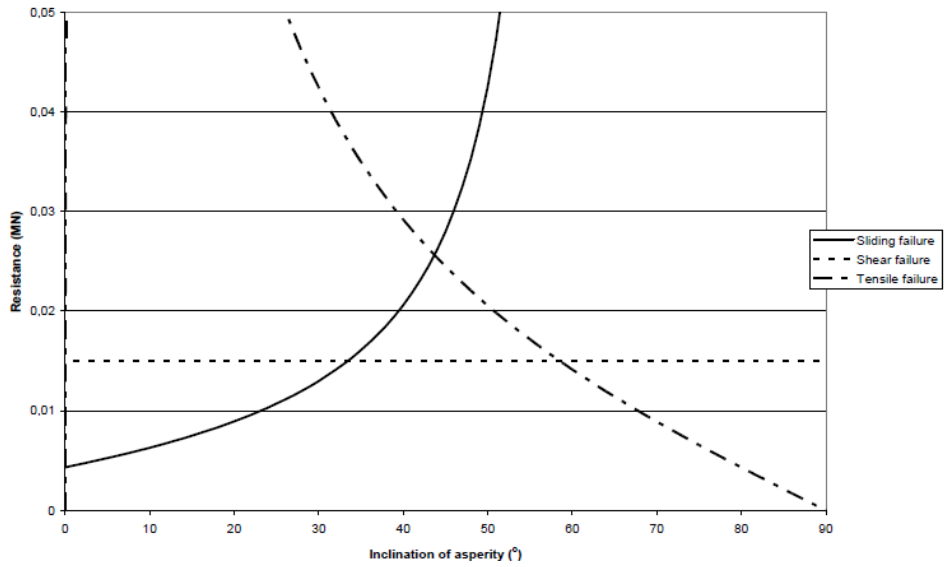

Figure 9. Resistances fro different failure modes for an idealized asperity where the inclination angle of the asperity varies (sliding failure, equation 3.22; shear failure, equation 3.23; and tensile failure, equation 3.24 (taken from (Johansson, 2009))

According to Johansson (2009) the results match with the observations made by Patton (1966), the shear behavior is determined by sliding failure for low values of asperity inclination. On the other hand, for higher values of i the failure mode turns into shearing off the asperities. From figure 4.5, the threshold value of i at which the transition between sliding failure and shearing failure occurs is 30-35º. As it can be seen in the figure 9, the tensile failure will take place for values of i above 70º.

A calculation of the total friction angle for different values of i was also carried out for the idealized asperity. The results are presented in Figure 10.

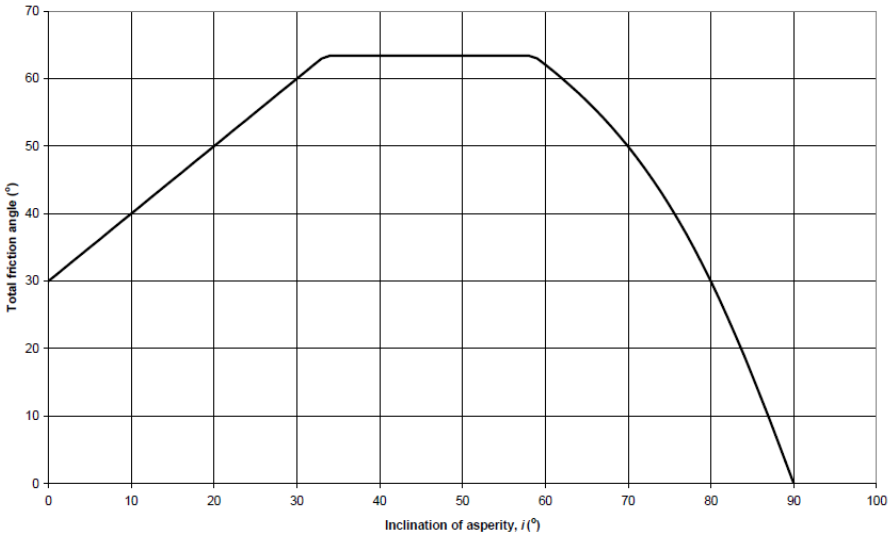

Figure 10. Total friction angle for an idealized asperity with a varying angle of inclinations i (taken from (Johansson, 2009))

Johansson (2009) argues that the geometry and strength of the intact rock of the asperity strongly influence the inclination angle at which different failure modes take place. This means that the horizontal line representing shear failure mode may increase or decrease depending on the strength of the asperity. Also he stated that the sliding over the asperities is the governing failure mode for full sized joints, and the average angle of the contacting asperities will be equal to the dilation angle, i, and therefore, for a full sized rock joint the friction angle at peak can be defined as the sum of the basic friction angle and the dilation angle.

The equation derived by Johansson (2009) to estimate the dilation angle for a full sized joints shows the influence of the roughness, the strength of the surface, the normal stress and increased scale. See appendix B for derivation of i_n.

$$i_n = \left(\theta^*_{max} - 10^{\frac{log\cdot\frac{\grave{\sigma_n}}{\sigma_{ci}} - log\cdot A_o}{C}} \cdot \theta^*_{max} \right) \cdot \left(\frac{L_n}{L_g} \right)^{kH-k} \tag{3.25}$$

Where θ^*_{max} is the maximum measured dip angle measured on the sample, A_o is the potential contact area, L_n is the length of the asperity to full sized joints, L_g is the length of the asperity to grain size scale, H is the Hurst exponent, k is an empirical constant ranging between 0-1, depending on the degree of matedness, $\grave{\sigma_n}$ is the effective normal stress, σ_{ci} is the uniaxial compressive strength and C is a roughness coefficient.

According to Johansson (2009), the conceptual behavior of the dilation angle can be seen in Figure 11.

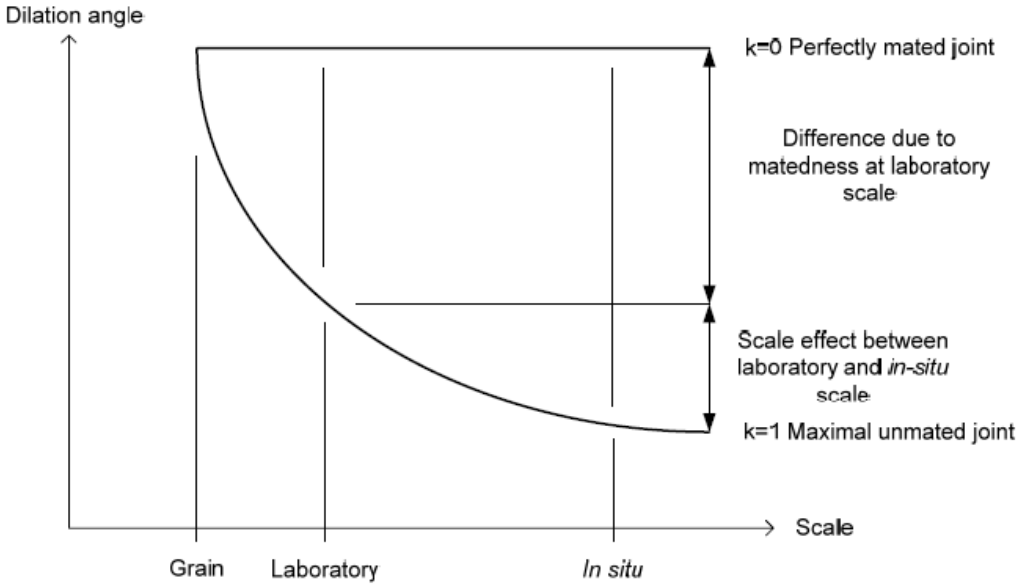

Figure 11. Conceptual behavior of the dilation angle at different scales and matedness (taken from (Johansson, 2009))

By substituting equation 3.25 into equation 3.22, the peak shear strength equation can be rewritten as:

$$\tau_p = \grave{\sigma_n} \cdot tan\left(\phi_b + \left(\theta^*_{max} - 10^{\frac{log\cdot\frac{\grave{\sigma_n}}{\sigma_{ci}} - log\cdot A_o}{C}} \cdot \theta^*_{max}\right) \cdot \left(\frac{L_n}{L_g}\right)^{kH-k}\right) \quad (3.26)$$

Where τ_p is the peak shear strength, $\grave{\sigma_n}$ is the effective normal stress, ϕ_b is the basic friction angle and i_n is the dilation angle for a full sized joint.

3.2.3 JRC models

A different approach to the problem of estimating the shear resistance of rough rock joints was proposed by Barton and Choubey (1977). The following empirical shear strength criterion was derived based on an extensive laboratory test program on natural rough joints:

$$\tau = \sigma_n \cdot tan\left(\phi_b + JRC \cdot log_{10}\left(\frac{JCS}{\sigma_n}\right)\right) \quad (3.27)$$

Where τ is the peak shear strength, σ_n is the effective normal stress, ϕ_b is the basic friction angle, JRC is joint roughness coefficient and JCS is the joint wall compressive strength.

Barton and Choubey suggested that the residual friction angle shall be used instead of the basic friction angle if the rock joint presented weathered. The following formula was proposed by Barton and Choubey (1977) to estimate the residual frictional angle by using the results from Schmidt rebound tests:

$$\phi_r = 10 + {}^{r}/_{R} \cdot (\phi_b - 10) \quad (3.28)$$

Where r is the rebound on weathered joint surface and R is the rebound on unweathered rock surface.

The JRC is an index that represents the roughness of the rock joint, this can be estimated by comparing the profile of the rough rock joint with a series of profiles provided by Barton and Choubey (1977) that are shown in figure 2. JRC index vary from a value of 0 to 20, where 0 represent a completely smooth surface, and 20 represents a very rough and ondulating surface.

Barton and Choubey (1977) suggested two different methods to determine the JRC parameter. Firstly, the JRC can be estimated by comparison of roughness with profiles given in figure 1. The alternative method is by back-analyzing the shear tests. According to Barton and Choubey (1977) the following equation can be used to express the JRC:

$$JRC = \frac{\arctan\left({}^{\tau}/_{\sigma_n}\right) - \phi_b}{log_{10} \cdot \left({}^{JCS}/_{\sigma_n}\right)} \quad (3.29)$$

Where ϕ_b is the basic friction angle, τ is the peak shear-strenght, σ_n is the normal effective stress and JCS is the joint compressive strength.

The estimation of JRC by visual comparison with the profiles provided in the Figure 12 has the limitation that is subjective. On the other hand, the back-analysis to determine JRC is not

very useful because the objective is to estimate the peak shear strength, not to determine JRC by knowing the test results before-hand.

According to Barton and Choubey (1977), JCS will be substituted by the compressive strength of the intact rock when the joint does not present weathering.

The following figure shows the roughness profile that are presented by Barton and Choubey (1977) and that are used to estimate the JRC parameter.

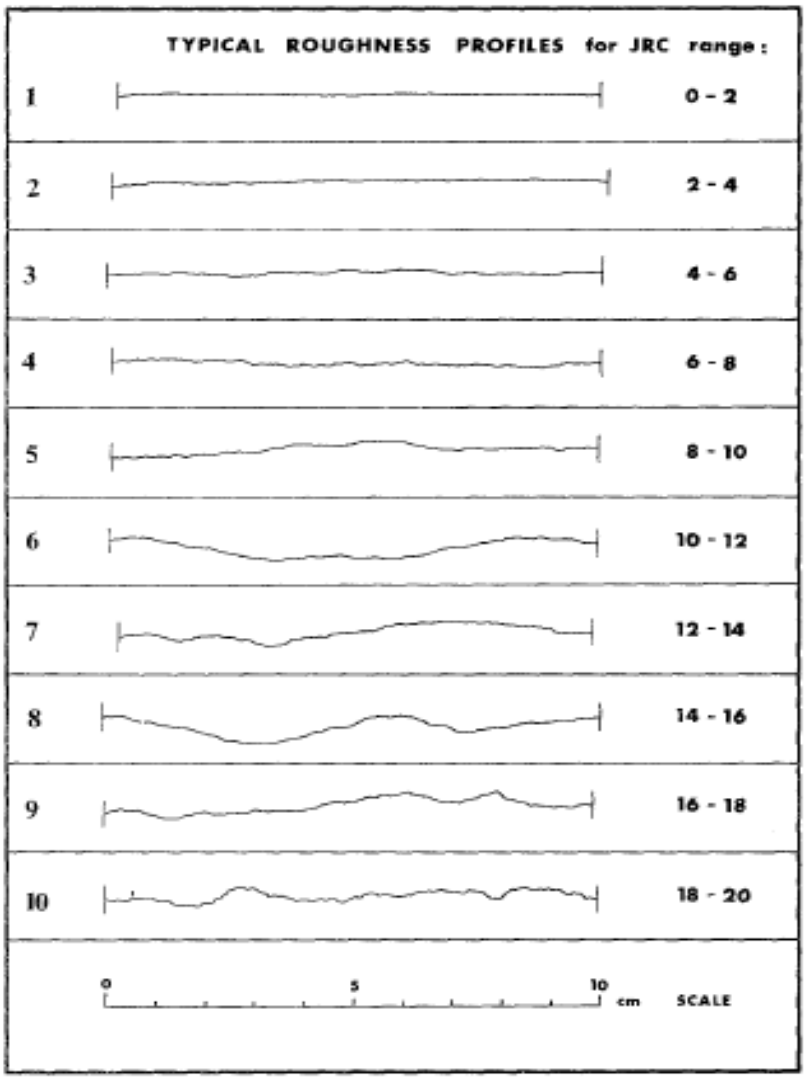

Figure 12. Standard profiles used for visual estimation of the parameter JRC (taken from (Barton and Choubeu. 1977))

Barton and Bandis (1982) proposed a modification of the peak shear strength given by Barton and Choubey in order to take into account the scale effects. The following equations were derived:

$$JCS_n = JCS_o \cdot \left(\frac{L_n}{L_o}\right)^{-0.03 \cdot JRC_o} \tag{3.30}$$

$$JRC_n = JRC_o \cdot \left(\frac{L_n}{L_o}\right)^{-0.02 \cdot JRC_o} \tag{3.31}$$

Where L_n is the length of the rock blocks along the joint being sheared, L_o is the length if the sample. The subscripts (o) and (n) means laboratory and *in situ* scale respectively.

$$\tau = \sigma_n \cdot tan\left(\phi_b + JRC_n \cdot log_{10}\left(\frac{JCS_n}{\sigma_n}\right)\right) \tag{3.32}$$

3.3 Previous results

The following chapter contains a review of different investigations carried out in order to estimate the shear resistance parameters, the cohesion and the friction angle. This section also presents a series of investigations conducted regarding the concrete-to-rock joints shear behavior. The objective it to increase the knowledge of the shear behavior of the rock-concrete interface and the influence that the roughness has into the shear strength and also to increase the knowledge on the condiction of direct shear tests.

3.3.1 Ruggeri G. (2004) ICOLD

In 2004 the ICOLD European working group published a report called "Sliding safety of existing gravity dams: Final Report". The objective of this work was to study the problem of the safety re-assessment against sliding for existing gravity dams. The report contains the following sections:

a) Overview of guidelines, standard practices and rules that are currently used when evaluating the sliding stability in concrete dams in different countries.
b) Use of specific site data to assess the safety against sliding stability including information about the data that can be found regarding the dam condition by using instrumental monitoring, surveys, inspections, in situ and laboratory tests.
c) Experiments regarding the behavior of the concrete lift joint and concrete-to-rock contact surface.
d) Application of numerical models to assess the sliding stability of concrete dams.

Since the aim of this thesis is to study the shear behavior of concrete-to-rock joints, only the results of the investigations regarding the shear strength of the concrete-to-rock interface will be described

3.3.1.1 Rocha M. (1964)

In-situ shear tests were carried out by Rocha M. in order to study the parameters that defined the shear strength of the concrete-to-rock interface at the dam foundation. The tests consisted of casting on the rock concrete blocks with dimensions 70x70x35 cm. The tests took place in six different dam sites. The table 12 shows the results from the in-situ shear tests:

Rock-type dam	*Number of tests*	*Cohesion (MPa)*	*Angle of friction (º)*	*Coefficient of friction (tan ϕ)*
Granite/Alto Rabagao	8	0.2	56	1.5
Shale/Bemposta	8	0.2	60-63	1.7-1.9
Shale/Valdecañas	3	0.4	62	1.9
Shale/Miranda	16	0.4-0.7	60-62	1.7-1.9
Shale/Alcantara	28	0.1	56	1.5
Sandstone/Cambambe	4	0.2	53	1.3

Table 12. Results from the in-situ shear tests conducted (taken from (Rocha M. , 1964))

The results show that the friction angle decrease as the weathering of the rock increases (Rocha M. 1964). The cohesion values vary in a range of 0.1-0.7 MPa while the friction angle values are in the range of 53-63º.

3.3.2.2 Lo et. Al (1991-1990)

During the years 1991-1994 several investigations were done by Lo, K.Y. et. Al regarding the shear strength parameters for both bonded and un-bonded concrete-to-rock interfaces and the results are presented in the following reports:

1. *"Evaluation of strength parameters of concrete-rock interface for dam safety assessment"*, Canadian Dam Safety Conference, Toronto, 1990.

2. *"The evaluation of stability of existing concrete dams on rock foundations and remedial measures",* 17th ICOLD Congress, 1991

3. *"Recent experiences with safety assessment of concrete dams on rock foundation"*, Canadian Dam Safety Confer

This research was done as a part of the 10-year program of assessment of safety of dams started by Ontario Hydro. Samples were obtained by drilling bore-holes at the dam site and cores from the concrete-to-rock interface were recovered. With these samples, a series of shear tests were carried out both for bonded and unbounded specimens. The results reported were as follows:

Peak shear strength:

- $\varphi = 62º\ ;\ c = 2.2\ MPa$

Residual shear strength:

- $\varphi = 32 - 39\ º$

3.3.2.3 EPRI (1992)

Investigation that aimed to study the shear strength parameters (friction angle and cohesion) was carried out by the Electric Power Research Institute (EPRI). Data of shear strength of concrete-to-rock interfaces were obtained for eighteen different dams. The study included 2 large scale in-situ tests. The number of samples tested was sixty-five, evaluating both peak and residual shear strength. Samples are considered bonded if they are intact and unbounded if they are broken. The results for peak and residual shear strength are presented in tables 13 and 14 respectively.

Peak Strenght	**Best fit lines**	**Lower bound lines**
Friction angle	54-68º	53-68º
Cohesion for most rock types (Mpa)	1.3-1.9 (average:1.7)	0.3-1.1 (average:0.6)
Cohesion for shale (MPa)	0.1 MPa	0 MPa

Table 13. Peak shear strength obatined (taken from (Ruggeri, 2004))

Residual Strenght	**Best fit lines**	**Lower bound lines**
Friction angle	24-39º	13-32º
Cohesion (Mpa)	0-0.2 (average:0.1)	0

Table 14. Residual shear strength obtained (taken from (Ruggeri, 2004))

3.3.3 Ghosh, A.K. (2010)

In-situ shear tests were performed in order to estimate the shear strength parameters (the friction angle and the cohesion) of the rock-concrete interface at the dam foundation. The tests were carried out at the Upper Tunga Dam, at the river Tunga in southern India. A total of 6 blocks 700x600x600 mm were casted on the foundation rock mass at the downstream part of the spillway. The rock mass in contact with the concrete was found to be a good quality granite with some schistose areas. Figures 13 and 14 show the set-up for one of the locations of the tests and the forces acting during the test, respectively.

Figure 13. Complete test setup at one of the locations (taken from (Ghosh, 2010))

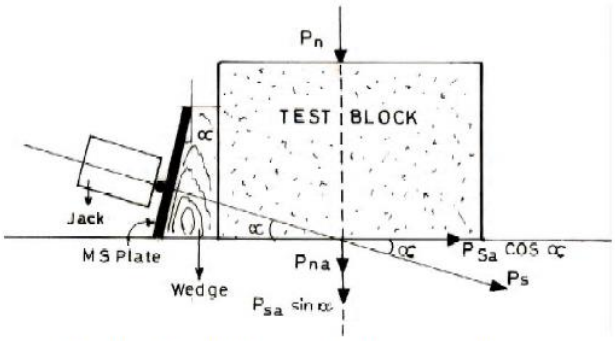

Figure 14. Forces applied in the test (taken from (Ghosh, 2010))

The Figure 15 shows the results from the in-situ shear tests. The peak shear strength was found to be a value between 50-60 MPa. The friction angle found was 59º and the cohesion 10 MPa.

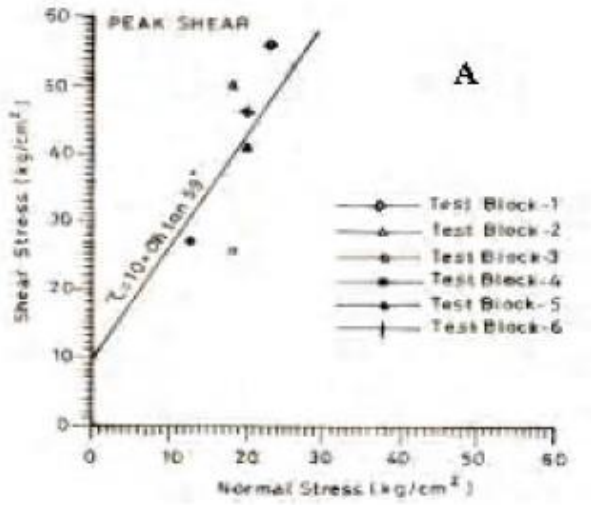

Figure 15. Peak shear strength envelop (taken from (Ghosh, 2010))

3.3.4 Xue F. Gu et. Al (2003)

The aim of this paper was to study the shear behavior of the contact surface between the concrete pile and the surrounding rock in the rock socketed piles. In order to be able to simulate the constant normal stiffness condition of the piles socketed in rock (see Figure 16), the laboratory tests were conducted under constant normal stiffness (CNS).

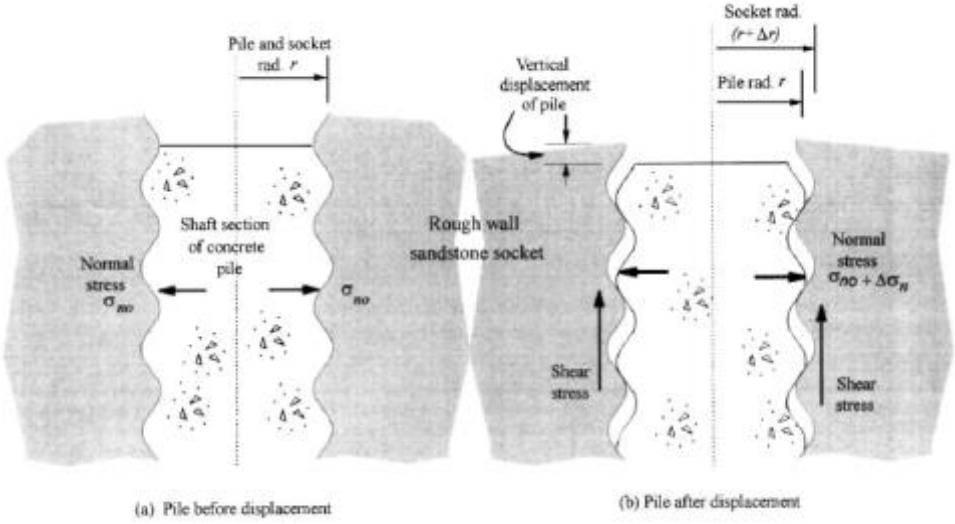

Figure 16. Constant normal stiffness condition (taken from (Xue F. Gu et Al, 2003))

To model the contact surface between the pile and the rock two half specimens with a predefined roughness have been used. (See Figure 17). Since the shear strength of the socketed piles is strongly influenced by the roughness of the concrete-to-rock interface, the main goal of the test program was to increase the understanding of the roughness influence on shear behavior.

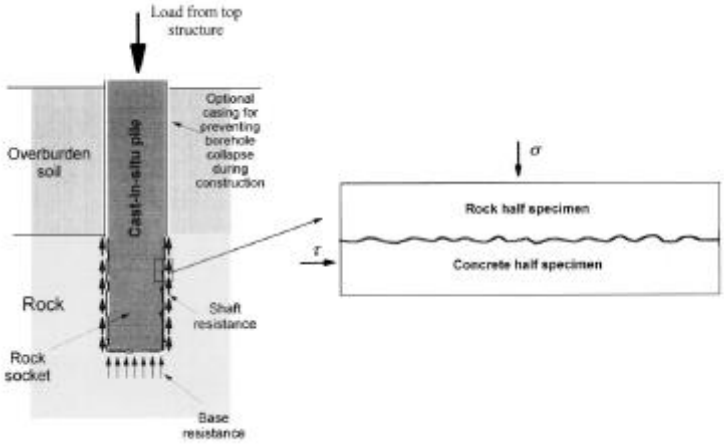

Figure 17. Laboratory model of socket interface (taken from (Xue F. Gu et Al, 2003))

Samples consisted of 2 halves, the rock half (sandstone) was given the required roughness by using water-jet cutting. A sample after the use of water-jet cutting is shown in Figure 19a. The other half of the sample, the concrete, was casted onto the pre-prepared sandstone surface. To prevent bonding, a thin film of food-wrap was placed on the sandstone surface before the concrete casting. The Figure 19b shows a sample ready to be tested. Five profiles with triangle asperities with an angle ranging from 5º to 10º were used and four fractal profiles with mean angle asperities ranging from 5º to 15º (See Figure 18).

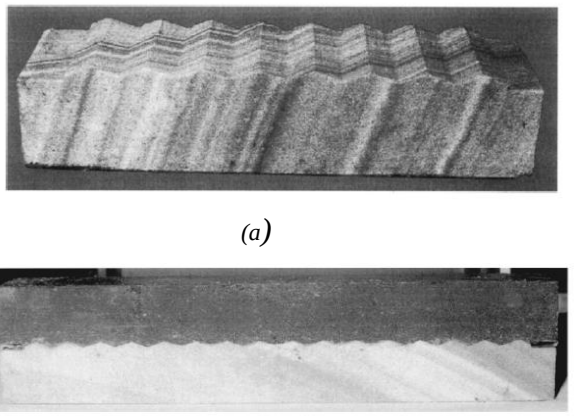

(a)

(b)

Figure 18, (a) Water-jet cut samples with regular profiles; (b) Sample ready for testing (taken from (Xue F. Gu et Al, 2003))

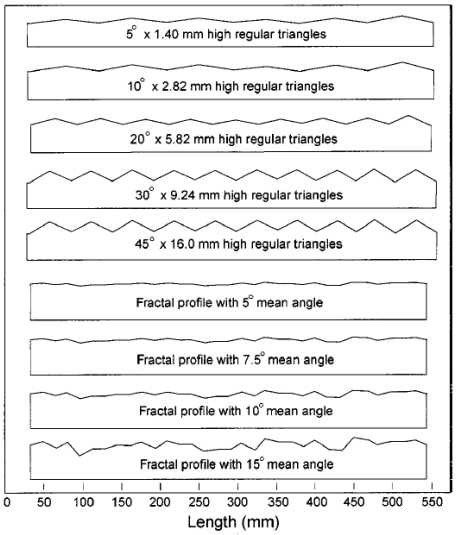

Figure 19. Roughness profiles

A total of 112 direct shear tests were carried out comprising regular triangular asperity and fractal profiles under constant normal stiffness (CNS) and under constant normal load (CNL). Each sample was tested for three different normal loads, 200 KPa, 400 KPa, and 800 KPa and for values of 600 KPa/mm, 800 KPa/mm, 1600 KPa/mm and 3200 KPa/mm. Some of the results are shown in Figure 20.

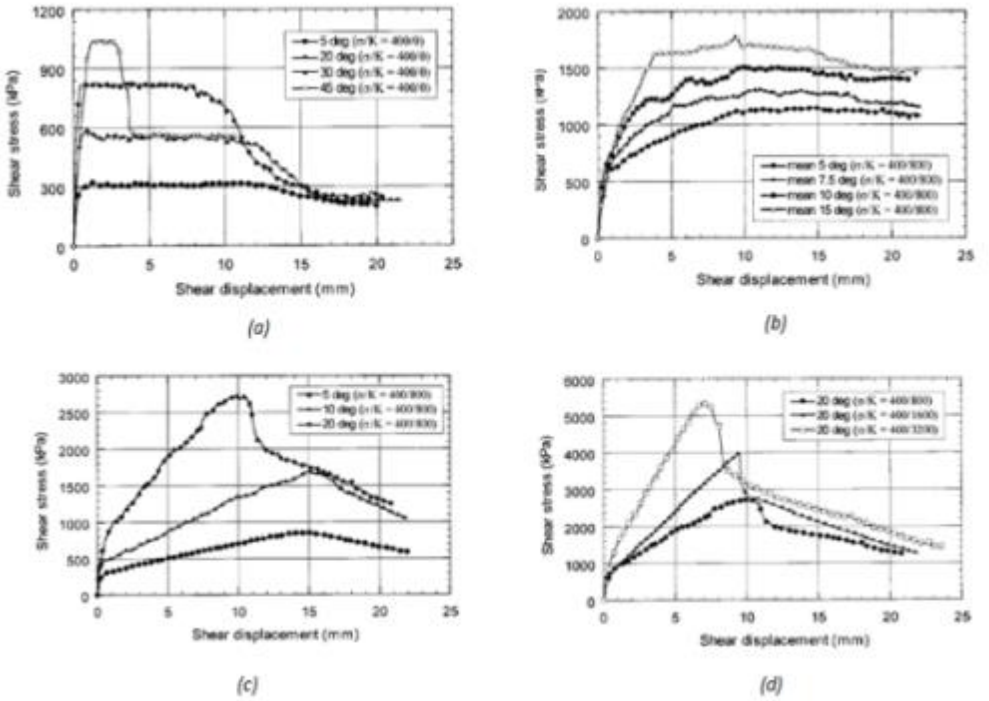

Figure 20. (a) Shear responses for 5, 20, 30 and 45 regular asperity profiles under σ=400 kPa, K=0 kPa/mm; (b) Shear response for different mean angle of fractal profile under σ=400 kPa, K=800, 1600 and 3200 kPa/mm; (c) Shear responses for 5, 10 and 20 regular asperity profiles under σ=400 kPa, K=800 kPa/mm ; (d)) Shear response for 20 asperity profile under σ=400 kPa, K=800, 1600 and 3200 kPa/mm (taken from (Xu F. Gu et Al, 2003))

The wear of the sandstone asperities was also studied and a video was recorded to analyze how the aspetity was weared during the tests. Figure 21 shows a video still of the tests when the horizontal displacement was 11 mm.

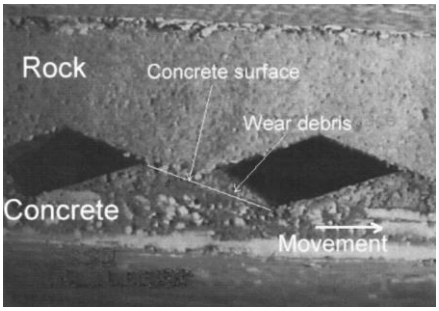

Figure 21. Video still of direct shear test at 11 mm of shear displacement (taken from (Xue F. Gu et Al, 2003))

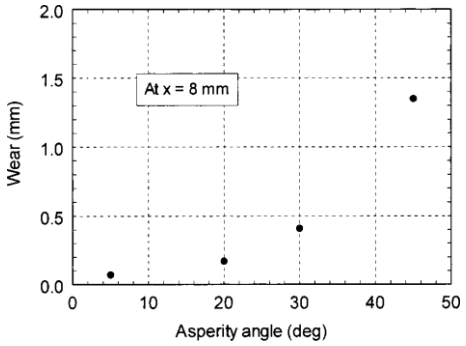

Figure 22. Wear at 8 mm shear displacement with different asperity angles (taken from (Xue F. Gu et Al, 2003))

Photographs from one single asperity were taken before and after the test in order to show the evolution of the wear during the test. Figure 23 shows a digitized asperity profile where it can be seen that the wear of the asperity surface during the shear test is evident.

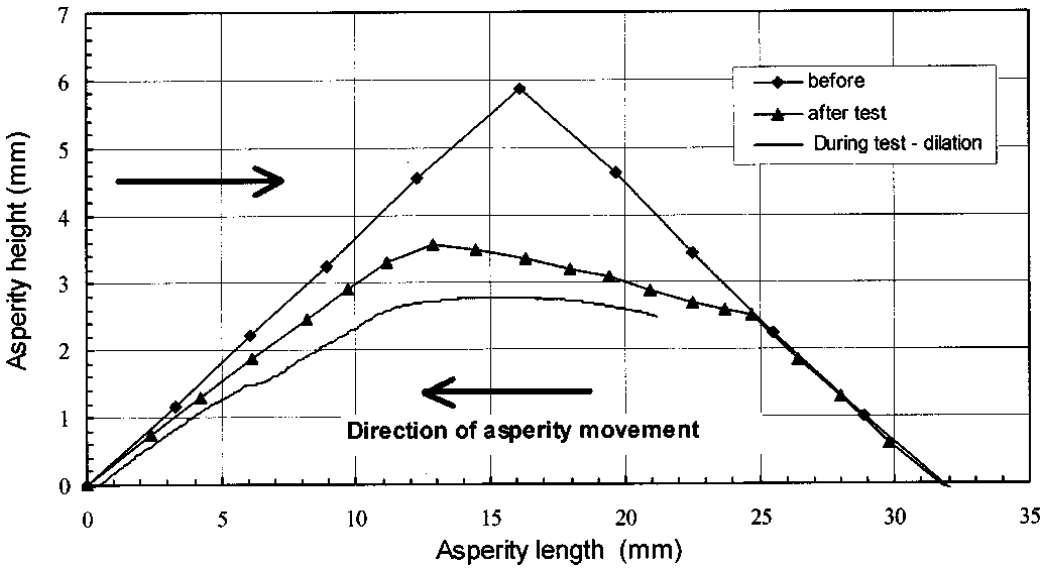

Figure 23. Digitized surface profiles from before and after testing (taken from (Xue F. Gu et Al, 2003))

According to Xue F. Gu et. Al (2003) the following conclusions were made:

- Roughness of the sandstone-concrete joints has a strong influence on the shear behavior. As the interface roughness increases, the peak shear strength increases as well, and the shear response will become more brittle.
- The peak shear strength is influenced by the normal stiffness, by increasing the normal stiffness, higher values of peak shear strength are obtained. The shear response is more brittle as the normal stiffness is increased.
- The peak shear strength also increases as the normal stress is increased. Again, the shear response becomes more brittle for higher values of normal stress.
- Fractal profiles present a more ductile behavior than the regular asperity profiles.
- Wear of the sandstone-concrete joint occurred during sliding. The amount of wear increases with the asperity angle and the shear resistance decreases due to wear.
- Wear of the sandstone-concrete joint is also dependent of the stress boundary conditions (CNL or CNS).

3.3.5 Reena Negi (2012)

During his M.Sc. Thesis Reena Negi studied the influence of the asperity profile and the normal stress on the shear behavior of artificial regular rock joints. Samples were made of Plaster of Paris and the joints were given a profile with regular triangle asperities. Two different set of samples were tested, the first a profile made by asperities with an angle of 15º and the second one with an angle of asperities of 30º (Se figure 24). The dimensions of the samples were 60x60x25 (mm)..

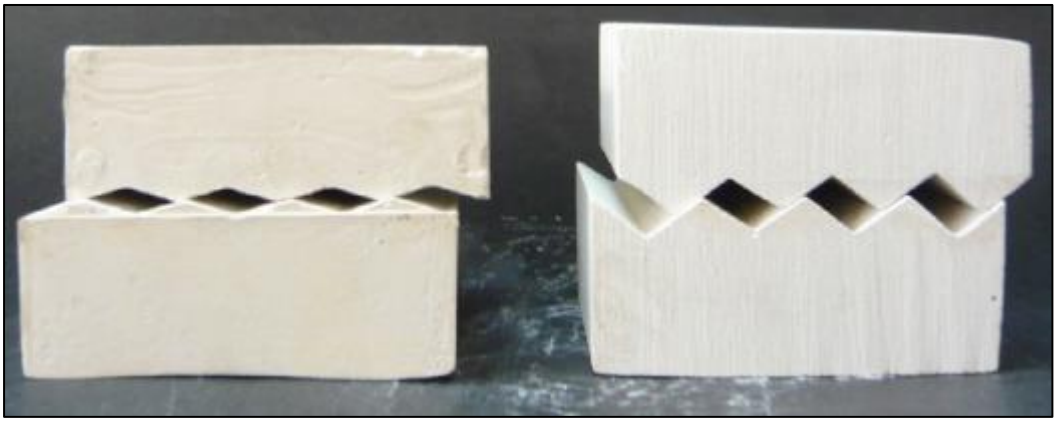

Figure 24. Specimens tested with 15 asperity profile and 30 asperity profile (taken from Negi R. (,2012))

Direct shear tests under constant load conditions were conducted. Each sample was tested under five different normal load; 0.05 MPa, 0.1 MPa, 0.20 MPa, 0.25 MPa and 0.5 MPa. The results are shown in figures 25 and 26. Figure 1 and 2 shows the shear stress-shear displacement curves for different normal loads and for the 15º asperity angle profile and for the 30º asperity angle profile, respectively.

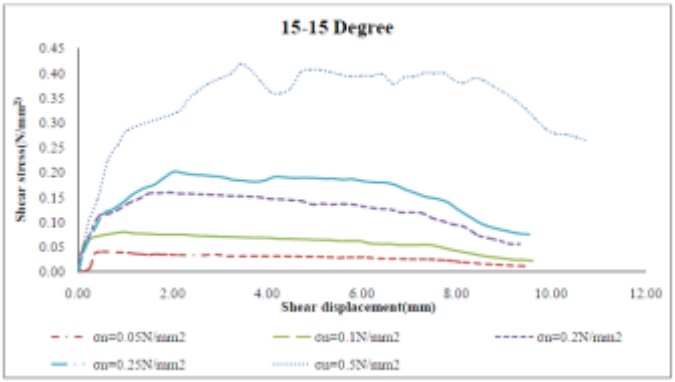

Figure 25. Shear stress response for 15 asperity profile (taken from (Negi R. 2012))

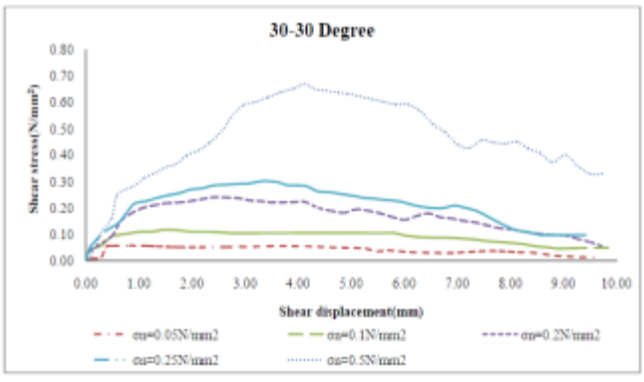

Figure 26. Shear stress response for 30 asperity profile (taken from (Negi R. 2012))

The results show that for the 15º asperity angle profile, the peak shear strength obtained was $\tau_p = 0.418\ MPa$ for a normal stress of $\sigma_n = 0.5\ MPa$ and a shear displacement at peak of 3.45 mm.. For the 30º asperity angle profile, the peak shear strength was $\tau_p = 0.669\ MPa$ for a normal stress of $\sigma_n = 0.5\ MPa$. The failure envelope for both the 30º asperity profile and the 15º asperity profile is shown in Figure 27.

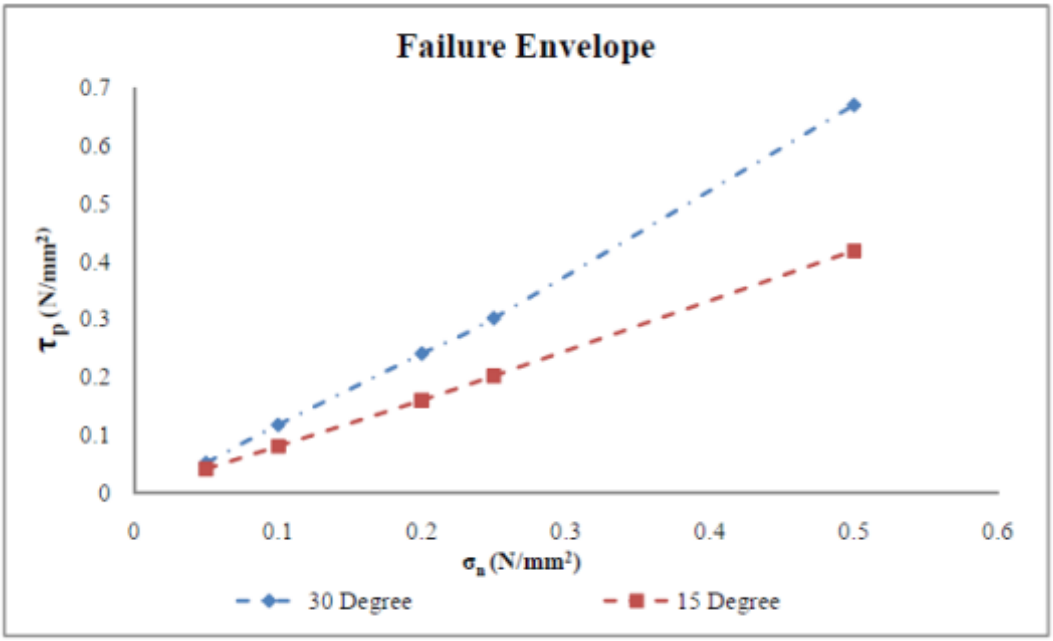

Figure 27. Failure envelopes for the specimen with 15 and 30 asperity profile (taken from (Negi R. 2012))

Negi R. (2012) made the following conclusions out of the results:

- Peak dilation angle decrease as the normal load applied increases; Reena Negi (2012) pointed out that the reason of the resistance provided by the normal load against the dilation.
- Peak shear stress increases when the normal load is increased.
- Peak dilation angle increases with the asperity angle for the same normal load.
- Peak shear stress increases when the angle of asperity increases. According to Negi R. (2012), this is because of the larger surface area of discontinuity in the asperity of 30º than in the asperity of 15º.
- Peak shear displacement increases with an increase in the asperity angle.

3.3.6 Kodikara and Johnston (1993)

In order to study the shear behavior of rough concrete-to-rock joints, Kodikara and Johnston (1993) conducted a series of direct shear tests. To simulate the roughness, the interface was prepared with both regular and irregular asperities triangles. The tests were carried put both under constant normal stiffness condition (CNS) and constant normal load condition (CNL). The material selected for the tests was a synthetic soft rock known as Johnstone. The concrete specimens were manufactured by casting micro-concrete over the rock specimen. Seven triangular profiles were tested, 2 regular (every asperity in the surface with the same inclination angle) and 5 irregular. The asperity angles for the regular profiles were 12.5º and 22.5º and for the irregular profile contained variations of those angles of $\pm$2.5º, $\pm$5º, and $\pm$7.5º (see Figure 28). The width and the height of the specimens were 71 mm and 80 mm, respectively. The length varied depending on the length required to accommodate the asperities.

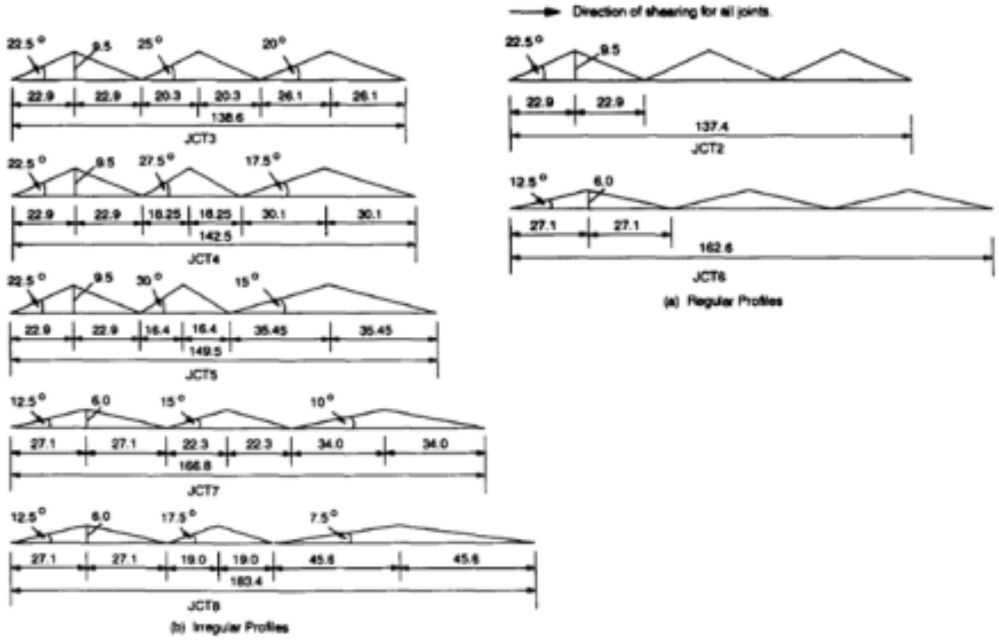

Figure 28. Joint profiles used in the direct shear tests (taken from (Kodikara and Johnston, 1993))

The principle of the test technique is described in figure 29 and an assembled concrete-to-rock joint is shown in figure 30.

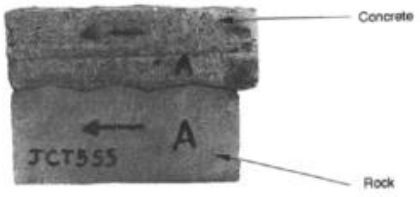

Figure 29. Typical rock and concrete components of a joint (taken from (Kodikara and Johnston, 1993))

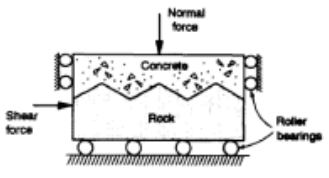

Fig. 4. Principle of test technique.

Figure 30. Principle of the test technique (taken from (Kodikara and Johnston, 1993))

Both CNL and CNS conditions were used to tests the specimens. 54 tests were carried out; 44 under constant normal stiffness and 9 under constant normal load conditions. The range of normal stiffness and loads used during the testing was:

- Normal Stiffness: 0-960 kPa/mm
- Normal stresses: 0.135-0.6 MPa

Some of the results obtained are shown below:

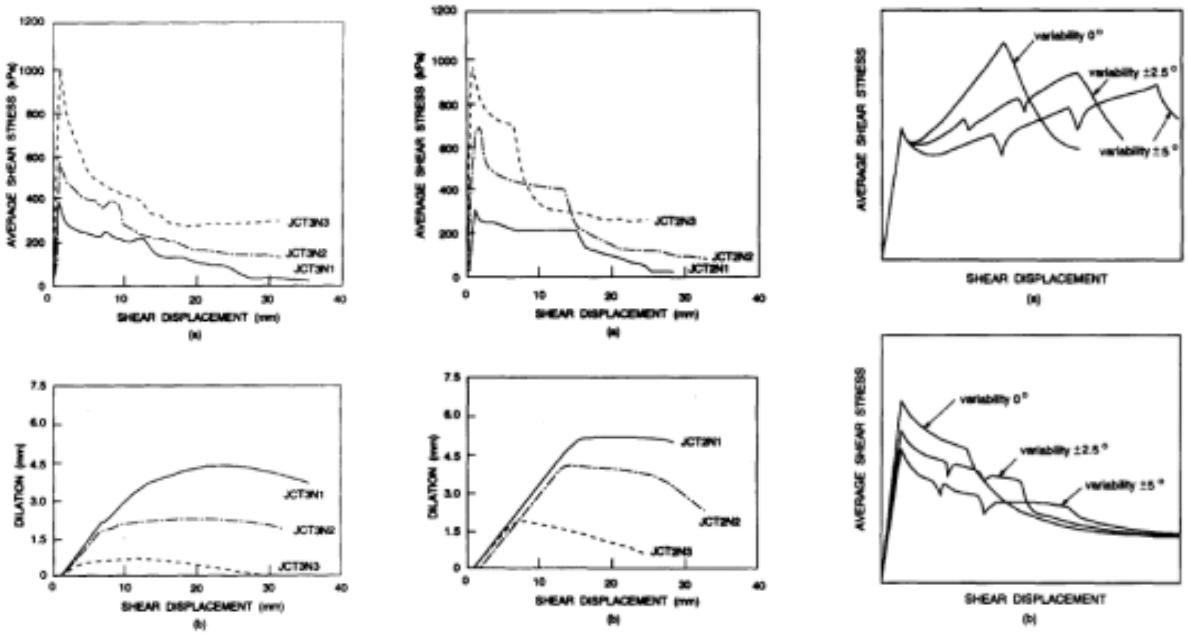

Figure 31. Results obtained from the shear tests (taken from (Kodikara and Johnston, 1993))

The following conclusions were made by Kodikara and Johnstone (1993):

- Test under CNS presented a significant work strengthening response after initial sliding.
- For the test under CNL the peak shear resistance was obtained when sliding occurred and therefore the work strengthening that occurred during CNS tests was absent.
- The influence of roughness variations was mainly that the regular profiles showed a relatively brittle response with a high shear resistance at a small shear displacement and on the other hand, the irregular were more ductile with a lower peak shear stress and occurred at a larger shear displacement (in the CNS case).

3.3.7 Indraratna et Al (1997)

In order to investigate the shear behavior of a regular saw tooth rock joints under constant normal stiffness conditions (CNS) a series of direct shear tests were conducted by Indraratna et Al (1997). One of the goals of this research was also to compare the results of the tests carried out under constant normal load (CNL) with the results from the CNS tests.

According to Indraratna et Al (1997), the direct shear tests under CNL condition can estimate realistically the shear strength of planar interfaces where the normal load applied remains constant, as in the case of rock slope stability problems. However, for situations where the normal stress in the field varies and dilation is constrained during the shearing, the CNL conditions will lead to underestimated shear resistance values of the joint.

In order to study the shear resistance of soft rock joints under CNS, direct shear tests were carried out. The apparatus used for the tests was able to perform both tests under CNS and CNL. To simulate the constant normal stiffness of the rock mass surrounding the joint an assembly of springs of known stiffness (k=8.5 kN/mm) was used. The tests were conducted both under CNL and CNS conditons and the normal load tested were 0.16, 0.30, 0.56, 1.10, 1.63 and 2.43 MPa.

The interface profiles were given a regular triangular asperities shape with different asperity angles (9.5º, 18.5º and 26.5º) as it can be seen in figure 32.

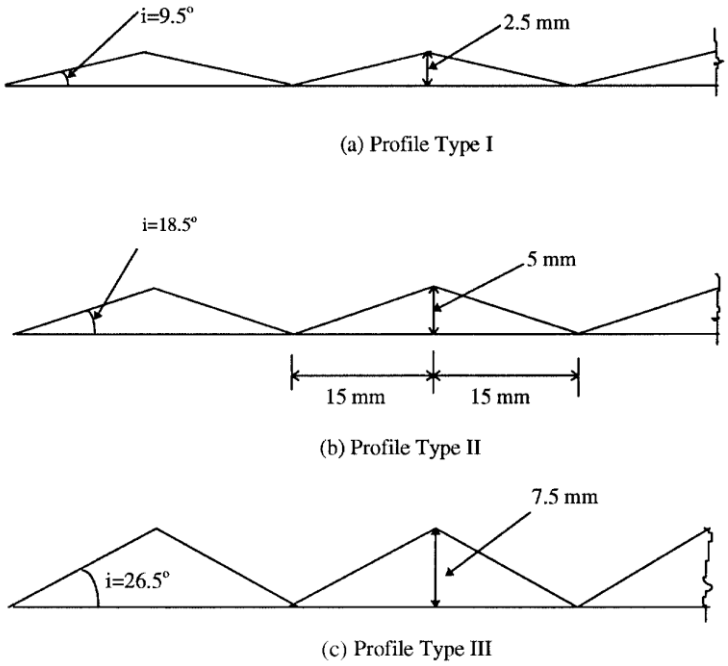

Figure 32. Asperity profiles tested (taken from (Indraratna et Al, 1997))

The figure 33 shows the shear stress response for different normal stresses applied and for both CNL and CNS. It can be seen that in all the cases the CNL underestimates the shear

capacity of the rock joint. Therefore, the CNS results would lead to more economical design in jointed rock masses (Indraratna, 1997).

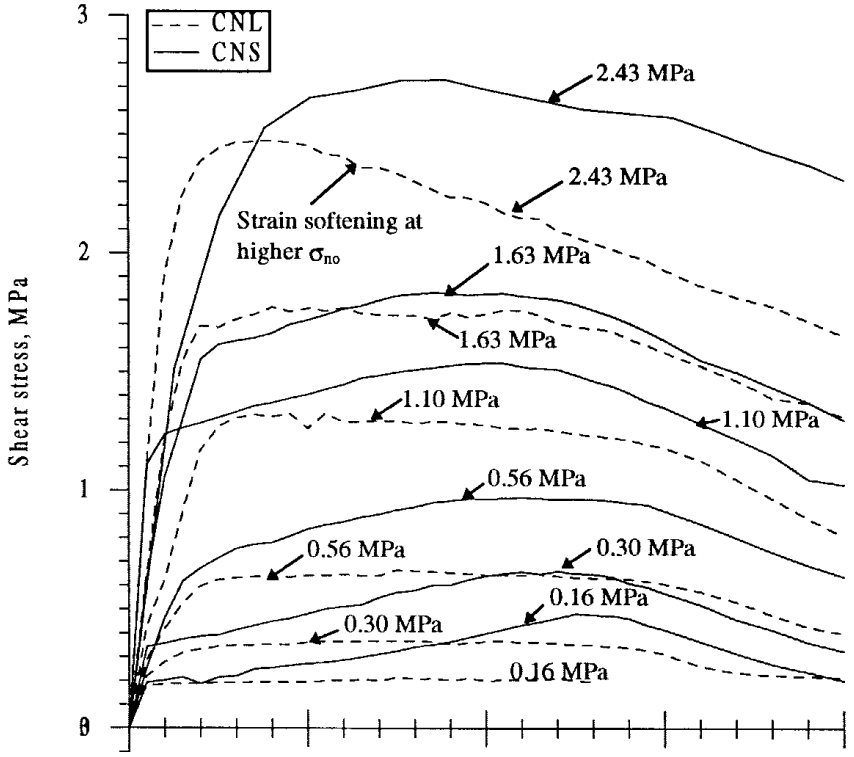

Figure 33. Variation of shear stress and normal stress with horizontal displacment for 9.5 asperity profile (taken from (Indraratna et Al, 1997))

13.4 Summary

The shear capacity between the dam and the rock foundations is the most important factor that affects the sliding stability of concrete dams. Nowadays, this shear resistance is determined by the Mohr-Coulomb model, which does not account the roughness of the joint. Many different authors have tried to introduce the effect of the joint roughness into the shear capacity but they seem to rely too much in empirical parameters and therefore are difficult to implement in the guidelines and regulations. The models to estimate the peak shear strength that have been studied within this chapter are based on the same thing, according to Johansson (2009) they are based on the assumption that the total friction angle can be divided in two components, the first part is set to constant and depends on the rock type. The second part is depending on the surface roughness and it is a function of the surface roughness, the strength of the joint, the normal stress and the scale.

Therefore, according to Johansson (2009) the shear strength of a rough rock joint is depending on the following parameters:

- Normal stress
- Uniaxial compressive strength of the joint
- Roughness
- Scale
- Rock type

The model derived by Patton, which is basically the Mohr-Coulomb model but applied in the direction of the angle that the asperity forms with the horizontal, describes pretty well the shear behavior when sliding is the failure mechanism occurring but when the angle of asperities increases and its implementation in the guidelines is not easy as the natural rock joints are not perfectly triangular and they present many irregularities.

Maksimovic (1997) and Layandi & Archambault (1970) proposed models to estimate peak shear strength incorporating the influence of the rock joint roughness where they tried to correct the limitation of the model proposed by Patton (1966).

Barton and Choubey also developed a model to incorporate the roughness effect into the shear resistance but it seems to be too subjective because one has to decide the JRC parameter by visual comparison with the real rock joint.

In order to study the scale effects on the shear strength of rock joints, Barton and Bandis (1982) proposed a modification of the Barton and Choubey (1977) failure criterion. Johansson F. (2009) also proposed a model to incorporate the scale effect on the shear strength of unfilled rock joints, but the estimation of the parameters needed to implement this model seems to be very difficult and this it is not easy to implement in the guidelines.

Due to the new technologies, some authors have developed models based on the three-dimensional characterization of the surface. For example, Graselli (2001) and Cai-Chu Xia et.

Al (2013). These methods have the inconvenient that to measure the surface roughness it is need equipment that is very expensive.

The literature study on previous results shows that the roughness strongly influences the shear resistance of a concrete-to-rock joint. For example, Kodikara and Johnston (1993), Negi R. (2012), or Xue F. Gu et Al (2003), proved through direct shear tests that an increase of the angle of the asperities of the surface leads to an increase in the shear strength of the joint.

As the literature study shows, many different models have been proposed in order to estimate the peak shear strength of rock joints and concrete-to-rock joint (which is the case that we are studying) but the major drawbacks of these models are that they rely too much in empirical parameters and sometime it is difficult and expensive to estimate those parameters. Therefore, there is a need of a model capable to include the effect of the roughness into the shear strength of concrete-to-rock joints in order to implement it in the guidelines.

4. DIRECT SHEAR TESTS AT LTU.

4.1 Introduction

A series of direct shear tests was decided to be implemented in this thesis. The laboratory tests were carried out at Luleå University of Technology (LTU) at the COMPLAB, which is the largest laboratory at LTU. The reason because of which this laboratory was chosen is that a direct shear test apparatus is located which was used to perform rock-concrete direct shear test during Simen Liahagen thesis in 2012, and the tests that were carried out in this thesis are very similar to the Liahagen´s tests performed in last year.

In this chapter, a review of the tests carried out by Liahagen (2012) is presented and a presentation of the direct shear tests conducted within this thesis along with the discussion of the results.

4.2 Review of 2012 direct shear tests at LTU

4.2.1 Introduction

A series of direct shear tests were carried out by Simen Liahagen during his M.Sc. Thesis in 2012. These laboratory tests took place at Lulea University of Technology. The goal of this chapter is not only to introduce and show the results of the Simen Liahagen´s work during his thesis but also to analyze the results from last year´s tests. First of all a description of the tests conducted in 2012 at LTU are described, then the results from the tests are analyzed and discussed, next the tests results are tested into commonly used methods to estimate the shear resistance to see how they match or how they differ. Next, a comparison between the results and the NVE regulations is carry out and finally a model to estimate the peak shear stress for concrete-to-rock joints with triangular asperity profiles based on these tests is presented.

4.2.2 Test description

In total 12 shear tests were conducted under constant normal load condition (CNL). The rock type used for the tests was granite with a compressive strength of approximately 260 MPa. In order to study the influence of the roughness in the shear capacity, the surface profiles of the specimens was artificially manipulated with triangular asperities; each asperity had the same geometry over the whole surface. Four different types of profiles were tested, each profile corresponding to a different inclination angle of the asperities; the asperity angles selected were 0º, 10º, 20º and 40º (See Figure 34). The rock specimens had dimensions of 240x240 mm and a height of 130m, without counting the asperities height which varied depending on the angle of asperity. The height of the asperities was 16.8, 7.3 and 3.5 mm for the 40º, 20º and 10º asperity angle, respectively. 100-110 mm was casted on the rock specimens, the

concrete used was B35. Ten samples were casted by placing an adhesive plastic on the rock surface and two of them were casted without the adhesive plastic, this was done to test some samples with bonding and without bonding (See figure 35).

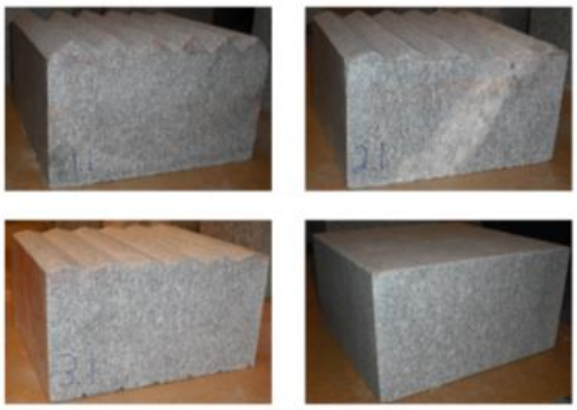

Figure 34. Surface profile tested (40, 20, 10 and 0) (taken from (Liahagen, 2012))

Figure 35. Formwork removed from rock sample and plastic wrap being removed (taken from (Liahagen, 2012))

Once the specimen was placed in the shear box, in order to measure the vertical displacement of the specimen, four LVDTs (Linear variable differential transformers) were glued to the specimen (See Figure 36). The shear rate selected for the tests was 0.5 mm/min. To study the influence of the normal load on the shear capacity, three normal load levels were used; 0.4 Mpa, 0.8 Mpa and 1.2 Mpa.

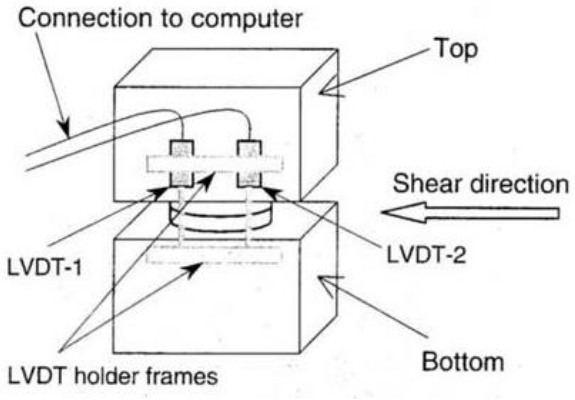

Figure 36. Location and setup for the LVDTs (taken from (Johansson, 2009))

Figure 37. Specimen ready for testing (taken from (Liahagen, 2012))

Figure 38. LVDTs glued to the specimens (taken from (Liahagen, 2012))

4.2.3 Results

The results of the direct shear test are shown in the table 15 below. The table shows normal stressσ_n, peak shear stress, "τ_{max}", shear displacement at peak, δ_P, maximum friction angle, ϕ_{max} and the horizontal maximum displacement.

Test	i [°]	N [kN]	V [kN]	δ_P [mm]	σ_n [MPa]	τ_{max} [MPa]	ϕ_{max} [°]	δ_{Hmax} [mm]	Comments
1.1	40	27.52	90.53	4.00	0.48	1.57	73.08	15.23	
1.2	40	46.91	131.19	3.03	0.81	2.28	70.32	15.44	
1.3	40	72.47	299.17	3.58	1.26	5.20	76.41	5.07	bonded
1.4	40	68.49	183.42	1.44	1.19	3.18	69.52	26.34	
2.1	20	27.57	50.74	6.39	0.48	0.88	61.48	24.99	
2.2	20	47.77	100.59	2.86	0.83	1.75	64.60	21.98	
2.3	20	68.36	162.83	2.30	1.19	2.83	67.23	20.07	
3.1	10	24.82	35.38	9.78	0.43	0.61	54.95	33.16	
3.2	10	45.98	58.70	6.55	0.80	1.02	51.93	32.94	
3.3	10	67.65	85.43	2.83	1.17	1.48	51.63	33.23	
4.1	0	67.85	240.00	2.49	1.18	4.17	74.24	14.59	bonded
4.2	0	67.23	52.04	33.23	1.17	0.90	37.74	33.23	

Table 15. Results from the direct shear tests conducted by Simen Liahagen at LTU in 2012

The following figures show the results for each test carried out, three curves are presented for each series of test: shear stress-shear displacement (τ-x), normal stress-shear displacement (σ-x) and friction angle-shear displacement (θ-x). Note that friction angle values are plotted on the secondary vertical axis. The results of each series of tests are presented.

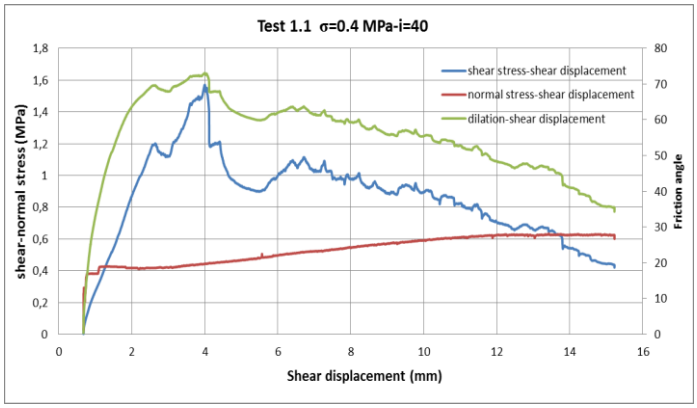

(a)

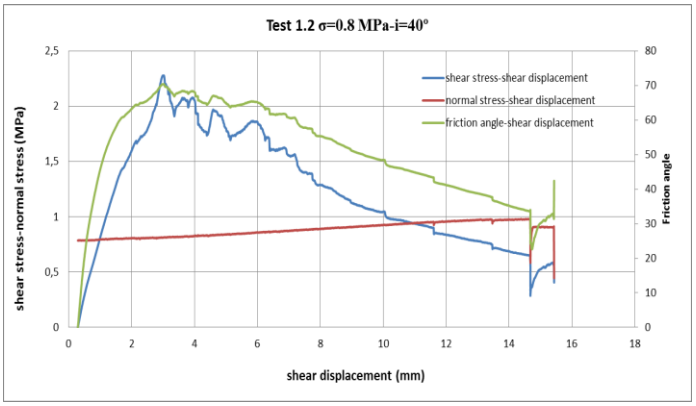

(b)

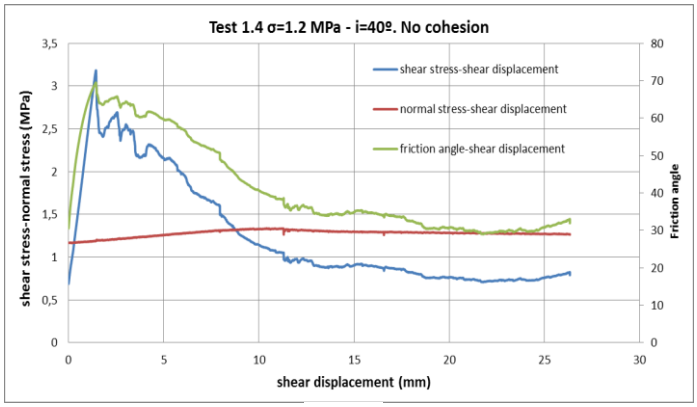

(c)

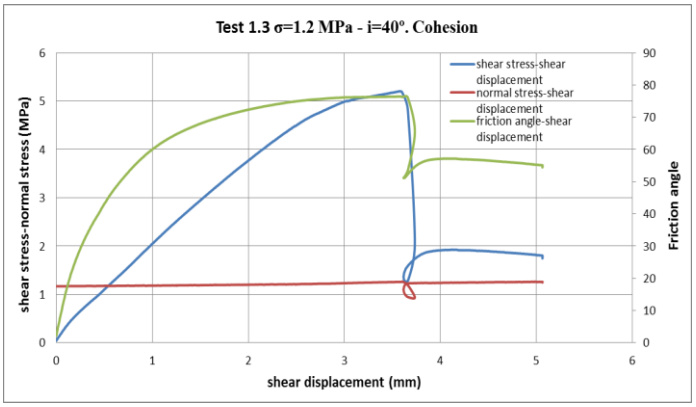

(d)

Figure 39. (a) Results from the tests with 40º asperity profile and a normal stress of 0.4 MPa. (b) Results from the tests with 40º asperity profile and a normal stress of 0.8 MPa. (c) Results from the tests with 40 asperity profile and a normal stress of 1.2 MPa. (d) Results from the tests with 40º asperity profile and a normal stress of 1.2 MPa with cohesion.

The figure 39a shows the direct shear test with a normal pressure of 0.4 MPa and the angle of asperities is 40 degrees. The figure shows 39 three curves, the green one is the variation of the friction angle over the shear displacement, the red one shows the variation of the normal stress with the shear displacement and the green curve represents the variation of the friction angle over the shear displacement. The figures 39.a and 39.b shows the same results but in this case for different normal stress applied (0.8 and 1.2 MPa respectively), and the figure 39.d represents the same test than the test 1.3 (figure 39.c) but in this case the cohesion was considered.

The figure 40 show the results for the tests 2.1, 2.2, 2.3 where the angle of asperities in the rock-concrete interface was 20 degrees. Figure 40.a is showing the results for a normal stress

applied of 0.4 MPa, Figure 40.b is showing the results for a normal stress applied of 0.8 MPa and Figure 40.c is showing the results for a normal stress applied of 1.2 MPa.

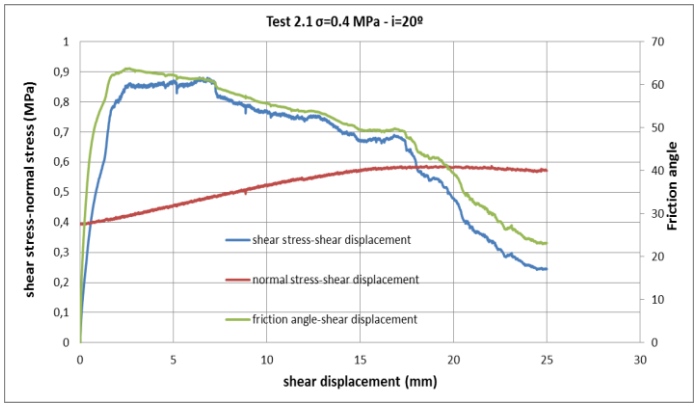

(a)

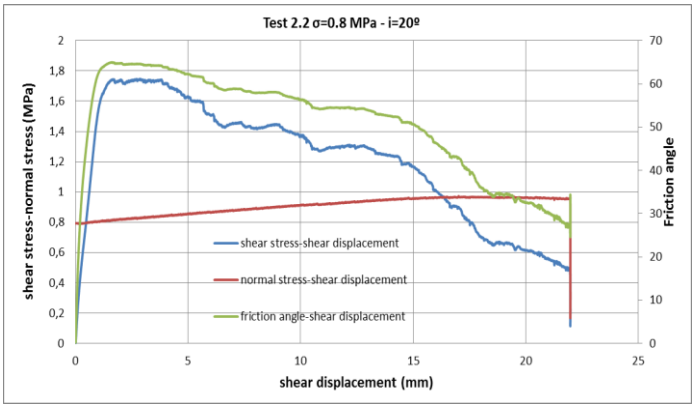

(b)

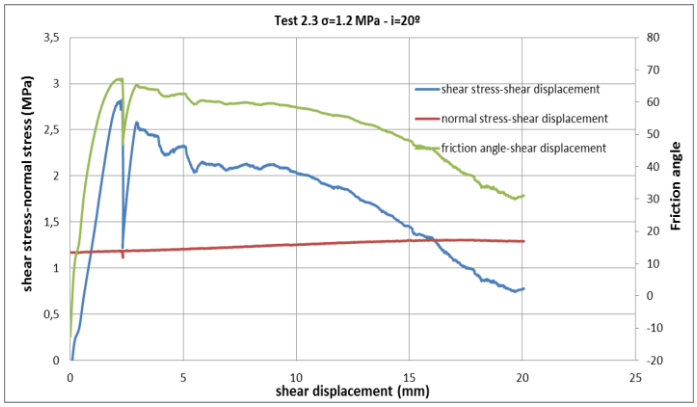

(c)

Figure 40. (a) Results from the tests with 20º asperity profile and a normal stress of 0.4 MPa. (b) Results from the tests with 20º asperity profile and a normal stress of 0.8 MPa. (c) Results from the tests with 20º asperity profile and a normal stress of 1.2 MPa.

The figure 41 shows the results for the tests 3.1, 3.2, 3.3, where the angle of asperities in the rock-concrete interface was 10 degrees. Figure 41.a is showing the results for a normal stress applied of 0.4 MPa, Figure 41.b is showing the results for a normal stress applied of 0.8 MPa and Figure 41.c is showing the results for a normal stress applied of 1.2 MPa.

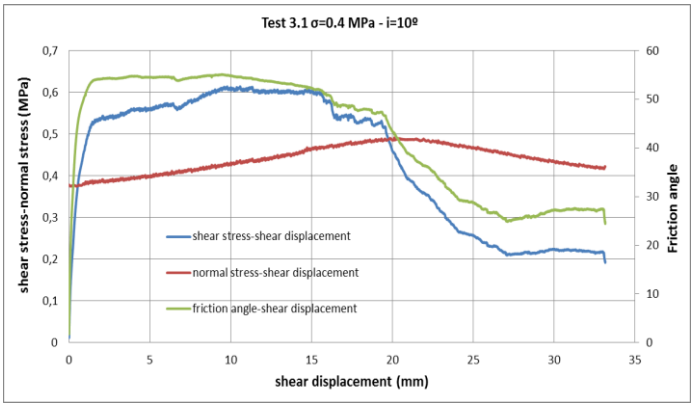

(a)

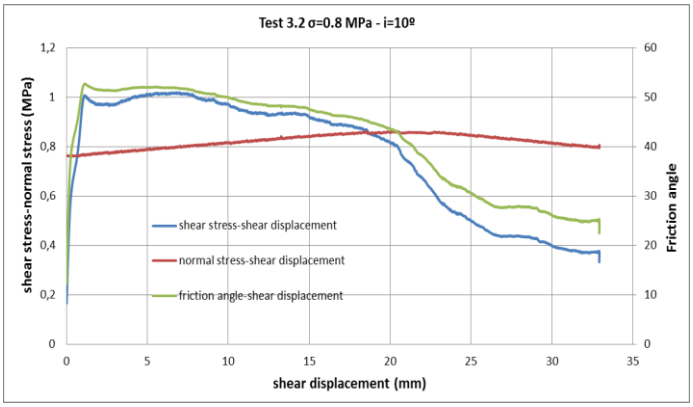

(b)

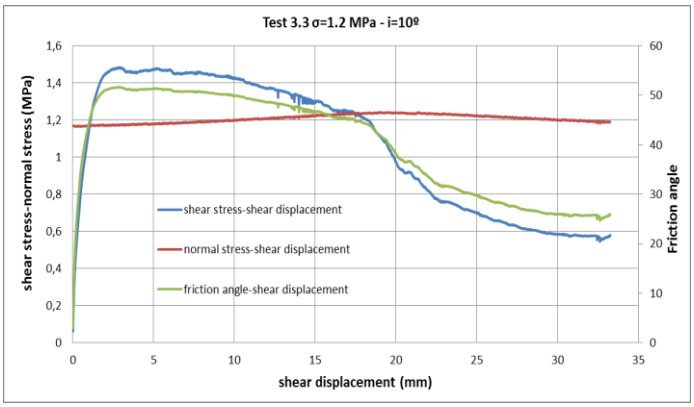

(c)

Figure 41. (a) Results from the tests with 10º asperity profile and a normal stress of 0.4 MPa. (b) Results from the tests with 10º asperity profile and a normal stress of 0.8 MPa. (c) Results from th tests with 10º asperity profile and a normal stress of 1.2 MPa.

The figure 42 shows the results for the tests 4.1 and 4.2 where the angle of asperities in the rock-concrete interface was 0 degrees. Figure 41.a is showing the results for a normal stress applied of 1.2 MPa for the samples tested with bonding and Figure 42.b is showing the results of the specimens tested without bonding for a normal stress applied of 1.2 MPa.

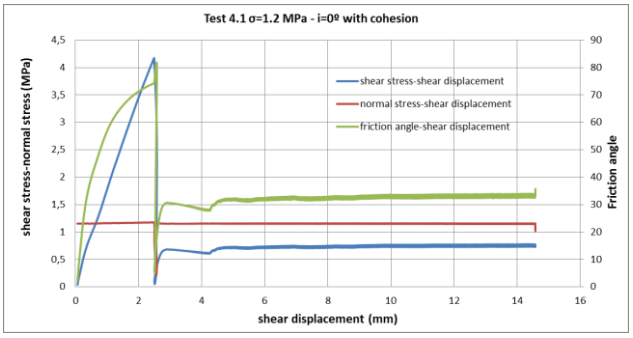

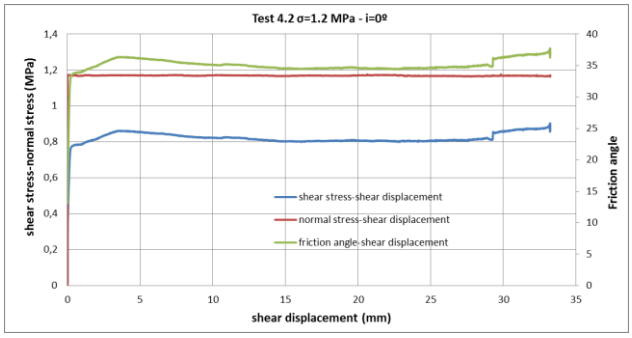

Figure 42. (left) Results from the tests with 0º asperity profile and a normal stress of 1.2 MPa with bonding. (right) Results from the tests with 0º asperity profile and a normal stress of 1.2 MPa without bonding.

4.2.4 Discussion of laboratory results

Within the following pages the results of the direct shear tests are analyzed and interpreted, the topics that are subject of study here are the following; how the shear capacity of the rock-concrete interface is affected by the roughness (angle of asperities) and by the normal load applied, as well as the influence of the normal load applied and the roughness in the friction angle obtained. Another important topic that is evaluated in this section is the effect of the bonding in the shear resistance and also in the friction angle. The role played by the roughness and the normal load applied in the failure mode of the samples during the testing is also analyzed.

The results showed that an increase of the asperity angle lead to an increase in the shear resistance of the joint, as we can see in Figure 43, 44 and 44 which show the shear response for the three asperity angle profiles tested (40, 20 and 10) for normal stress of 0.4, 0.8 and 1.2 MPa, respectively. It can be seen that for angles of asperity of 10 and 20, the curve is similar, there are small deformations (which are due to the initial elastic deformations of the asperities) until the peak is reached and then there is a the shear stress variation keeps steady with the horizontal deformation. This means that sliding is the governing failure mode, which is in line with Joahansson (2009), who indicates that asperity angles up to 35, sliding over the asperities is occurring. On the other hand, for higher angle of asperity, as 40 degrees, the shear response is different, it is characterized by a rapid drop of the shear stress once the peak shear stress has been reached, and the curve is full of up and downs. The same situation occurs when the asperity angle is 20 and the normal stress 1.2 MPa. This is because of the fact that asperities are sheared off.

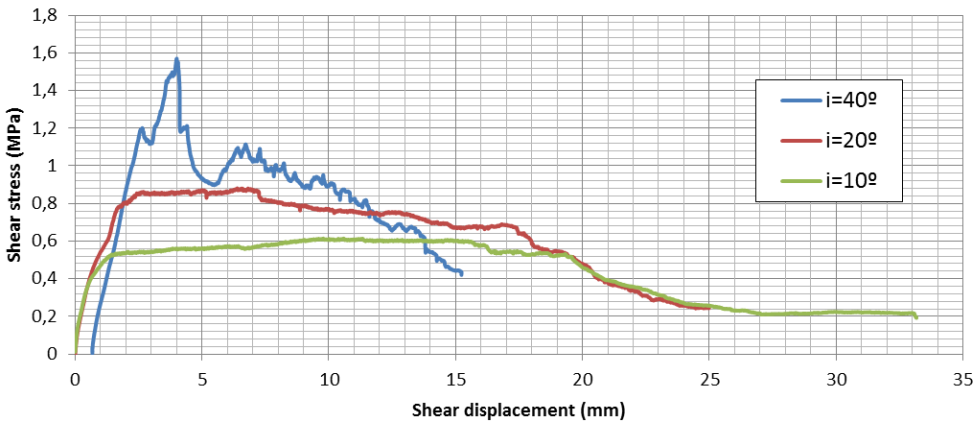

Figure 43. Shear stress response for the different asperity angles tested and a normal stress of 0.4 MPa.

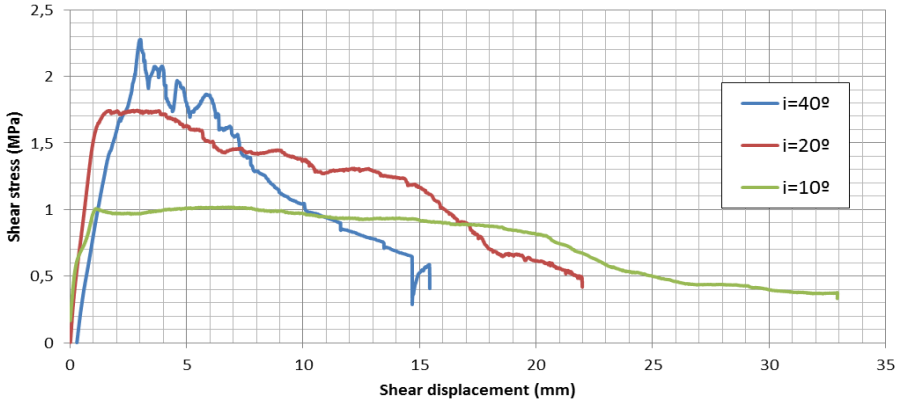

Figure 44. Shear stress response for the different asperity angles tested and a normal stress of 0.8 MPa.

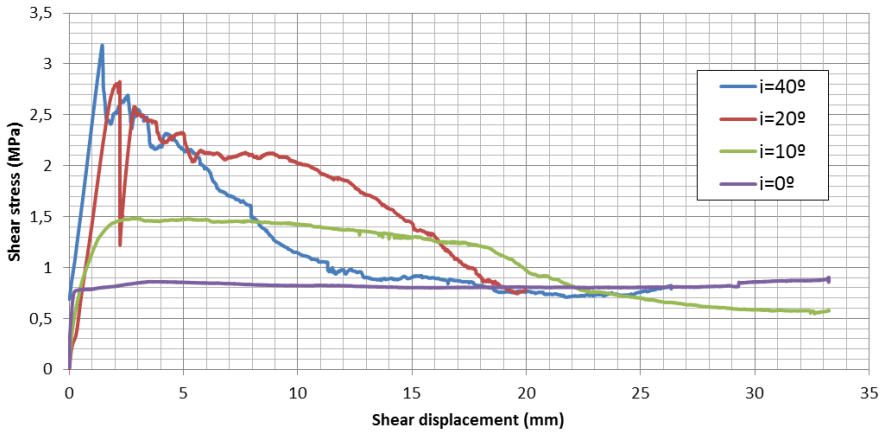

Figure 45. *Shear stress response for the different asperity angles tested and a normal stress of 1.2 MPa.*

If the peak shear stress for an asperity angle of 10 and 40 are compared, it is evident how the roughness influences the shear capacity. For a normal stress of 0.8 MPa, the maximum shear stress reached is 51.93 MPa and 70.32 MP for an asperity angle of 10 and 40, respectively. If we compare the peak shear stress for a normal stress of 1.2 MPa when the angle of asperity is zero, which is 0.9 MPa, and for 40 asperity angle, which is 3.18 MPa, the influence of the roughness in shear capacity becomes more evident.

The normal stress applied also plays a key role on the shear stress of the concrete-to-rock interface. As it can be seen in Figure 46, for all the asperity angles tested an increase in the normal stress applied implies an increment in the peak shear stress. For example, for a fixed asperity angle of 20º, the peak shear stress obtained for a normal stress of 1.2 MPa and 0.4 MPa is 2.83 MPa and 0.88 MPa, respectively. This means that the shear resistance experiences an increment of 321,6 % when the normal stress varies from 0.4 to 1.2 MPa. The Figure 47 shows the shear stress variation with the horizontal displacement for 40º asperity angle profile and for the three different normal stress levels tested. As it can be seen the shear

capacity experiences a significant increase as normal stress applied increases. It is also important to note that the three curves of shear response showed in Figure 47 have a similar shape, with many up and drops, which is reflecting the shearing off the asperities due to the high asperity angle.

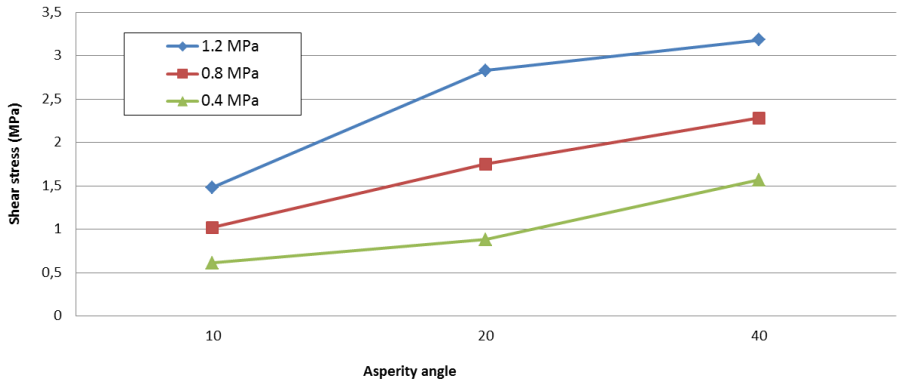

Figure 46. Variation of the peak shear stress with asperity angle for a normal stress of 0.4, 0.8 and 1.2 MPa.

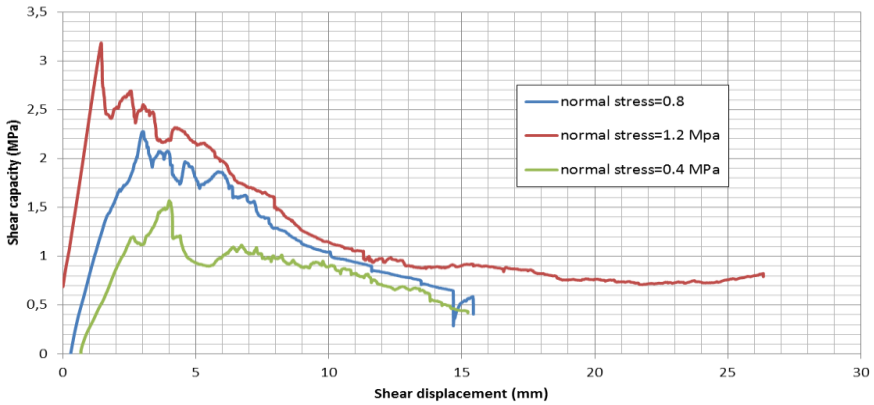

Figure 47. Shear stress response for different normal stresses and 40 asperity angle.

In order to study the effect of the cohesion in the shear resistance of the joint, two tests were carried out with bonding. The Figure 48 is showing the shear stress response for the tests with an asperity angle of 40º with and without bonding, and for the test with an asperity angle of 0º with and without bonding. The shear response for the specimens tested with bonding is characterized by a brittle behavior, as it can be seen from the Figure 48, after it reaches the peak shear stress, it experiences an abrupt drop. The bonding strongly influence the shear resistance of the joint, for example for the test with i=40º carried out with bonding the peak shear stress reached is 5.2 MPa and the specimen with the same asperity angle and without bonding is 3.18 MPa, which means that the peak shear stress is increased in a 163.52% due to bonding. For the specimen tested with flat surface interface with bonding the maximum shear stress obtained is 4.17 MPa and without bonding is 0.9 MPa. This illustrates how significant

is the presence of the bonding on the shear resistance of the concrete-to-rock joint. It is interesting the fact that the angle of asperities, when bonding is present, does not influence the shear capacity as when there is no bonding. If the peak

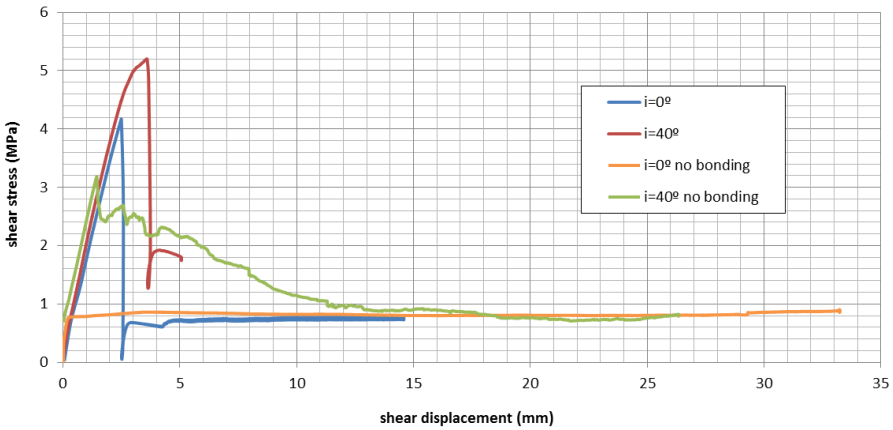

Figure 48. Shear stress response for tests with bonding and without bonding for i=40º and i=0º.

shear stress when there is no bonding is compared for i=40º and i=0º (both for $\sigma_n = 1.2\ MPa$), an increment in the shear capacity of 252% is observed. On the other hand, when the bonding is present for the same tests, then the shear capacity is only increased in a 25%. This indicates that when bonding is present, the roughness does not contribute that much to the shear resistance of the joint as when there is no bonding. The physical explanation of this phenomenon is, according to Øystein E. (2012) that *"this failure mode is not bound to follow the surface of the foundation, but may propagate through the materials" (page 23).* The failure will follow the interface if the adhesive bond at the interface is weaker than the ones in the intact material (Øystein E. (2012)).

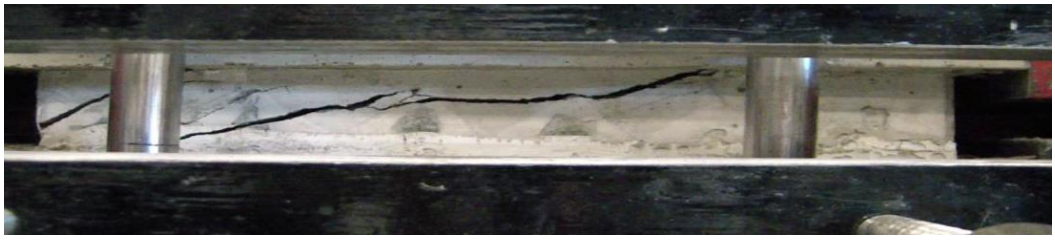

Figure 49. Failure for the specimens tested with bonding for i=40º and $\boldsymbol{\sigma_n = 1.2\ MPa}$.

The failure occurred in a different way depending of the roughness, when the angle of asperity is 40º, the failure started in the concrete block and finish in the rock specimen (See Figure 49). On the other hand, when the surface interface is flat, the failure occurs along the surface interface (See Figure 50).

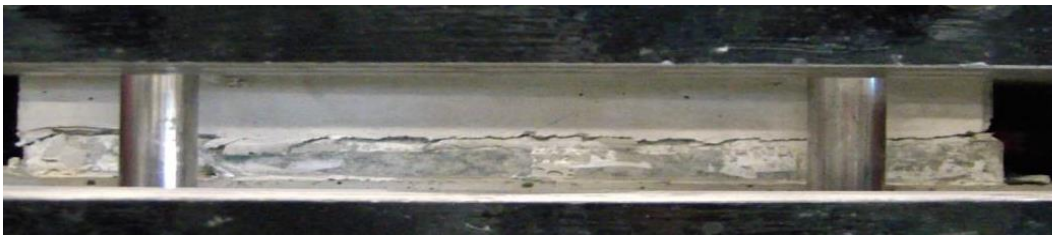

Figure 50. Failure for the specimens tested with bonding for i=0º and $\boldsymbol{\sigma_n = 1.2\ MPa}$.

A higher maximum friction angle was observed in the specimens tested with bonding compared to those tested without bonding. For example, for bonded specimens with a 40º asperity angle, the maximum friction angle obtained was 76.41 MPa and for the same specimen tested without bonding it was 69.52 MPa.

The asperity angle and the normal load applied also influence the failure mode of the interfaces. For low asperity angles, as 10º and 20 º, sliding was the governing failure mode observed (See Figure 51 and 52). On the other hand, for higher angle of asperities as 40º, the concrete asperities were sheared off. The rock also presented wear for 40º asperity angle. It is remarkable that the wear of the rock was not sensitive to the normal stress applied but to the angle of the asperities, for 10º and 20º the rock did not present significant wear for none of the normal stress applied, but for the 40º asperity angle it was observed significant wear of the rock (See Figures 53, 54 and 55). The concrete seemed to be sensitive to both normal stress and the angle of asperities. For the same asperity angle, as the normal load increased, the wear of the concrete asperities increased as well.

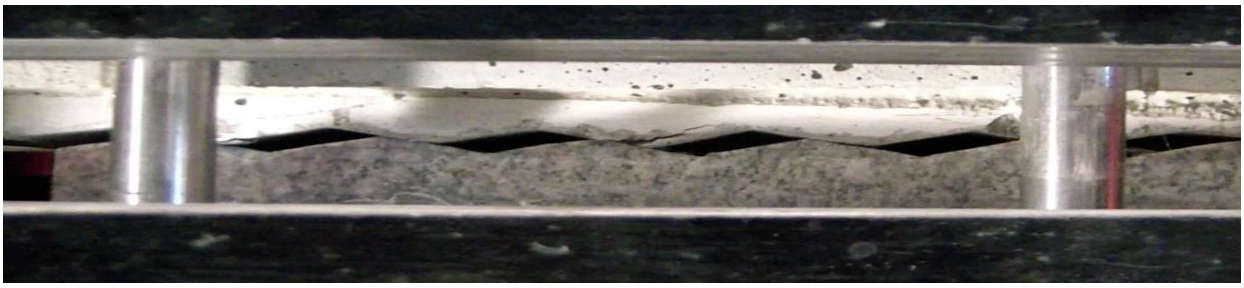

Figure 51. Test 3.1 Interface when peak shear stress is reached (taken from (Liahagen, 2012)).

Figure 52. Test 2.1 Interface when peak shear stress is reached (taken from (Liahagen, 2012)).

Figure 53. Test 1.1 Concrete-to-rock interface after the test is finished (taken from (Liahagen, 2012)).

Figure 54. Test 1.2 Concrete-to-rock interface when peak shear stress is reached (taken from (Liahagen, 2012)).

Figure 55. Test 1.4 Concrete-to-rock interface when peak shear stress is reached (taken from (Liahagen, 2012)).

The angle of asperities also influence the maximum friction angle reached. As it can be seen in Figure 56, for a fixed normal stress, the maximum friction angle increases as the angle of the asperities increase. For example, when the normal stress is 0.4 MPa, the maximum friction angle obtained is 73.08º, 61.48º and 54.95º for an asperity angle of 40º, 20º and 10º, respectively. Regarding the influence of the normal stress applied on the friction angle, an increase of the normal stress will lead to a reduction of the maximum friction angle reached. When the angle of asperities is 20º, this relation is not satisfy and as the normal stress is increased, the maximum friction angle reached increases as well.

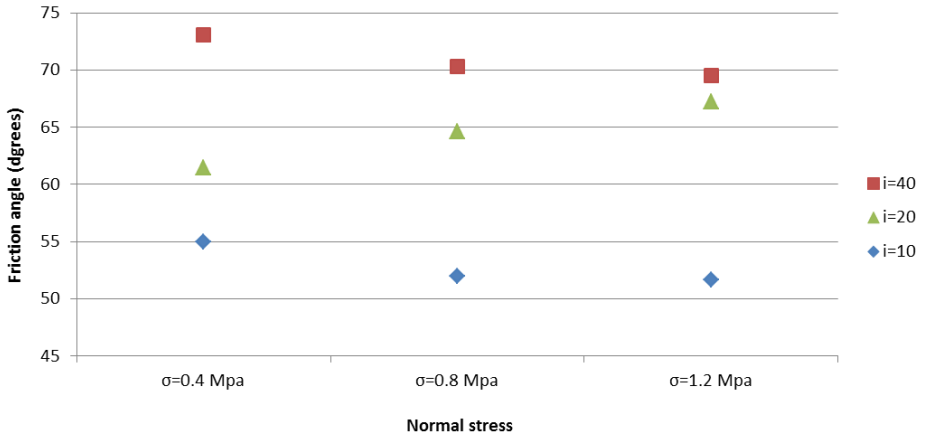

Figure 56. Influence of the asperity angle in the friction angle.

The Figure 57 shows the variation of the friction angle with the shear displacement for the different surface profiles tested and for a normal stress of 1.2 MPa. If we take a look at the test with flat surface, (i.e. 0 º asperity angle profiles), we can see that the curve reaches it maximum friction angle and then it keeps a constant value of friction angle which is the basic friction angle of the surface. In this case, the basic friction angle of this concrete-to-rock joint can be estimated as 35º.

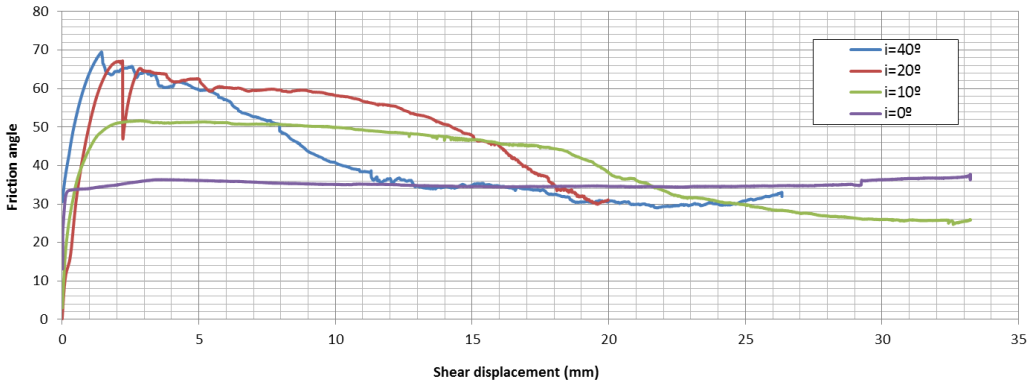

Figure 57. Friction angle variation with the shear displacement for the different roughness.

Figure 58 shows the horizontal displacement when the maximum shear stress is reached. As it can been seen, the peak shear displacement increases as the angle of the asperities decreases, for example for a normal stress of 0.4 MPa and 10 asperity angle the peak shear displacement is 9.78 mm and for the same normal stress level and a 40 asperity angle, the displacement at peak has a value of 4 mm. It is remarkable that when the normal stress is 0.8 MPa, the peak shear displacement has the same value for 20 and 40 asperity angle profiles. Regarding the influence of the normal stress on the peak shear displacement, we can see that as the normal stress increases, the horizontal displacement at peak decreases.

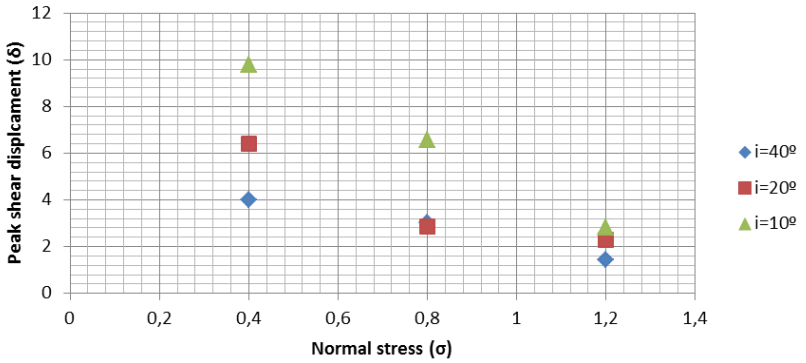

Figure 58. Peak shear displacement variation with the normal stress and roughness.

The variation of the stiffness with the roughness and the normal stress level applied is shown in Figure 58. The stiffness of the joint has been calculated as the peak shear stress divided by the horizontal displacement at peak:

$$k_s = \frac{\tau_{peak}}{\delta_{H,peak}}$$

As it can be seen from Figure 59, the influence of the roughness on the stiffness of the joint is evident. As the asperity angle increases the stiffness increases as well. An increase on the normal stress also leads to an increase of the stiffness of the joint.

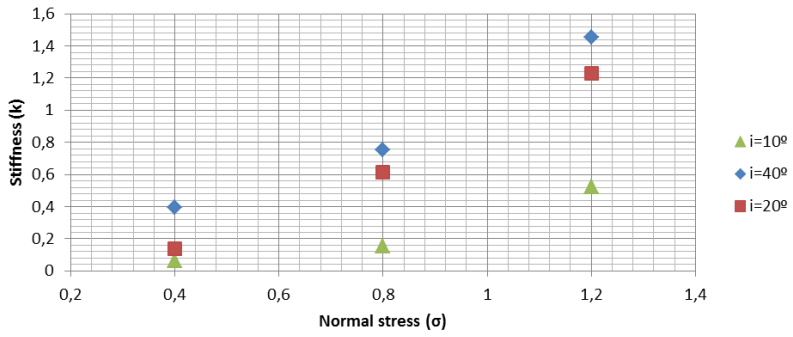

Figure 59. Stiffnes variation with normal stress and roughness.

4.2.5 Testing results into shear strength failure criterions

The results of the tests conducted by Liahagen (2012) have been testes into commonly used models to estimate the shear resistance. Four models have been used in this analysis, first of all, the Mohr-Coulomb equation has been used, then the Patton`s bilinear model is tested, Barton & Choubey`s model is also used to compare predicted and observed values and finally the hyperbolic model developed by Maksimovic is tested. As an input data, the normal stresses 0.4, 0.8 and 1.2 MPa have been used, and the basic friction angle used is 35º (the one that was calibrated from the Liahagen `s tests) The comparison between the observed values in the tests and the values predicted by each shear failure criterion asperity angle tested.

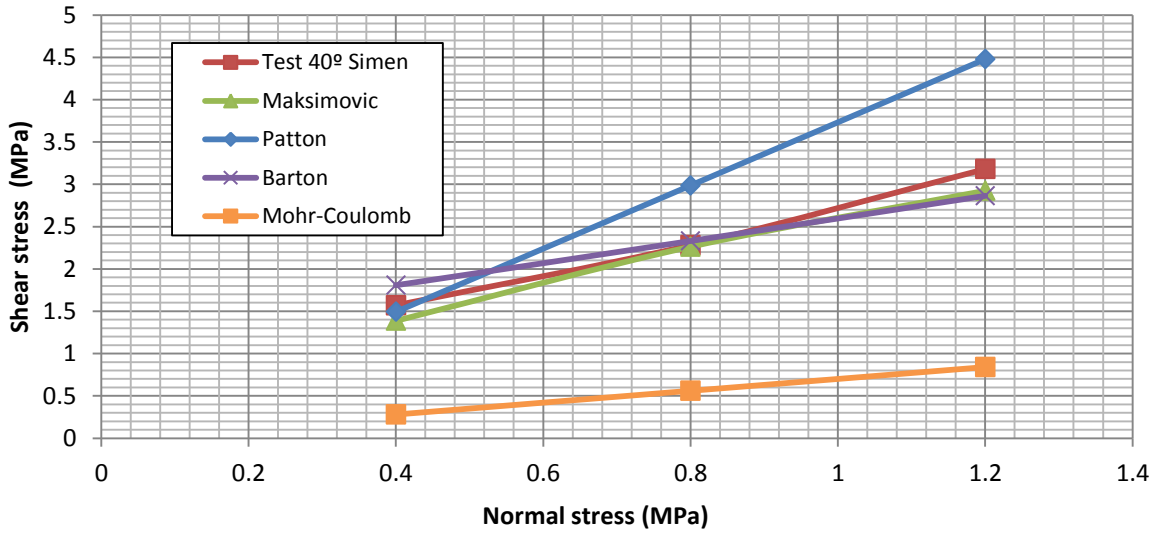

(a)

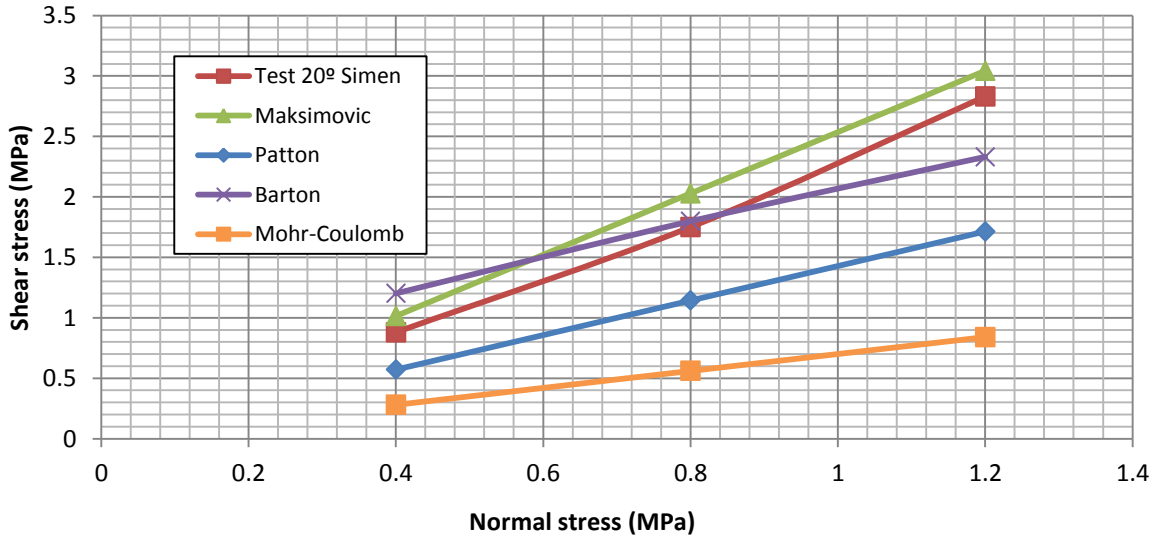

(b)

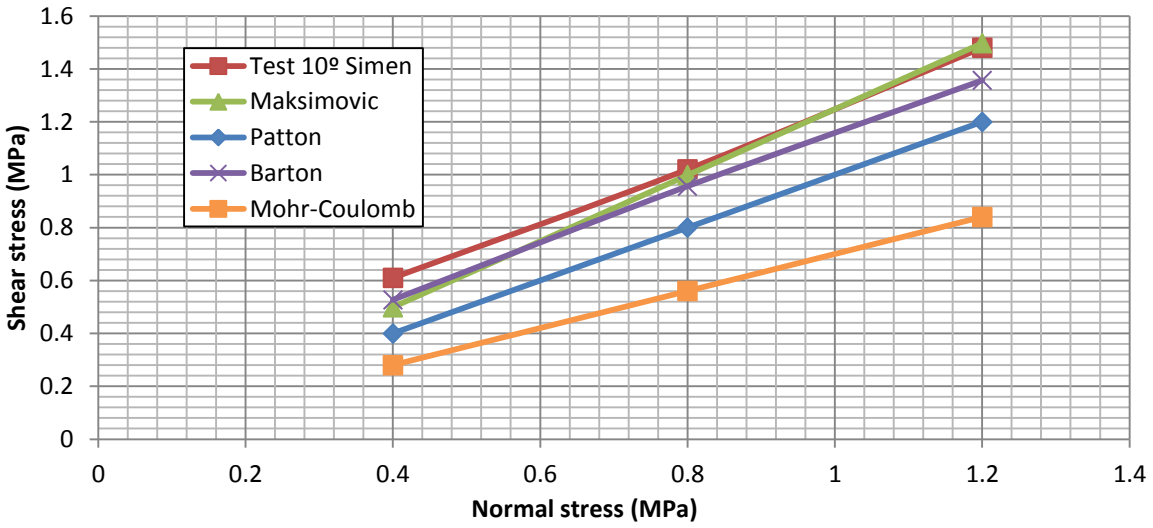

(c)

Figure 60. (a) Comparison between observed and predicted shear capacity envelopes for i=40º (b) Comparison between observed and predicted shear capacity envelopes for i=20º (c) Comparison between observed and predicted shear capacity envelopes for i=10º

As the results show there is a significant difference between the results obtained from the shear tests and the values obtained by using the Mohr-Coulomb model. The reason behind these is the fact that Mohr-Coulomb equation does not incorporate the influence of the roughness interface into its formula, and as the literature and the direct shear tests conducted by Liahagen (2012) have shown, an increase of the joint roughness greatly increase the shear capacity of the surface interface. By looking at the comparison, one can realize how conservative is to use the Mohr-Coulomb to evaluate the shear resistance of a potential failure plane where roughness is present, the Mohr-Coulomb approach clearly underestimates the shear resistance for surface with roughness. For example, for an interface with an angle of asperities of 20º, the shear resistance of the plane is 2.83 MPa for a given normal stress of 1.2 MPa. If the Mohr-Coulomb criterion is used, the value of shear capacity for the same normal stress level would be 1.2 MPa, which is a value 42.40% lower than the actual shear capacity. As it is shown in figure 4, when the asperity angle is low, in this case 10º, the difference between the observed values and the predicted values of shear capacity are not that high as in the case of the tests with asperity angles of 20º and 40º. Therefore, as the roughness in the concrete-to-rock interface, the Mohr-Coulomb model gives less accurate values due to the fact that the roughness component is not included in its equation.

The Figure 60 shows the failure envelopes for the tests with the different asperity angle and the Mohr-Coulomb failure envelop, among others. It can be seen clearly in this figure how the difference between the actual and predicted values increase as the roughness of the joint increases. For low asperity angle values, as the 10º, the actual failure envelope is similar to the Mohr-Coulomb envelope, the less is the roughness of the interface, the more similar would be the actual shear capacity to the described in the Mohr-Coulomb model.

The results show that the Patton`s criterion underestimates the peak shear values for 10º asperity angle and it can be seen that this asperity angle the predicted and observed failure

envelop has the same inclination, which means that discrepancies between shear stress values are not due to the applied normal load. For the 20º asperity angle profile, the Patton`s criterion again underestimates the shear resistance of the concrete-to-rock joints but this time as the normal load increases, the differences between the observed and predicted values become larger. Therefore there is a discrepancy between what is said in the theory and what is actually occurring, it seems that for these tests the Patton`s criterion is not able to reproduce well the sliding behavior. In theory, the model described by Patton (1966) should be able to describe fairly well the shear behavior for low asperity angles and for higher asperity angles it overestimates the peak shear stress. An interesting phenomenon was found relating to the variation of the Patton`s predicted values with the basic friction angle ($\phi_b$) used. It was found that for $\phi_b$ higher than 45º, the Patton`s criterion overestimates the actual shear stress values observed and for ϕ_b lower than 45º, it underestimates the shear capacity of the concrete-to-rock joint. Figure 34a and 34b shows the observed failure envelop and the failure envelop predicted by Patton for values $\phi_b = 50º$ and $\phi_b = 35º$, for an asperity profile of 20º and 10º, respectively (See Figure 61).

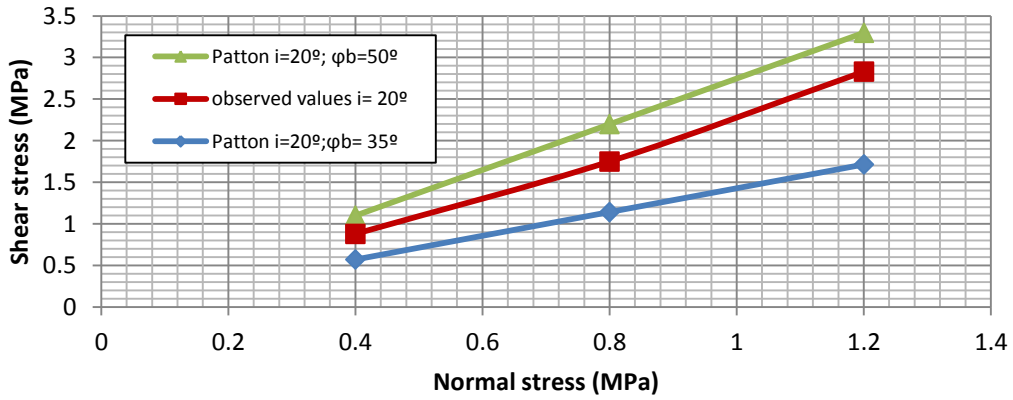

(a)

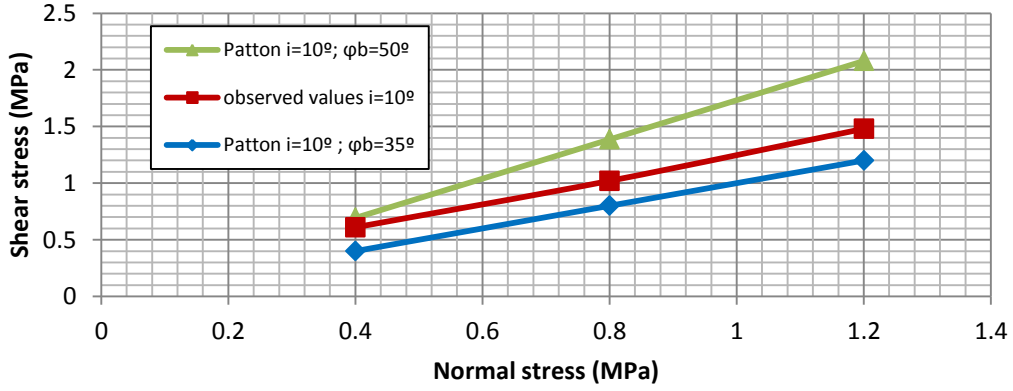

(b)

Figure 61. (a) Comparison between observed values for i=20º and predicted envelop by Patton`s model for a basic friction angle of 50º and 35º. (b) Comparison between observed values for i=10º and predicted envelop by Patton`s model for a basic friction angle of 50º and 35º.

According to the theory, for high asperity angles the asperities are sheared off and sliding is no longer the governing failure mode and therefore the Patton`s model overestimates the shear capacity. This is what is actually occurring in the reality, in the tests with 40º asperity profile, the asperities are sheared off. As it can be seen from Figure 60, for this type of asperity profile the shear stress values obtained with Patton`s equation are higher than the observed values.

When using the Barton & Choubey`s model to predicted the peak shear stress values, the parameters JRC and JCS used in the formula has been calibrated and the values used are:

JRC (roughness parameter)	JCS (MPa)
21.5	38
18.5	38
9	38

Table 16. JRC and JCS used in Barton`s and Maksimovic's model.

The values predicted by using the Barton`s model seem to fit very well with the observed values in the tests for all the asperity profiles testes, 40º, 20º and 10º. When $i = 10°$ and the normal stress is 0.4 MPa the predicted shear stress value is a bit lower than the actual value recorded in the tests, but for 0.8 and 1.2 MPa it fits very well. For the normal stress 0.4 MPa, the Barton`s equation seems to overestimates a bit the shear resistance for both $i = 20°$ and $i = 40°$ asperity profile. On the other hand, for a normal stress of 1.2 MPa, it underestimates the shear capacity for both $i = 20°$ and $i = 40°$. For the rest of the cases the predicted and observed values fits perfectly.

The last model that has been tested is the model developed by Maksimovic (1997) which is described in chapter 3 as the others model tested. According to this model, the frictional component of a joint can be divided in three parameters; $\Delta\phi$, which is defined as the "joint roughness angle" may be estimated according to Maksimovic (1997) as $\Delta\phi = 2 \cdot JRC$, the median angle pressure, which may be estimated as $p_n = JCS/10$, and the basic friction angle of the surface, which has been calibrated from the tests and it is 35º. The same values calibrated for JRC and JCS for Barton`s model have been used for testing the Maksimovic model. The predicted values when using this model fit very well with the actual shear capacity observed in the tests, except for 20º asperity profile, where the model seems to slightly overestimate the shear strength of the joint.

Out of the comparison presented on Figure 60, it seems that the Maksimovic`s model is the model that gives the best correlation between observed and predicted shear resistance.

It was the author`s intention to test the model developed by Johansson (2009) as well. But our tests were not suitable to use with the Johansson model because the samples of tests carried out by Liahagen (2012) have regular shaped asperities and the model proposed by Johansson (2009) is based on the assumption that natural rock joints have different scales of asperities with different angles of inclination.

4.2.6 Comparison of test results with NVE guidelines

A factor of safety has been calculated for each test, since each test can be assimilated as a mini concrete dam and then these values of factor of safety have been compared with the factors of safety calculated by using the NVE guidelines. The objective of this analysis is to study how an increase in the roughness affects to the factor of safety.

The shear friction method is used to estimate the factor of safety against sliding in the NVE guidelines:

$$SF_{NVE} = \frac{\sum H_f}{\sum H_t} \tag{4.1}$$

Where $\sum H_f$ is the maximum shear resistance of the sliding plane considered $\sum H_t$ is the horizontal load applied to the sliding plane.

For a normal loading case, the factor of safety considered by NVE (2005) is 1.5 and the maximum shear resistance of the sliding plane is calculated according to the Mohr-Coulomb equation, where the basic friction angle (ϕ_b) is assumed to be 45°.

$$\tau_p = \sigma_n \cdot tan(\phi_b)$$

The factor of safety for each test is calculated as follows:

$$SF_{tests} = \frac{H_{max,tests}}{\sum H_t} \tag{4.2}$$

If equation 4.1 is divided by equation 4.2, then the factor of safety for each tests can be calculated without the need of estimating the horizontal load applied to the sliding plane.

$$\frac{SF_{tests}}{SF_{NVE}} = \frac{\tau_{max,tests}/\sum H_t}{\sum H_f/\sum H_t} = \frac{H_{max,tests}}{\sum H_f} \tag{4.3}$$

Therefore, the safety factor for the tests can be estimated as the relation between the shear resistance estimated by using the Mohr-Coulomb equation which is used in the NVE guidelines (and 45º basic friction angle) and the shear resistance estimated from the tests, multiplied by the factor of safety proposed by NVE for a normal loading case.

$$SF_{tests} = SF_{NVE} \cdot \frac{H_{max,tests}}{\sum H_f} = 1.5 \cdot \frac{H_{max,tests}}{\sum H_f} \tag{4.4}$$

As it can be seen from Figure 62, as the roughness of the dam-rock interface increases, as the asperity angle increases, the factor of safety becomes higher. This show how conservative is the method use by the NVE guidelines to assess the sliding stability of concrete dams.

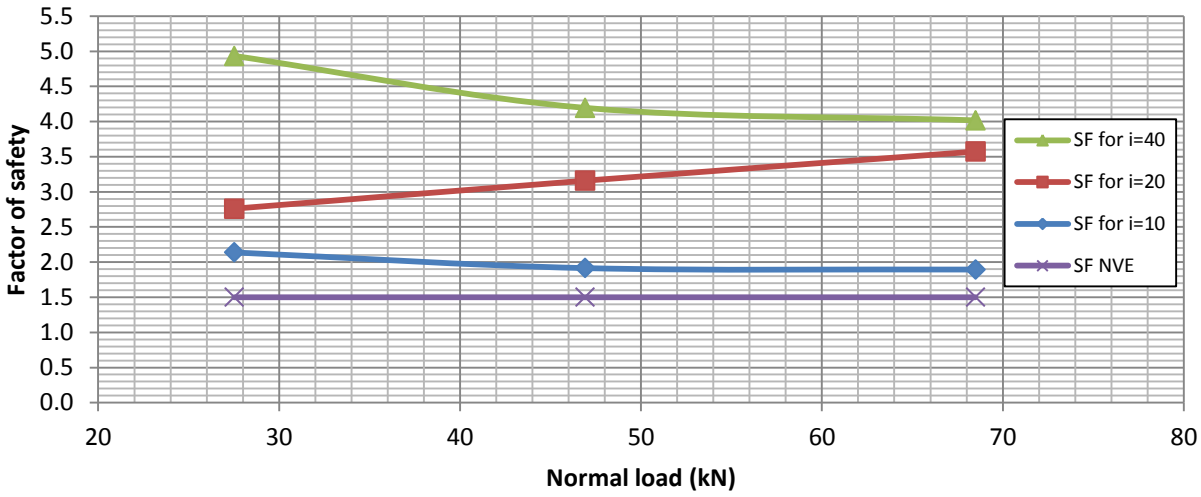

Figure 62. Variation of the safety factor with the asperity angle.

If the shear stress values are divided by the factor of safety for each case, then the maximum allowable horizontal loads can be calculated, this means that above those load levels, the dam will not meet the sliding stability requirements given by NVE (2005). To calculate the limiting horizontal load for each case the following equations have been used:

$$H_{max,allowable,tests} = \frac{H_{max,tests}}{SF} \quad (4.5)$$

$$H_{max,allowable,NVE} = \frac{H_{max,NVE}}{SF} \quad (4.6)$$

Figure 63 shows the maximum allowable horizontal loads in order to meet the NVE safety requirement for normal loading case (factor of safety 1.5). This has been calculated for each asperity angle profile and as it can be seen in Figure 63 as the roughness increases, the limiting horizontal load increases as well. It is remarkable the degree of conservatism of the current NVE guidelines if the values of maximum allowable horizontal load for 40 or 20 asperity angle and the values calculated according to NVE are compared. This means that if the roughness effect is taken into consideration when estimating the shear capacity of the sliding plane, the dam would be stable against sliding for higher loads. For the same loads, if the influence of roughness is ignored the dam would not be safe against sliding.

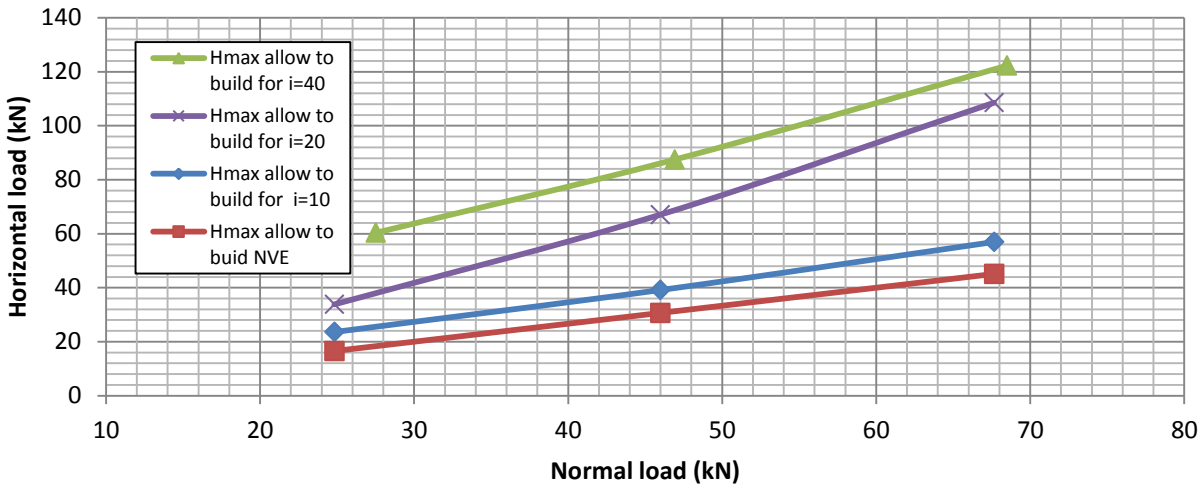

Figure 63. Variation of the maximum allowable horizontal loads envelopes for each asperity angle and for NVE guidelines.

Figure 64 shows the maximum horizontal load that allow in order to meet the NVE requirements for normal loading case with a safety factor of 1.5 for the specimens tested with bonding. This is done in order to show the influence of the bonding between the concrete and the dam in the shear capacity between the dam and the rock. Looking at the Figure 64, it becomes evident that the actual guidelines used by NVE greatly underestimate the shear resistance between the dam and the rock when bonding is present. For example, for an horizontal load of 150 kN, the dam would be considered as unstable against sliding according to NVE, but if the bonding between the dam and the rock was taken into consideration in the guidelines, we can see that the dam would be perfectly stable against sliding failure (the values under the blue line in Figure 64 are in the range of allowable horizontal loads, and for values above that line, the dam would be unstable against sliding).

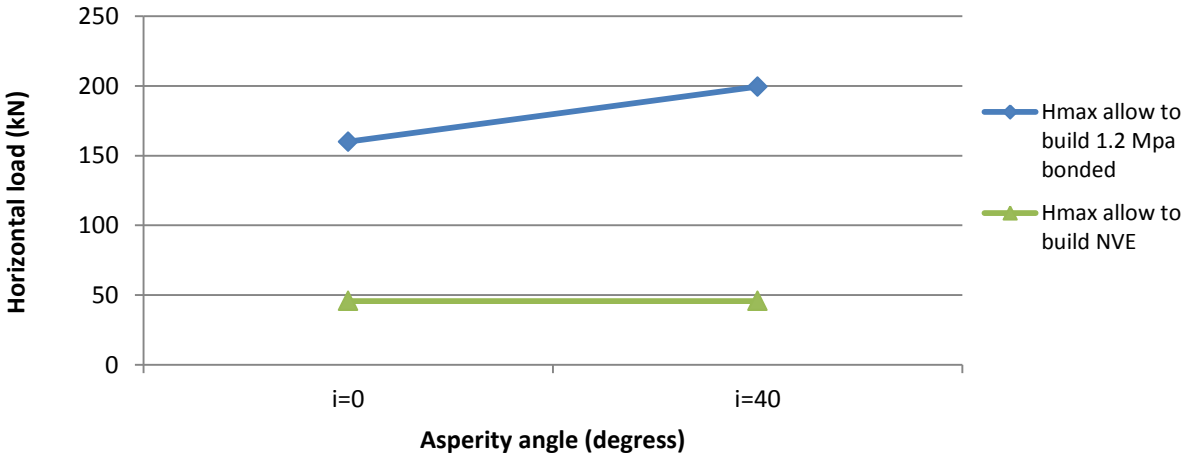

Figure 64. Comparison between the maximum allowable horizontal loads for bonded specimens and for NVE guidelines.

4.2.7 Proposed model to estimate shear strength

Both the literature study and the direct shear tests have shown that the roughness strongly influence the shear capacity of concrete-to-rock joints. The results from the direct shear tests revealed that an increase of the asperity angle at the interface rock-concrete originate an increase on the shear strength. For the tests carried out without bonding, the envelopes are similar to the Mohr-Coulomb envelope with the difference of the inclination of the line. It can be seen that when increasing the roughness by increasing the asperity angle, the line becomes steeper (See Figure 65). The different inclination of the lines respect to the Mohr-Coulomb envelope is due to the fact that the frictional component in the Mohr-Coulomb equation does not include the roughness effect.

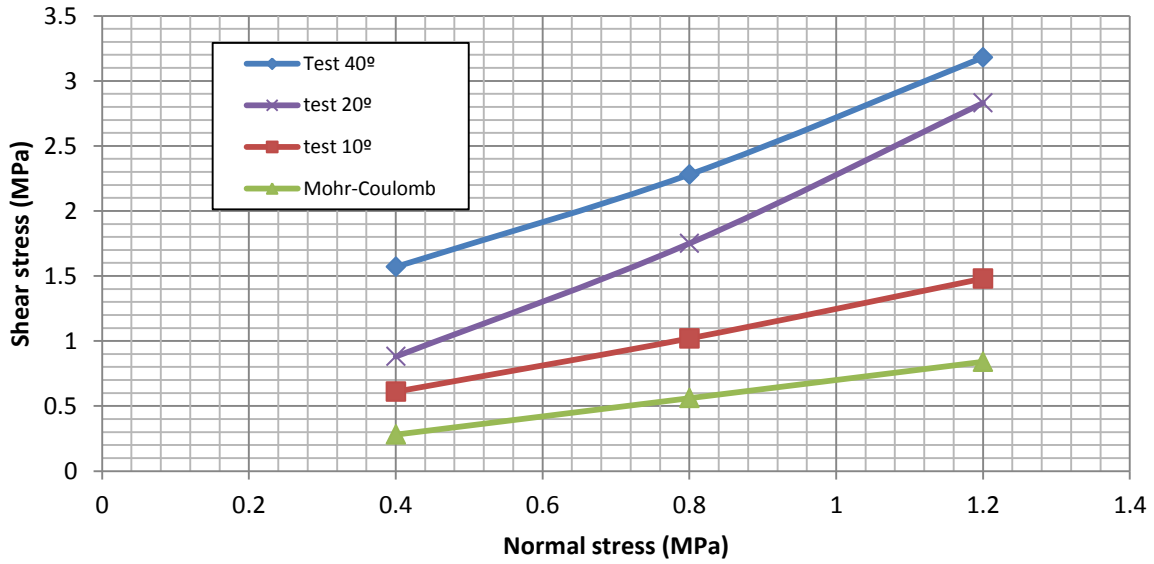

Figure 65. Shear resistance enveloped for each asperity angle tested and for Mohr-Coulomb model.

Therefore, an attempt to improve the Mohr-Coulomb equation, a model to estimate the peak shear strength has been developed in order to incorporate the roughness effect. This effect implies an increment of the gradient that will be depending on the roughness factor, which is considered the asperity angle (See figure 66).

$$\tau_p = \sigma_n \cdot tan(\varphi_b \cdot k)$$

Where τ_p is the peak is shear strength, σ_n is the effective normal stress applied, φ_b is the basic friction angle, k_r is the roughness factor and i is the angle of asperity.

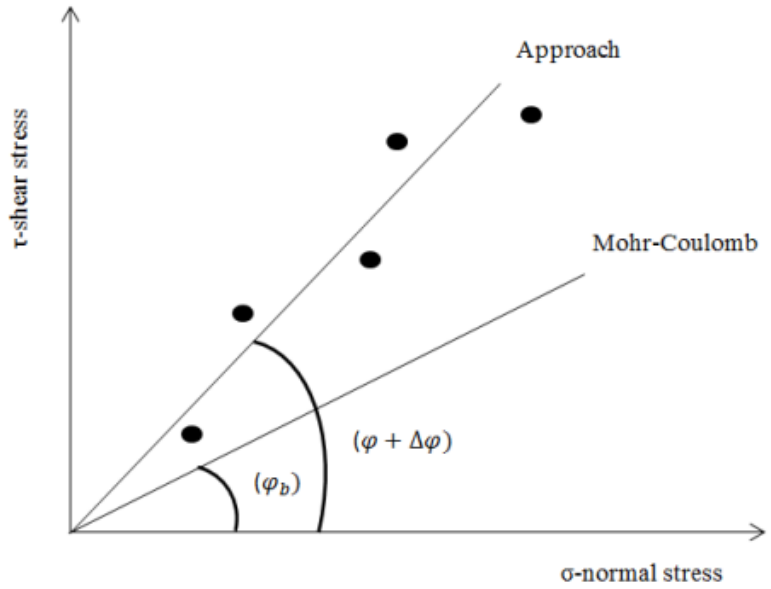

Figure 66. Increment of gradient by incorporating a roughness factor into Mohr-Coulomb model.

The equation to estimate the peak shear strength has been developed from the tests carried out by Liahagen (2012). The methodology of the model development is described below:

1. For each set of tests with different angle of asperities the 3 pair of points (τ_i, σ_i) are plotted and by using least squares a straight line which the ordinate in the origin is zero, therefore there is only one parameter to estimate with this method which is the gradient of the regression line approach.

2. After the gradient of each approach is calculated, the roughness factor is calculated for the three different approaches:

$$Gradient = \frac{\tau_i}{\sigma_i} = tan(\varphi_b \cdot k_r)$$

3. A roughness factor is computed for each asperity angle and then an equation showing how the k varies with the i is obtained.

$$k_r = \frac{arctan(\tau_i/\sigma_i)}{\phi_b}$$

The first approach is based on the Mohr-Coulomb equation, in this case the frictional component is increased by multiplying the basic friction angle of the surface by the roughness factor (k_r). The variation of the roughness factor with the asperity angle profile for both proposed models is shown in Figure 67.

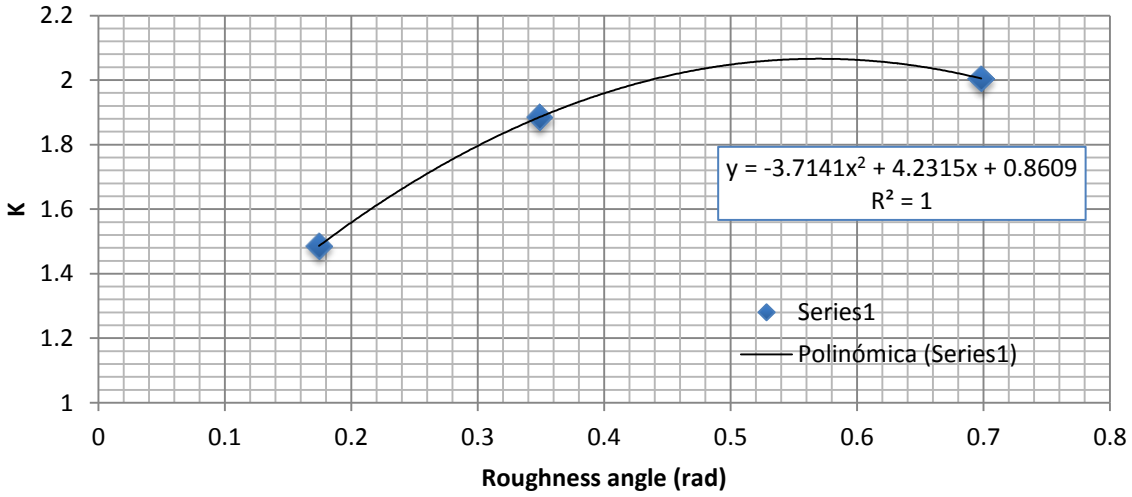

Figure 67. Variation of the roughness factor with the asperity angle.

The equation that defines the peak shear strength for proposed model, the Mohr-Coulomb model:

$$\tau_p = \sigma_n \cdot \left(tan(\phi_b \cdot k_r)\right)$$

Where is the peak shear strength, I the normal stress applied, is the basic friction angle and is the roughness factor, which can be calculated as a function of the asperity angle:

$$k_r = -3.7141 \cdot i^2 + 4.2315 \cdot i + 0{,}8609$$

The shear capacity has been estimated by using both models and the results have been compared to the direct shear test results conducted by Liahagen (2012). The Figure 68 shows a comparison between the failure envelopes estimated by using the proposed model and the one obtained from the tests. This is done for the three asperity angle profiles tested (40, 20 and 10).

From the Figure 68, it can be seen that the correlation between the observed and predicted by the proposed model is really good for all the asperity angle profile.

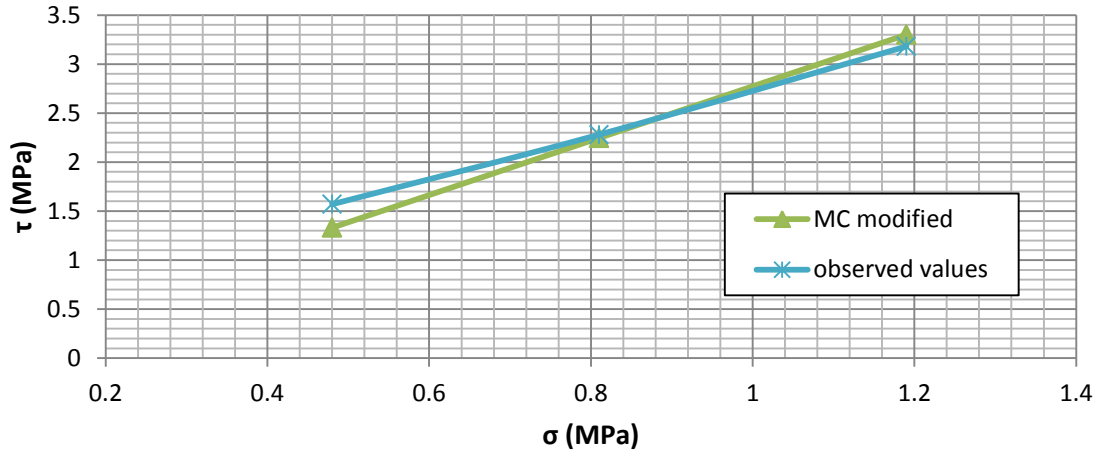

(a)

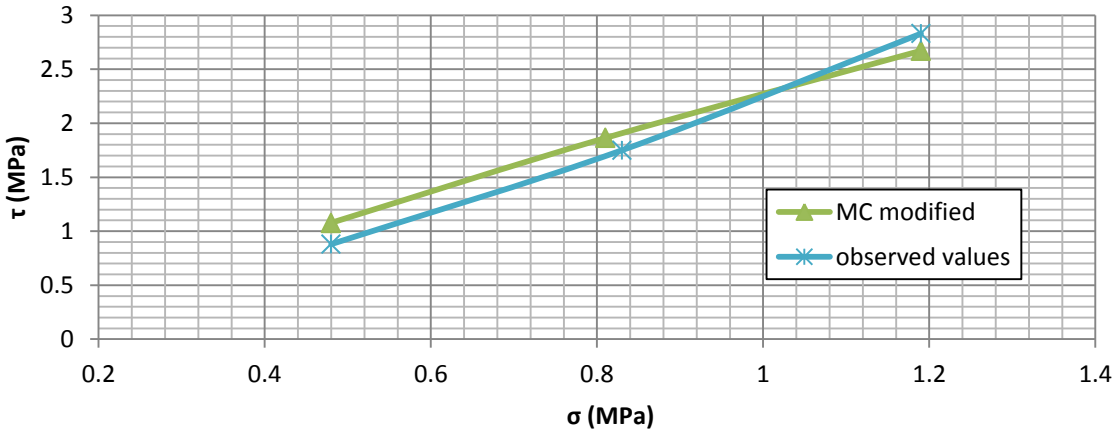

(b)

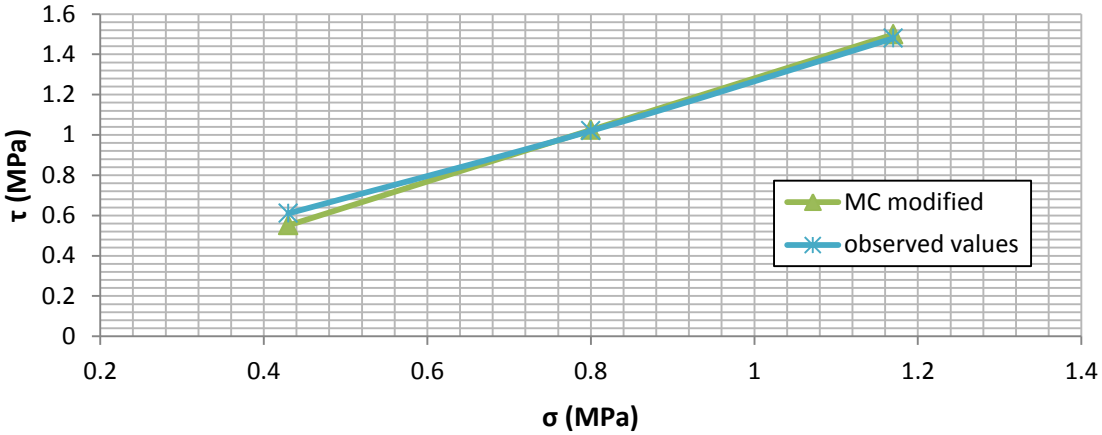

(c)

Figure 68. (a) Comparison between observed values and predicted values by using the proposed model for i=40º (b) Comparison between observed values and predicted values by using the proposed model for i=20º (c) Comparison between observed values and predicted values by using the proposed model for i=10º.

4.2.7 Summary

Throughout this section, an evaluation and review of the direct shear tests carried out at LTU by Simen Liahagen during his M.Sc. thesis in 2012 is presented. The aim of his work was to study the influence of the roughness on the shear resistance of concrete-to-rock joints. This was done by artificially manipulating the surface of the rock by shaping it with regular triangle asperities. The angle of asperities tested varied between 0º and 40º. In total, 12 tests were carried out, four of them with 40 º asperity angle, three of them with 20º and 10º asperity angle, respectively and finally two specimens were tested with flat surface (0º). The rock used was granite with a uniaxial compressive strength of 260 MPa and the concrete used was B35. In order to study the effect of the cohesion on the shear resistance between the rock and the concrete, 3 tests were run with bonding. To analyze the influence of the normal load applied in the shear capacity, three different normal load levels were used in the tests, these were 0.4 MPa, 0.8 MPa 1.2 MPa.

The results showed that the roughness strongly influenced the peak shear stress value obtained, for higher values of asperity angle, the shear capacity between the joint experienced an increase. This is consistent with what has been seen from the literature, see for example Negi R. (2012), Xue F. Gu et Al (2003) or Kodikara and Johnston (1993). The maximum friction angle reached was influenced by the asperity angle as well, higher values of ϕ_b were obtained. Regarding of the normal load on shear resistance between concrete and rock, it has been observed that as the normal load applied increased the peak shear stress obtained increased as well.

The failure mode of the concrete asperities was influenced by the angle of the asperities and the normal load applied. For lower asperity angles, as 10º and 20º sliding over the asperities was the governing failure mode observed, while for 40º asperity angle, the asperities were sheared off for all the normal load tested. This change in the failure mode with the angle of asperity is consistent with what it has been show in the theory, see for example Johansson F. (2009) and Patton (1966). The specimens tested with bonding showed a much higher shear capacity if we compare with the ones tested without bonding, this means that the effect of the cohesion strongly influences the shear resistance between the dam and the rock, and therefore, more research should be carried out within this topic with the objective of incorporating the effect of the cohesion into the sliding stability guidelines for concrete dams.

The test results were tested into four different models to estimate the shear capacity. These models were:

- Mohr-Coulomb
- Patton
- Barton & Choubey
- Maksimovic

Out of the comparison, the model which gave the best correlation between the observed and predicted values was the one proposed by Maksimovic (1997). The model proposed by Barton

and Choubey also seemed to describe fairly well the shear resistance. The Mohr-Coulomb model underestimated the shear capacity between the rock and the concrete and the model proposed by Patton (1966) gave values of the peak shear stress smaller than the observed ones for 10º and 20º asperity angle, while for 40º asperity angle it overestimated the shear capacity between the rock and the concrete.

A comparison between the results of the direct shear tests and the NVE guidelines was also carried out within this chapter. The analysis showed how the safety factor (estimated by using the shear friction method) varies with the interface roughness. As expected, the safety factor increased as the asperity angle increased. The NVE guidelines uses the Mohr-Coulomb criterion to estimate the shear resistance between the concrete-rock interface at the dam foundation and this model does not take into consideration the roughness influence in shear resistance. In order to show how conservative are the NVE, the envelope of the maximum allowable horizontal loads have been estimated for each asperity angle tested (40º, 20º and 10º) and this have been compared to the envelope estimated by using the NVE guidelines (Mohr-Coulomb criterion) for a safety factor of 1.5. This analysis shows that if the roughness effect is taken into consideration when estimating the shear capacity of the sliding plane, the dam would be stable against sliding for higher loads. For the same loads, if the influence of roughness is ignored (as NVE guidelines do) the dam would not be safe against sliding. An interesting fact was that the basic friction angle found for the concrete-to-granite interface was 35º and the NVE guidelines indicates that a friction angle of 45º shall be used to estimate the shear resistance at the dam-rock contact. This also evidences that the actual guidelines to estimate the shear strength of the concrete-to-rock interfaces does not reflect the actual shear behavior.

Finally, a model to estimate the peak shear stress of a concrete-to-rock rough joint is proposed. The model is based on the Mohr-Coulomb model but it aims to incorporate the effect of the roughness interface into the shear capacity by including a roughness factor, which is a function of the asperity angle. The model was developed out of the results of tests carried out by Liahagen (2012) and it gave a good correlation between the observed a predicted values. The model will be validated with the results of the tests carried out within this Master Thesis, and this validation will be shown in section 4.7.4.

4.3 Apparatus description

The Figure 5 shows the shear test machine that has been used to carry out the direct shear test at Lulea Technical University. It consists of a large and heavy steel frame which dimensions are 2.5 m-2.5 m. The samples to be tested are placed in the shear red box which is located in the lower middle part of the steel frame. The shearing is done by the means two hydraulic arms attached to the upper part of the shearing box, being this part the one that slides over the lower part. There is a hydraulic piston which responsible of the applied normal load, the maximum shear load and normal load that can be applied is 500 kN. The piston transmits the load and the two compressed steel plates which further leads down force on the cutting box. Vegetable oil is pressed between these steel plates by means of hydraulic pumps. Figure 17 shows the principal components of the shear machine.

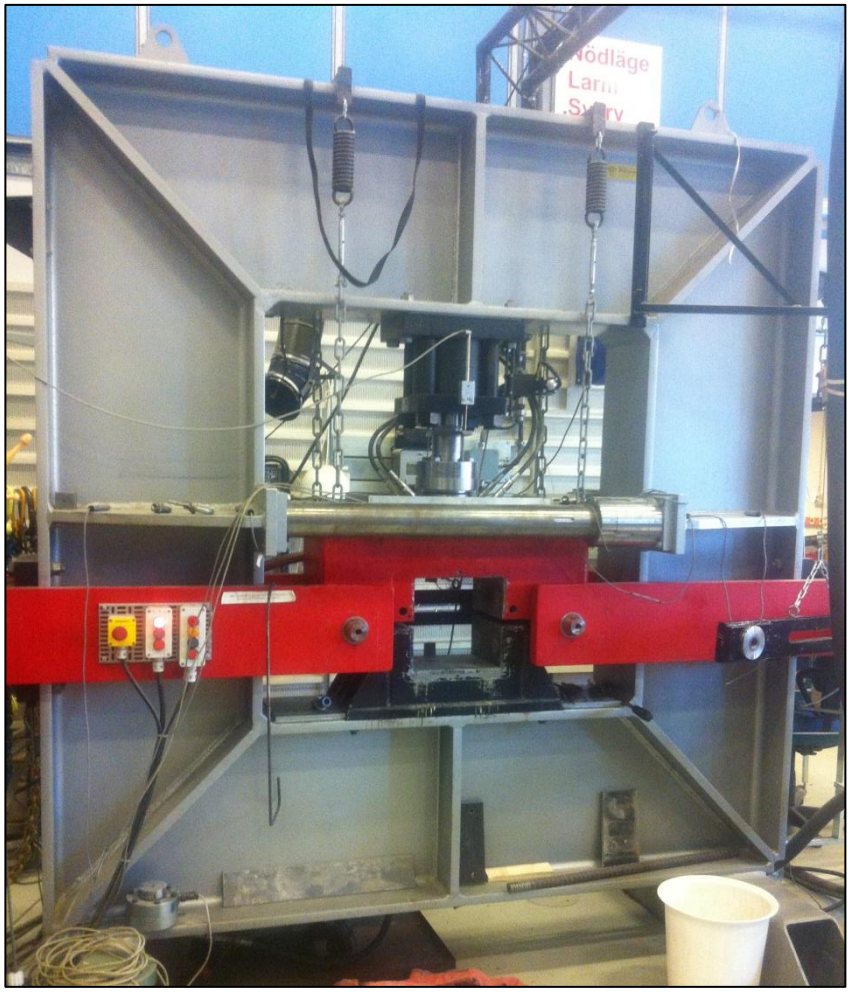

Figure 69. Direct shear test machine used in the tests at LTU.

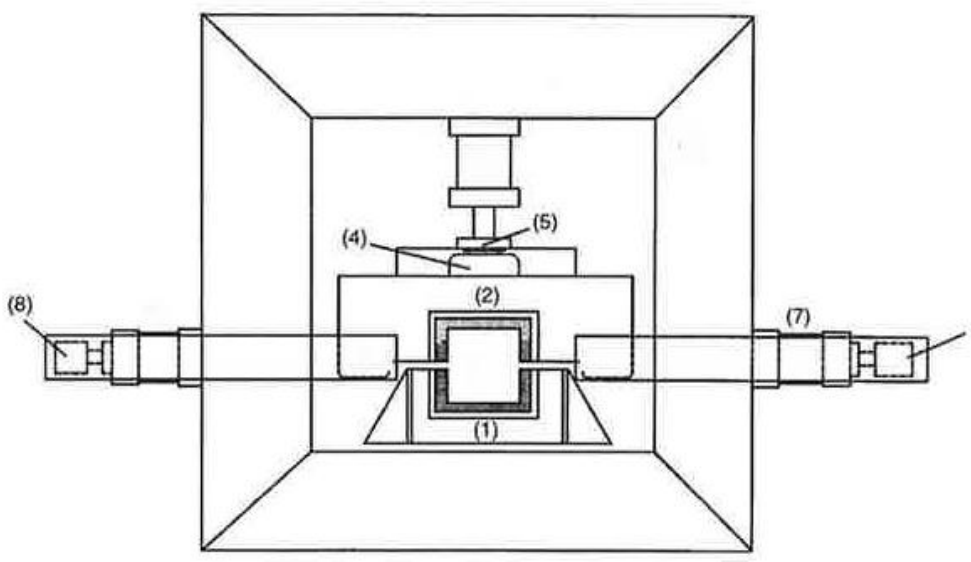

Figure 70. (0) stiff steel frame, (1) lower box, (2) upper box, (3) specimen holder, (4) hydrostatic bearing, (5) spherical bearing, (6) & (7) hydraulic actuators, (8) bucker up (taken from Saaiang et Al, 2005)

4.4 Samples preparation

4.4.1 Rock samples

The rock type used for the direct shear tests was gneiss, in the tests carried out by Liahagen (2012) sound granite was used, and therefore this year the intention was to select a poorer rock in order to study how the rock quality influences in the shear resistance.

12 rock samples were ordered from the company *Granitti Natursten,* located at Piteå, near Luleå. This company was selected to obtain the rock samples because it is located near Luleå. Since the objective of this Thesis is to study the influence of the concrete-to-rock interface roughness, it was decided to artificially manipulate the rock surface. This was done by using triangular asperities and each asperity had the same geometry over the whole surface. . Four different types of profiles were tested, each profile corresponding to a different inclination angle of the asperities; the asperity angles selected were 0º, 10º, 20º and 40º (See Figure 71). The rock specimens had dimensions of 240x240 mm and a height of 130 mm, without counting the asperities height which varied depending on the angle of asperity. The height of the asperities was 16.8, 7.3 and 3.5 mm for the 40º, 20º and 10º asperity angle, respectively. Figure 70 shows the 12 rock samples used in the test conducted by Liahagen (2012), the rock samples used in the direct shear tests looked exactly the same than the samples used last year, only the rock type is changed. There were four samples with 40º asperity angle, three samples with 20º asperity angle, three samples with 10º asperity angle and two samples with 0º asperity angle (flat surface).

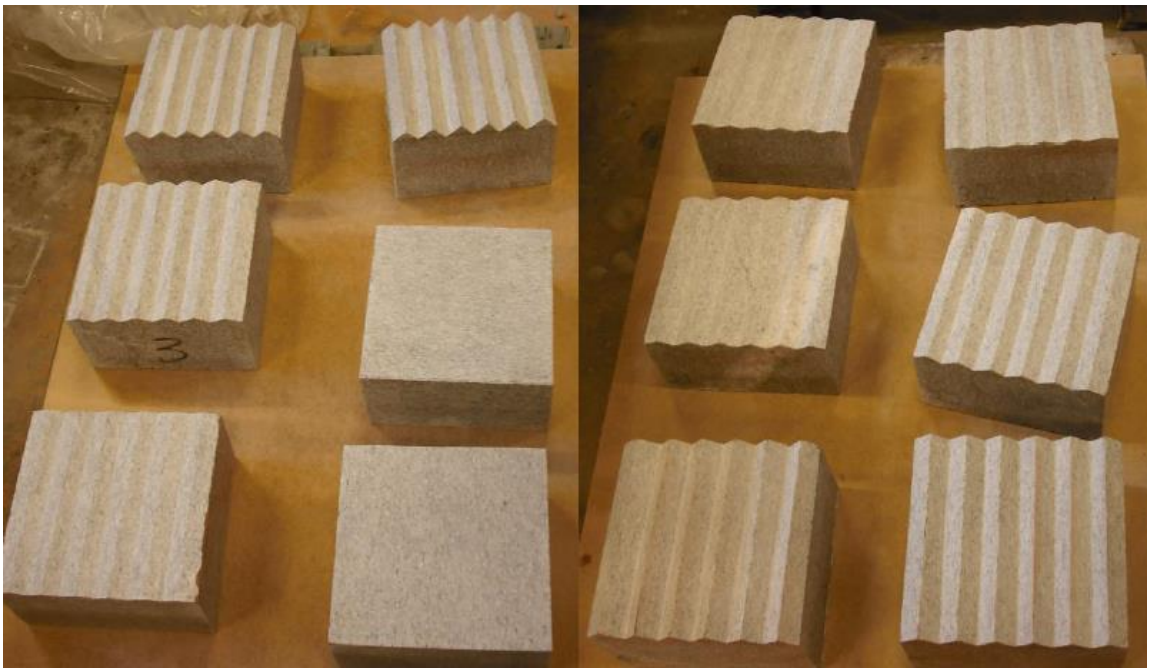

Figure 71. 12 rock samples used in the tests.

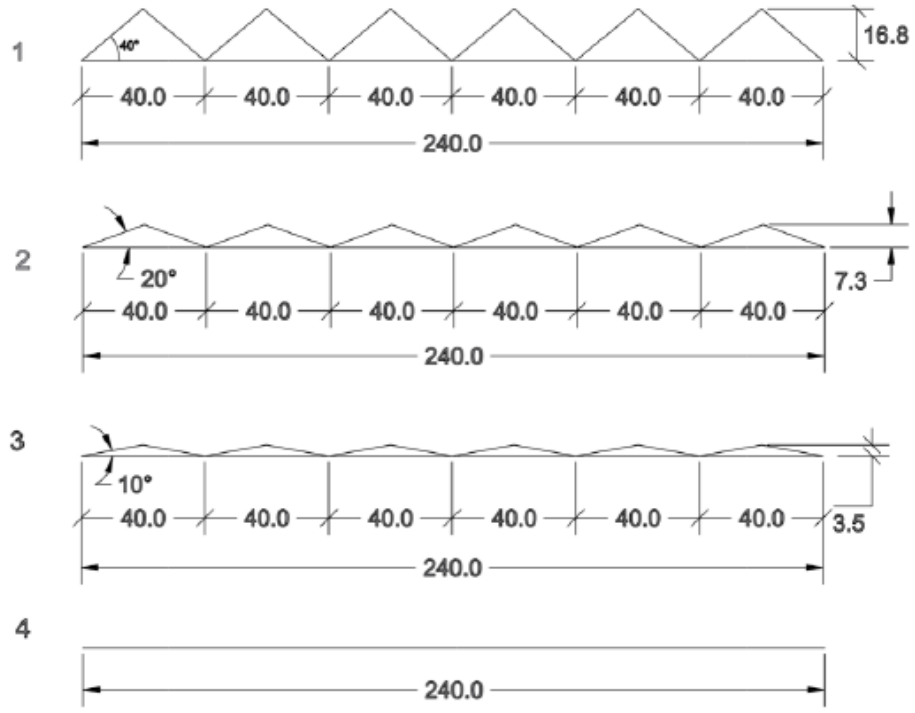

Figure 72. Four different profiles used.

4.4.2 Mechanical properties of rock samples

In order to estimate the strength of the rock used in the direct shear tests, gneiss, three cylindrical samples of the rock were tested at LTU (See Figure). The average strength value found was 158.8 MPa. The results of the test for each sample are shown in table 17.

sample	Height (mm)	Diameter (mm)	Weight (gr)	Area (mm2)	Volume (dm3)	Density (kg/dm3)	Fracture (Kn)	Strength (MPa)
1	148.5	53.4	893.7	2240	0.333	2.69	358.1	159.9
2	144.8	53.7	901.6	2265	0.328	2.75	342.6	151.3
3	150.4	53.6	901.3	2256	0.339	2.66	373.2	165.4

Table 17. Results from the uniaxial compressive strength tests carried out at LTU.

4.4.3 Casting of concrete

Concrete was casted on the rock specimens (See Figure 72 and 73), the concrete used was B45/45 (45 MPa is the compressive strength and 45 is the relation water/cement). The concrete was casted by using wooden formworks, as it can be seen in Figures .Ten samples were casted by placing an adhesive plastic on the rock surface and two of them were casted without the adhesive plastic, this was done to test some samples with bonding and without bonding (See figure 75 and 76).

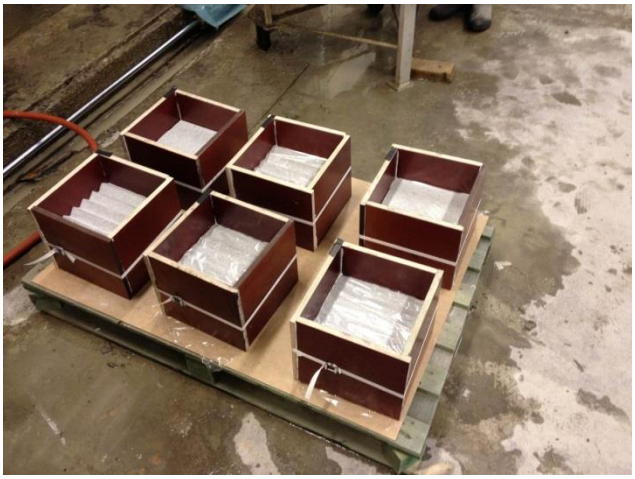

Figure 74. Samples ready for casting.

Figure 73. Casting completed.

Figure 75. Plastic adhesive to avoid bonding (ii).

Figure 76. Plastic adhesive to avoid bonding (i).

Once the samples had cured in water during 14 days, the samples were casted into the steel molds by using fast-setting concrete. Figures 76 and 77 show the process.

Figure 77. Casting on the steel molds (i).

Figure 78. Casting on the steel molds (ii).

4.4.4 Mechanical properties of concrete samples

Four concrete cubes from the concrete that was casted on the rock samples were subjected to compression strength test after 26 days of curing. This is done in order to control the strength of the concrete. The results showed an average compression strength of 62.2 MPa.

Test	1	2	3	4
$f_c\ (MPa)$	61.1	62.5	62.5	62.7

Table 18. Values of the concrete strength.

4.5 Test description

Once the two samples were placed on the machine, six linear variable differential transformers (LVDTs) were attach to the sample in order to measure the vertical displacements at the interface, two LVTDs were placed on the front-side and two more on the back-side of the sample. In order to measure the horizontal displacement at the interface, two more LVDTs were assembled to the samples, one at the front-side and another one at the back-side of the sample (See Figure 80). The tests were conducted under a shear rate of 0.5 mm/min.

In order to study the influence of the normal load applied in the shear resistance between the concrete and the rock, each sample was tested under three different normal stresses. During the direct shear tests conducted last year by Liahagen (2012), the normal load levels selected were 0.4 MPa, 0.8 MPa and 1.2 MPa. This year it was decided to increase the normal load applied in order to study the shear response of the concrete-to-rock interface for higher normal loads. The normal loads selected were 1.2 MPa, 2.2 MPa and 3.2 MPa. Test set-up is shown in Figure 79.

Profile type	1				2			3			4	
Asperity angle	40				20			10			0	
Test	1.1 (B)	1.2 (B)	1.3	1.4	2.1(B)	2.2	2.3	3.1	3.2	3.3	4.1(B)	4.2
σ (Mpa)	1.2	2.2	2.2	3.2	1.2	2.2	3.2	1.2	2.2	3.2	1.2	3.2
N (Kn)	69.12	126.72	172.8	172.8	69.12	126.72	172.8	69.12	126.72	172.8	172.8	172.8

Figure 79. Test set-up for direct shear tests at LTU.

Figure 80. Sample ready for testing.

4.6 Results

The results from the direct shear tests are presented in Table 19. Figures showing the results for all of the samples can be found in Appendix C, while photos of the samples during and after the shear tests are presented in Appendix D. The Table shows the normal load applied, N, the horizontal load applied, H, the normal stress, $\boldsymbol{\sigma_n}$, peak shear stress, "$\boldsymbol{\tau_{max}}$" , shear displacement at peak, $\delta_{h,peak}$, the maximum shear displacement, $\delta_{h,max}$, peak friction angle, ϕ_{max}.

Test	$\boldsymbol{i}$ [°]	**N** [kN]	**H** [kN]	$\boldsymbol{\delta_{h,peak}}$ [mm]	$\boldsymbol{\sigma_n}$ [MPa]	$\boldsymbol{\tau_{max}}$ [MPa]	$\boldsymbol{\phi_{max}}$ [°]	$\boldsymbol{\delta_{Hmax}}$ [mm]	**Comments**
1.1	40	69.12	325.76	3.16	1.2	5.65	77.72	27.89	bonded
1.2	40	126.72	418.75	3.71	2.2	7.27	73.19	27.90	bonded
1.3	40	126.72	272.45	1.93	2.2	4.73	65.2	25.38	
1.4	40	184.32	433.07	2.92	3.2	7.52	66.80	33.42	
2.1	20	69.12	272.45	2.34	1.2	4.73	75.93	33.18	bonded
2.2	20	126.72	203.90	1.96	2.2	3.54	59.08	28.14	
2.3	20	184.32	293.22	3.44	3.2	5.09	57.71	33.18	
3.1	10	69.12	89.10	3.27	1.2	1.54	51.90	30.4	
3.2	10	126.72	113.47	2.23	2.2	1.97	41.52	33.18	
3.3	10	184.32	145.15	1.60	3.2	2.52	38.34	33.18	
4.1	0	69.12	215.42	2.07	1.2	3.74	74.3	33.18	bonded
4.2	0	184.32	92.73	0.53	3.2	1.61	26.78	33.18	

Table 19. Results from the direct shear tests conducted at LTU.

4.7 Analsysis of the laboratory test results.

4.7.1 Discussion of the test results

The results showed that an increase in the angle of the asperities lead to an increase of the peak shear stress reached. Figure 81 and 82 show the shear stress-horizontal displacement curves for each surface profile tested and for a normal stress applied of 3.2 MPa and 2.2 MPa, respectively. Looking at the graphs, it becomes evident how an increase in the concrete-to-rock interface roughness influences the shear resistance. For example, for an asperity angle of 40º and 3.2 MPa, the peak shear stress obtained was 7.52 MPa, while for the flat surface profile the maximum shear stress reached was 1.61 MPa, which means that the peak shear stress when i=40º is almost 5 times higher than in the flat surface profile case. If the peak shear stresses obtained for i=40º and i=10º for a normal stress applied of 2.2 MPa are compared it is also evident how much the roughness plays a key role in the shear capacity of the joint. The peak shear stress reached for i=40º and i=10º was 4.73 MPa and 1.97 MPa respectively, which means that when the angle of the asperities is 40º, the shear capacity is almost 2.5 times higher than when the asperity angle is 10º. For the shear response for i=10º and i=0º, it is remarkable that the increase of the shear stress at the end of the curves is not representing that the shear capacity increases, this increment observed is due to the fact that sample has reached the other side of the box in the shear machine.

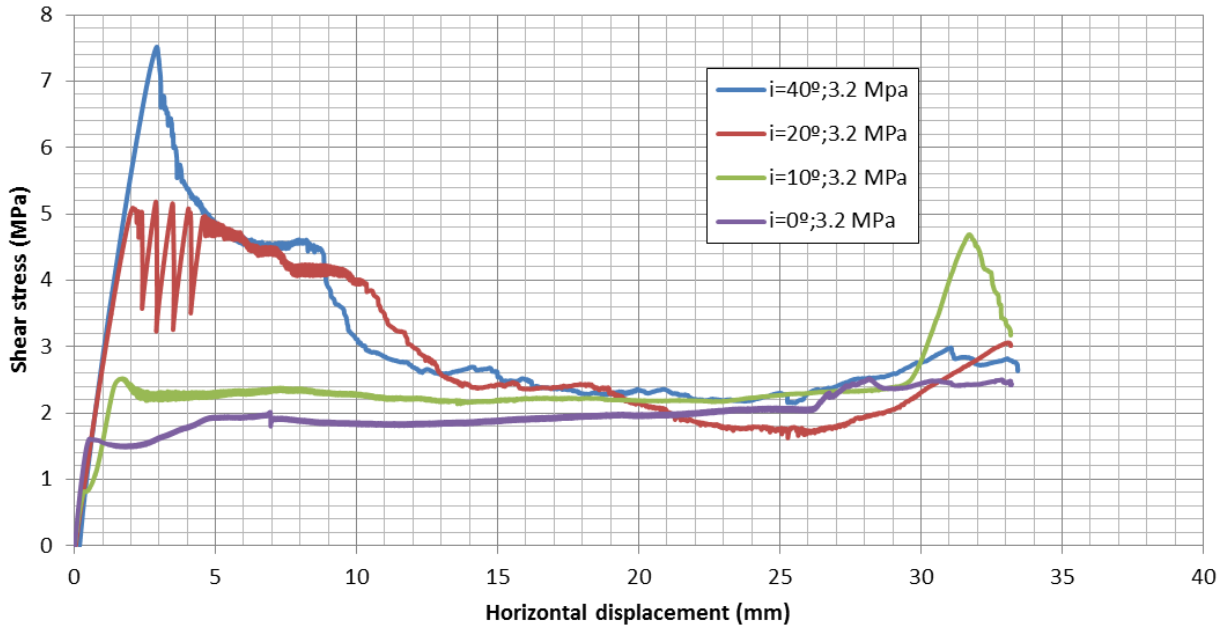

Figure 81. Shear stress response for the different asperity angles tested and a normal stress of 3.2 MPa.

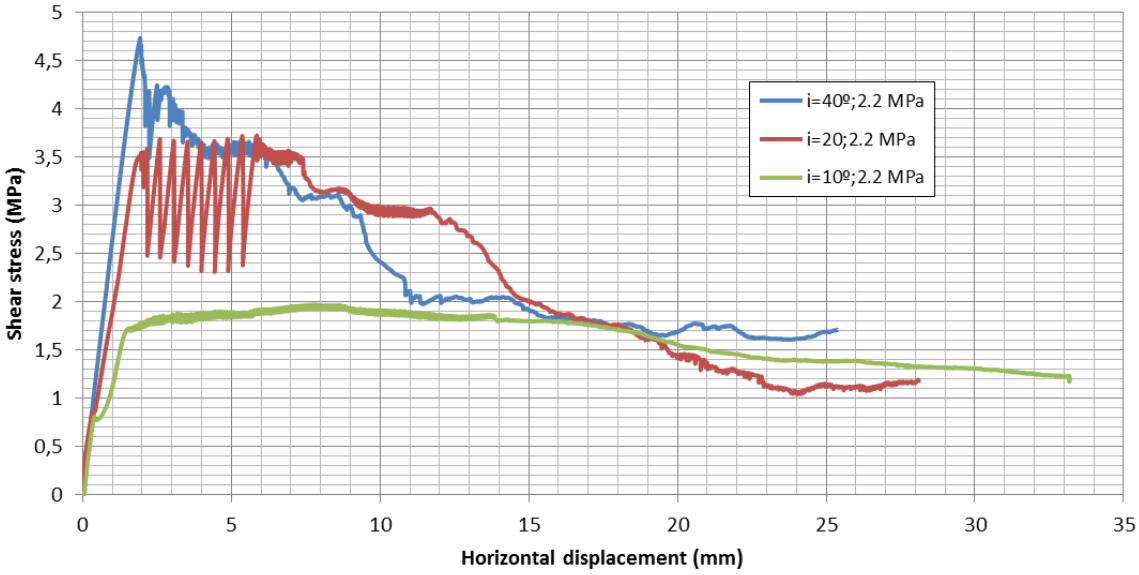

Figure 82. Shear stress response for the different asperity angles tested and a normal stress of 2.2 MPa.

The shear response is more brittle for higher asperity angles, as for example for i=40º and i=20º, we can see that after the peak shear shear has been reached, the curve is characterized by abrupt drops in the shear stress. On the other hand, for lower asperity angles as 10º or for flat surface profiles, the shear response seems to be uniform after the peak shear stress has been reached. The reason of these differences is that the asperites fail in different modes depending on their geometry (i.e. the angle of the asperities). For high values of asperity angle, 40º and 20º, the asperities are sheared off and for low values, sliding is the governing failure mode. These results are consistent with what has been presented in the literature study; see for example (Johansson, 2009). Comparing with the results obtained by Liahagen (2012) where the normal stresses applied were lower, for the i=40º and i=10º the shear response is similar, this means that the normal stress does not influence the shear behavour for 40º and 10º asperity angle. For the 20º asperity angle, the situation is different because for low normal stresses applied, sliding was the failure mode occuring but as the normal stress applied was increased, the initial failure mode was sliding, but this sliding was not uniform but it consisted of abrupt displacements which explains the sudden drops on the shear stress-horizontal displacement for i=20º in Figures 81 and 82. The shearing off the asperities started then because the normal load applied was too high for the small contact area.

Figure 83. Test 2.3 asperities failing.

It is remarkable the fact that the wear of the rock asperities seemed to be not influenced by the normal stress applied but for the angle of the asperities. For i=10º and i=20º, there was no

significant rock asperity wear for any of the normal stress tested but for i=40, the asperities showed more wear regardless the normal stress applied. On the other hand, the concrete asperities wear seemed to be depending both on the normal stress applied and on the asperity geometry. For the i=10º, the concrete asperites were not sheared off as the sliding was the failure mode occuring but it was observed wear of the concrete asperites. This wear increased as the normal stress applied increased for the same asperity angle.

The normal stress strongly influenced the shear resitance of the concrete-to.-rock joint tested. Figure 84 shows the shear stress-horizontal displacement curve for an asperity angle of 40 and for the two normal stresses tested, 2.2 MPa and 3.2 MPa. Lookiong at the Figure 84, it is evident that as the normal load increases, so it does the peak shear stress obtained. In this case, the maximum shear capacity reached for a normal stress of 3.2 MPa and 2.2 MPa was 7.52 MPa and for 4.73 MPa, respectively. This means that increasing the normal stress 1 Mpa for the same asperity geometry, the shear capacity reached is over 1.5 times higher.

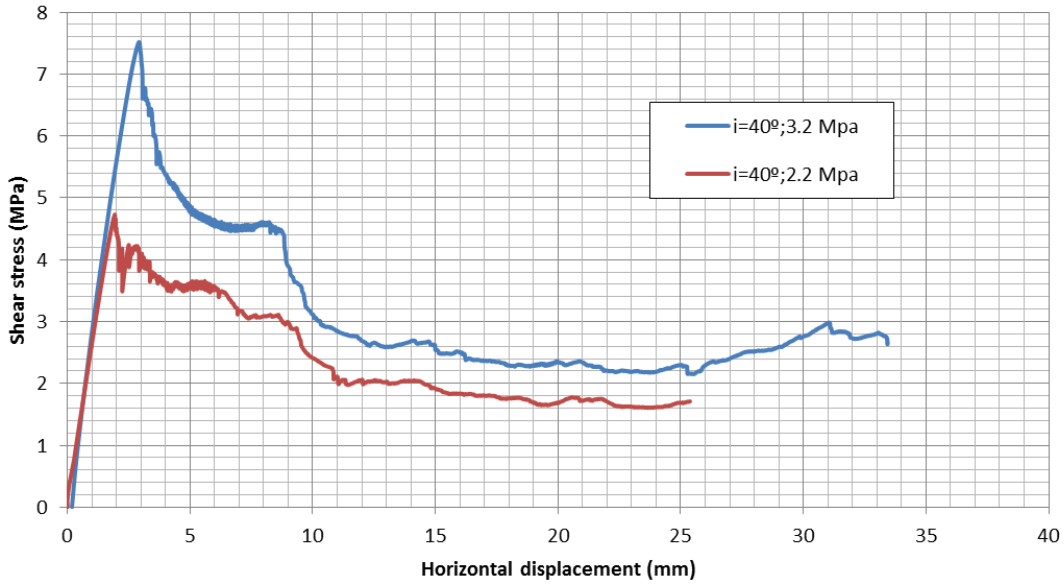

Figure 84. Shear stress response for different normal stresses and 40 asperity angle.

Figure 85 shows the comaprison of the shear stress response for the two normal stress levels tested (2.2 MPa and 3.2 MPa) and for 20 degrees asperity angle. As it can be seen, the curves are very similar due to the fact that the failure mode is the same in both tests (shearing off the asperities) but with the obvious difference in the peak shear stress reached. The maximum shear

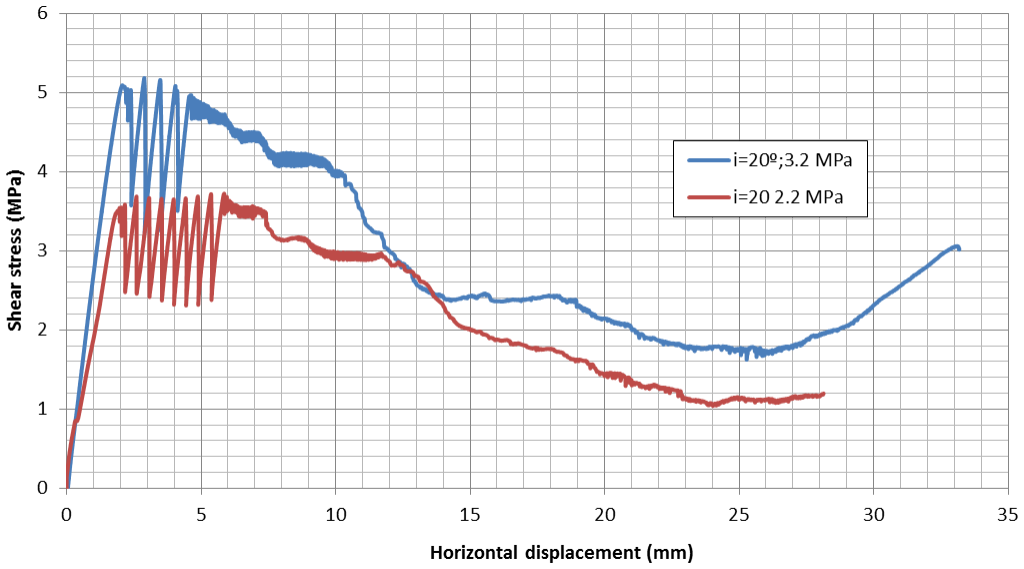

Figure 85. Shear stress response for different normal stresses and 20 asperity angle.

capacity obtained for 3.2 MPa was 5.09 MPa, while for 2.2 MPa, the maximum shear resistance reached a value of 3.54 MPa. The Figure 86 is showing the influence of the normal stress applied when the angle of the asperities at the interface is 10 degrees. Again and as it happened with the other asperity angles, as the normal stress applied increases, the shear capacity of the joint increases as well. In this case the peak shear stress reached for a normal stress of 3.2 MPa was 1.97 MPa and for a normal stress of 2.2 MPa was 1.54 MPa.

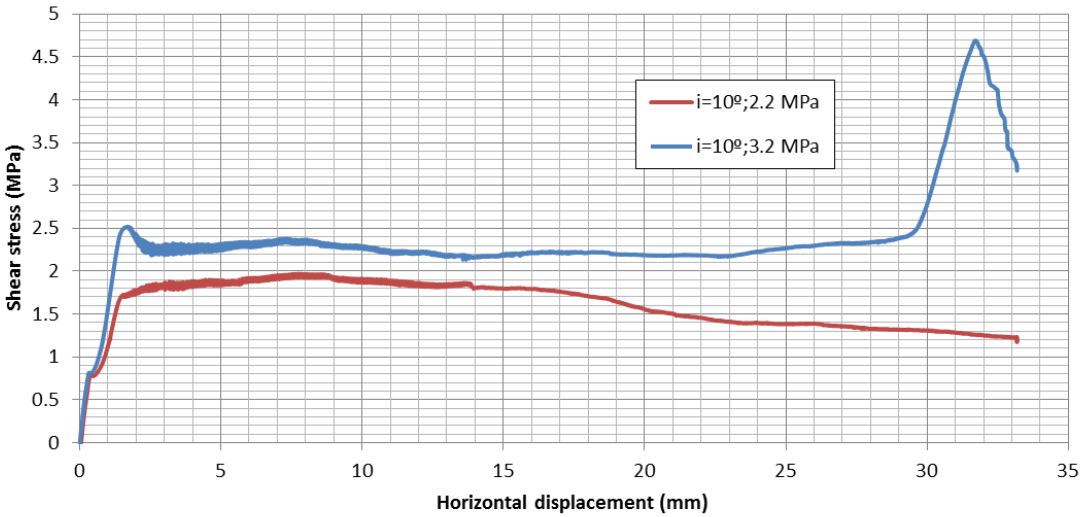

Figure 86. Shear stress response for different normal stresses and 10 asperity angle.

Figure 87 is showing the variation of the peak shear stress obtained for the different normal stress levels tested and for each surface profile. As it can be seen, it is evident that both the roughness and the normal stress applied play a key role in the shear capacity of the joint. It is remarkable that the influence of the normal stress in the shear capacacity becomes higher as the asperity angle increases. The difference between the maximum shear capacity obtained for 2.2 MPa and 3.2 MPa is 0.43 MPa, MPa and MPa for 40, 20 and 10 asperity angle, respectively. Figure 88 shows the shear capacity increment when the normal stress goes from 2.2 MPa to 3.2 MPa for each asperity angle tested.

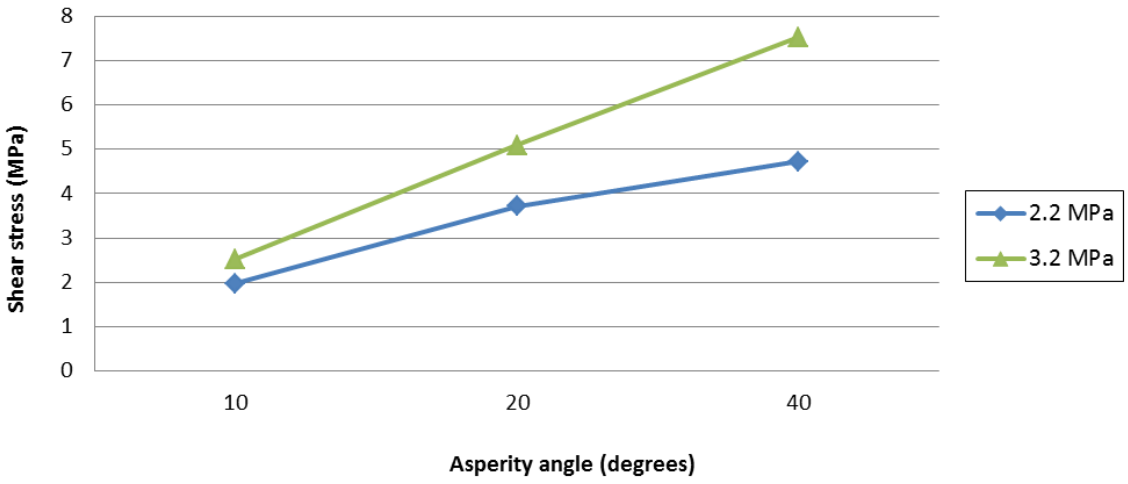

Figure 87. Variation of the peak shear stress with asperity angle for a normal stress of 2.2 and 3.2 MPa.

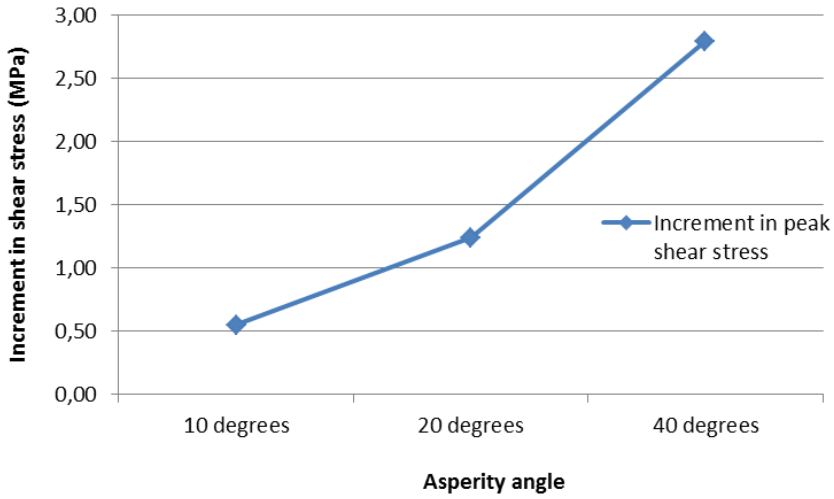

Figure 88. Variation of the shear capacity increment with the roughness.

As it was done in the direct shear tests carried out by Liahagen (2012), to study the effect of the cohesion in the shear capacity between the concrete and the rock, 4 tests were carried out

with bonding. The shear capacity experiences a strong increment when bonding is present, as we can see in Figure 89, where the shear stress response for i=40 and 2.2 MPa normal stress for bonded and unbonced specimens is compared. For the bonded specimen, the shear capacity obtained was 7.27 MPa while for the unbonded specimen a value of 4.73 MPa was observed.

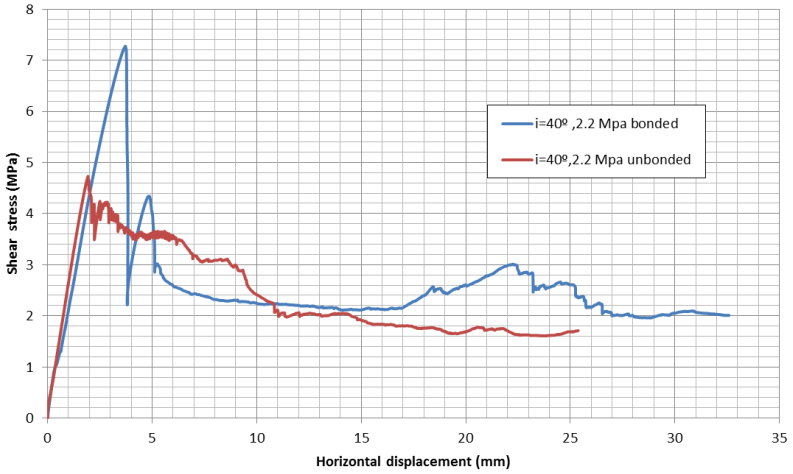

Figure 89. Shear stress response for test 1.2 and 1.3 (bonded and unbonded specimens).

The shear response for the specimens tested with bonding was characterized by a brittle behavour as it was observed in the tests conducted by Liahagen (2012). For the specimens tested with bonding the curve shear stress-horizontal displacement is very similar in shape, as it can be seen in Figure 90. It is characterized by an abrupt drop in shear stress right after the peak shear stress has been reached. The Figure 90 also shows that even when bonding is present, an increase in the roughness of the joint leads to a higher shear capacity.

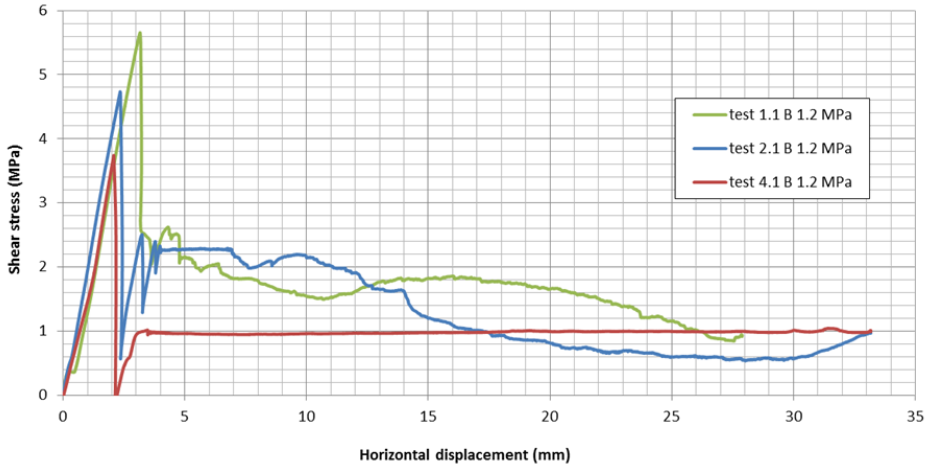

Figure 90. Shear stress response for tests 1.1, 2.1 and 4.1 (bonded specimens).

The different shape of the curves after the peak shear stress has been reached is due to different failure modes occuring. For example, for the red curve in Figure 90 which is the one corresponding to the test 4.1 (flat surface) the failure followed the horizontal interface and then it slided and that is why the curve is flat after the abruot drop. For the test 1.1 (i=40 degrees and 1.2 MPa) the failure also followed the interface and for the tests 1.2 (i=40 degrees and 2.2 MPa) the failure started in the concrete and then it ended up in the rock as it can be seen in Figure 100. It is important to remark that the specimen with bonding and i=40 degrees was initially tested for a normal stress of 3.2 MPa, but it reached an horizontal load of 500 kN, which is the maximum capacity of the shear machine, without breaking. Therefore it was decided to decrease the normal load applied and the specimen was tested with a normal stress of 2.2 MPa (test 1.2).

Even though Figure 90 shows that an increase in the roughness of the joint implies an increase of the peak shear stress reached, the influence of the roughness is not that relevant as it is when the bonding is not present. Figure 91 shows how the influence of the roughness in the shear capacity changes depending on whether the bonding is present or not. For example, if the peak shear stress when bonding is not present is compared for i=40 and i=0 (for a normal stress of 1.2 MPa), an increment in the shear capacity of 467 % is observed. On the other hand if we compared the shear capacity reached for i=40 and i=0 (for a normal stress of 3.2 MPa) when bonding is present, only an increment of 151 % is observed. This indicates that when bonding is present the influence of the joint roughness in shear capacity is not that significative as it is when there is no bonding.

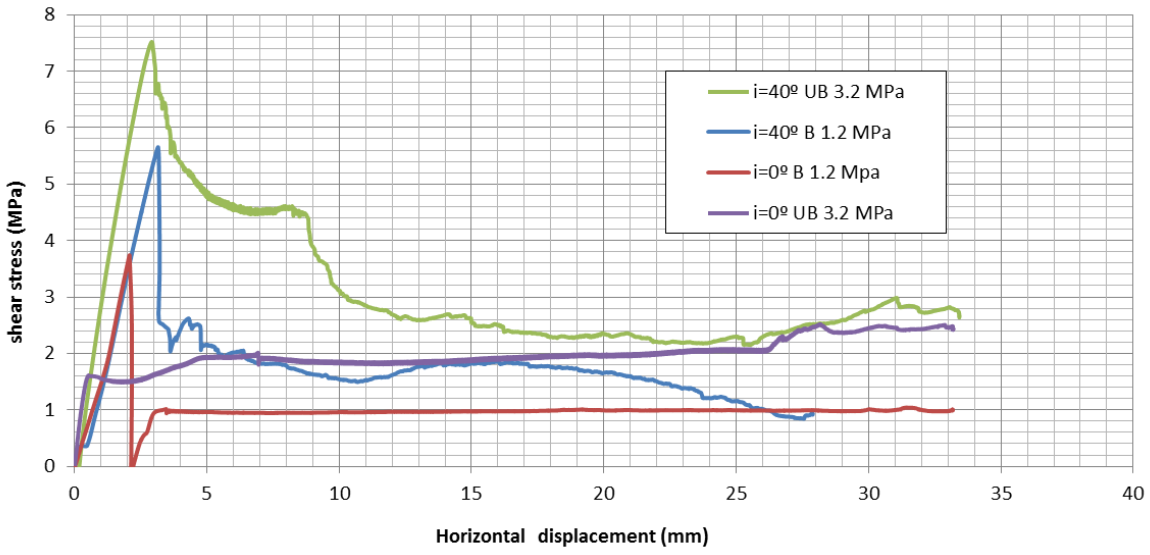

Figure 91. Shear stress response for tests with bonding and without bonding for i=40º and i=0º.

As it was the case in the tests carried out by Liahagen (2012), the angle of asperities strongly influenced the shear capacity of the concrete-to-rock joint. As it can be seen in Figure 91, for a fixed normal stress, the maximum friction angle increases as the angle of the asperities increases. For example, when the normal stress is 2.2 MPa, the maximum friction angle obtained is 65.2º, 59.08º and 41.52º for an asperity angle of 40º, 20º and 10º, respectively.

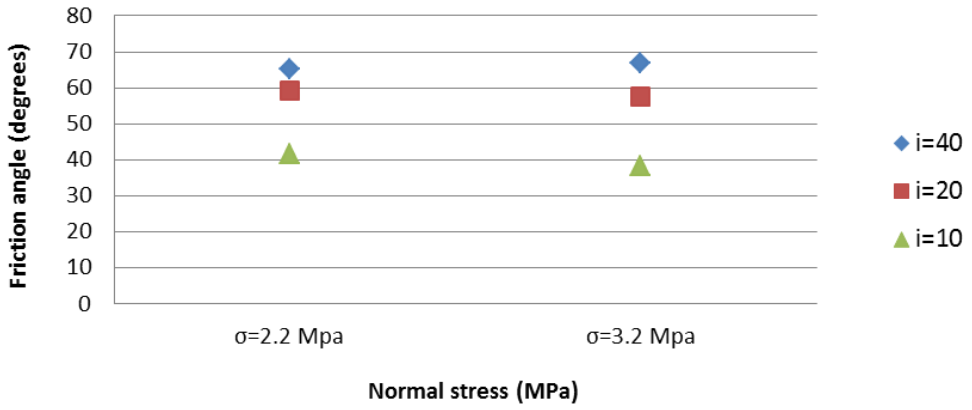

Figure 92. Variation of the friction angle with the asperity angle and normal stress applied.

The Figure 93 shows the variation of the friction angle with the shear displacement for the different surface profiles tested and for a normal stress of 3.2 MPa. If we take a look at the test with flat surface, (i.e. 0 º asperity angle profiles), the basic friction angle can be estimate as it was done in section 4.2.4 .In this case, the basic friction angle of this concrete-to-rock joint can be estimated as approximately 30º.

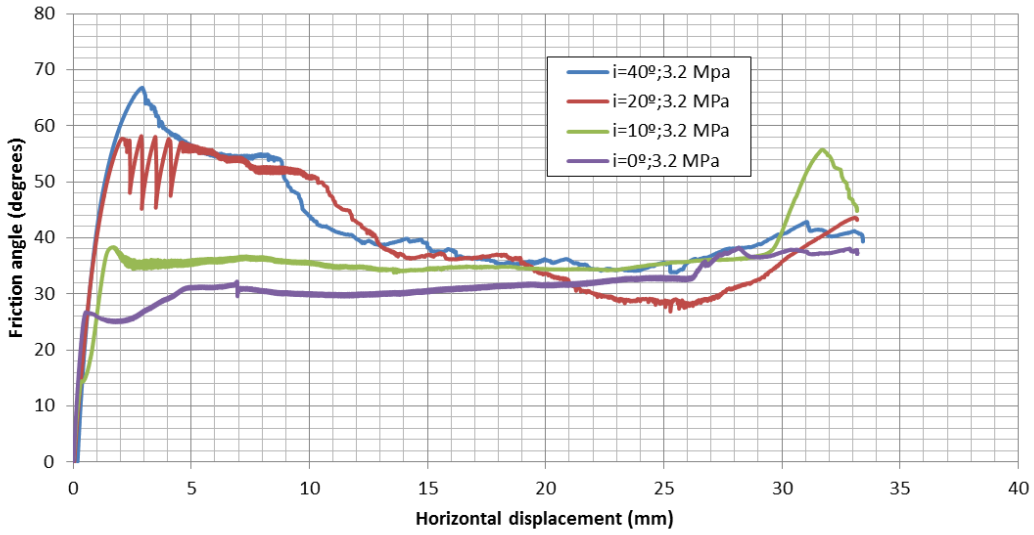

Figure 93. Friction angle variation with horizontal displacement for each roughness tested.

4.7.2 Testing results into shear strength failure criterions

As it has been done with the test results from Liahagen (2012), the results of the direct shear tests conducted in this thesis have been tested into commonly used models that are used to estimathe the shear capacity of rough rock joints. The same models that were used in section 4.2.5 have been used in this analysis. Thereofore, four different shear strength failure criterions have been used:

1. Mohr-Coulomb criterion.
2. Patton's bilinear criterion.
3. Barton & Choubey criterion.
4. Maksimovic criterion.

The normal stress levels used as input data are 2.2 MPa and 3.2 MPa, and the basic friction angle of the concrete-rock interface is 30 degrees. The comparison between the observed values in the tests and the values predicted by each shear failure criterion asperity angle tested is presented in Figure 94.

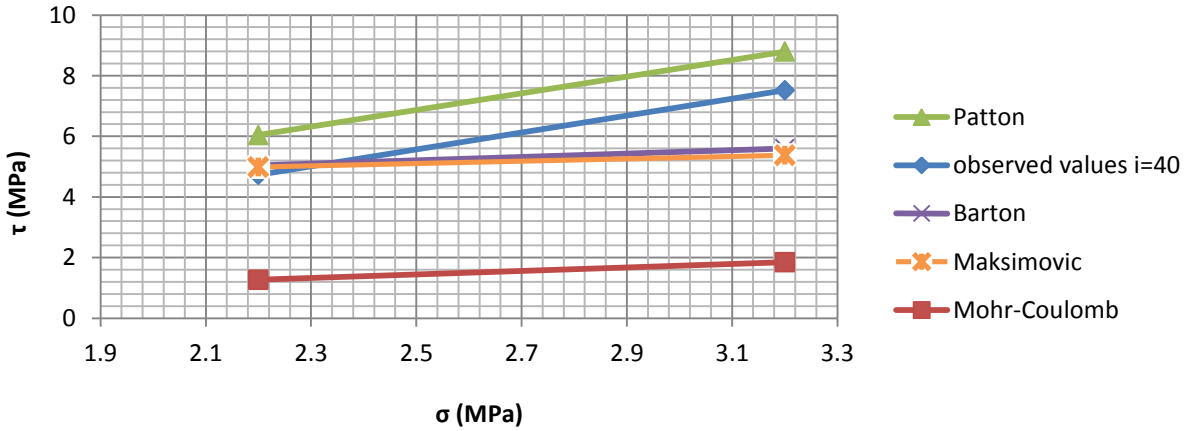

(a)

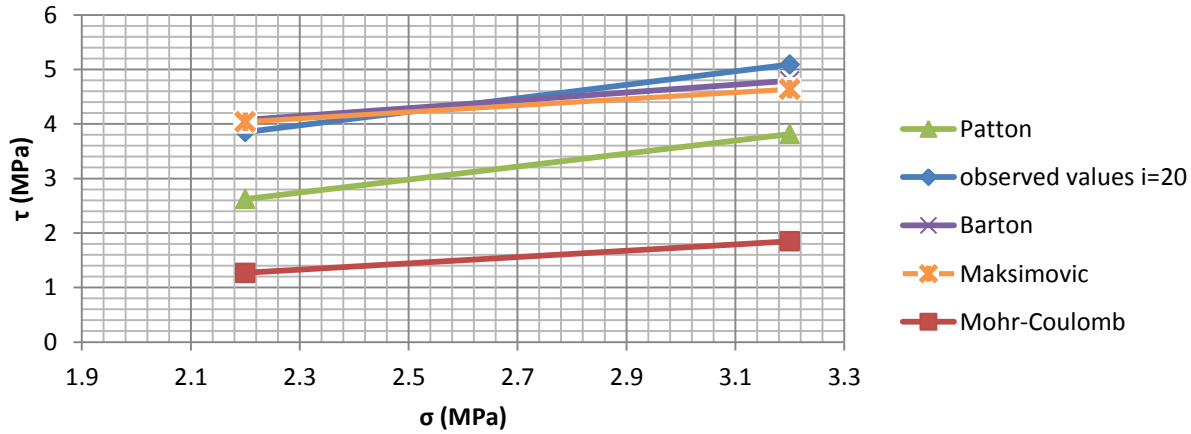

(b)

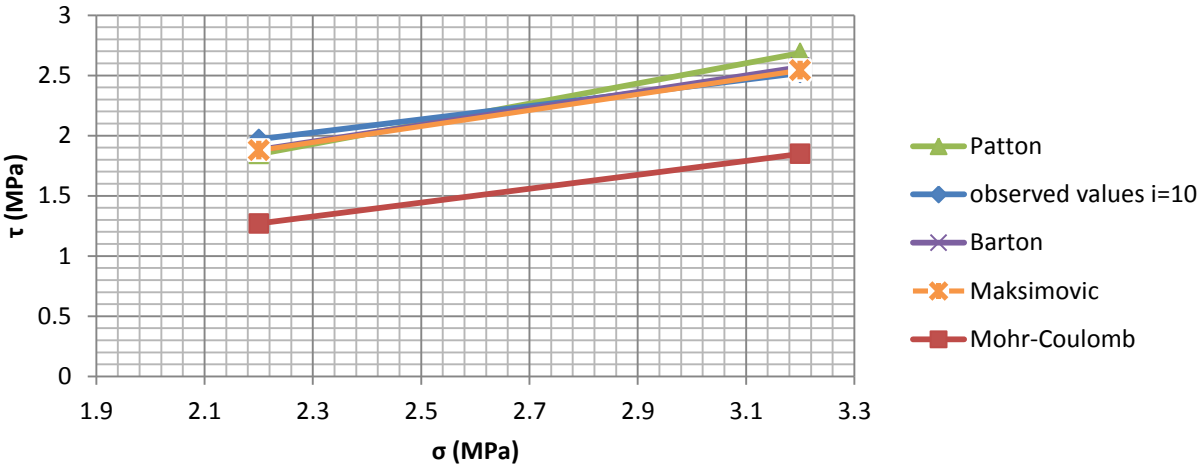

(c)

Figure 94. (a) Comparison between observed and predicted shear capacity envelopes for i=40º (b) Comparison between observed and predicted shear capacity envelopes for i=20º (c) Comparison between observed and predicted shear capacity envelopes for i=10º

As expected, the Mohr-Coulomb failure criterion is the one that gives the worst correlation between the observed and the predicted shear stress values. As it was explained in section 4.2.5, the reason of this is because this shear strength failure criterion does not take into consideration the roughness influence into the shear capacity and thus it underestimates the shear capacity between the concrete and the rock. For example, for i=40 and a normal stress of 3.2 Ma , the shear capacity observed was 7.52 MPa, while the Mohr-Coulomb model gives a value of 2.24 MPa, which is over three times lower than the actual shear resistance observed.

The bilinear shear strength criterion proposed by Patton (1966) does not give a good correlation between the actual and predicted values either. For 40 degrees asperity angle, the Patton's criterion gives overestimates the actual shear capacity of the joint, this is due to the fact that the asperities are sheared off for i=40 degrees. On the other hand, for 20 degrees asperity angle, this shear strength failure criterion gives shear stress values that are lower than the actual values observed. For low angle of asperities as for i=10 degrees, this model gives a good correlation between actual and predicted vales of peak shear resistance.

In order to test the failure criterions proposed by Barton & Choubey (1977) and Maksimovic (1997), the following JRC and JCS parameters were selected. The parameters were calibrated in order to give the best fit with the oberved peak shear stress values.

JRC (roughness parameter)	JCS (MPa)
38	20
33	20
11	20

Table 20. Table 21. JRC and JCS used in Barton`s and Maksimovic's model equation.

It is remarkable that the JRC parameters seleced for 20 and 40 degrees asperity angle are out of the range that Barton & Choubey (1977) proposed. The model proposed by Maksimovic (1997) also gives a good correlation for an asperity anlge of 20 and 10 degrees but for 40 degrees it does give correlation for a normal stress of 2.2 MPa, but not for a normal stress of 3.2 MPa. As it can be seen from Figure 94, the model proposed by Barton & Choubey is the one that gives the best correlation between the observed and predicted shear stress values.

4.7.3 Comparison between tests 2012 and 2013

The shear stress responses from the tests carried out by Liahagen (2012) and from the tests conducted within this thesis are presented together in Figure 95. The first figure is showing the shear stress-horizontal displacement for i=40 degrees and for each normal stress level tested. Note that the rock type used in the tests carried out in 2012 by Liahagen (2012) was granite and the rock type used in the tests conducted during this thesis is gneiss.

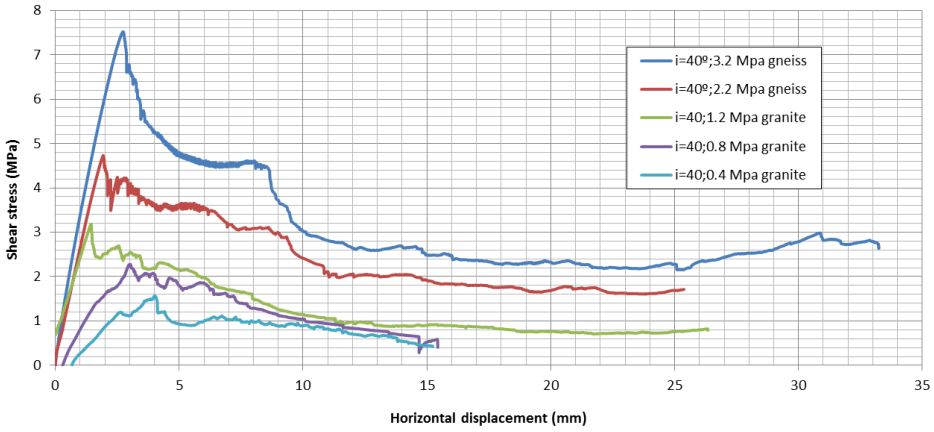

(a)

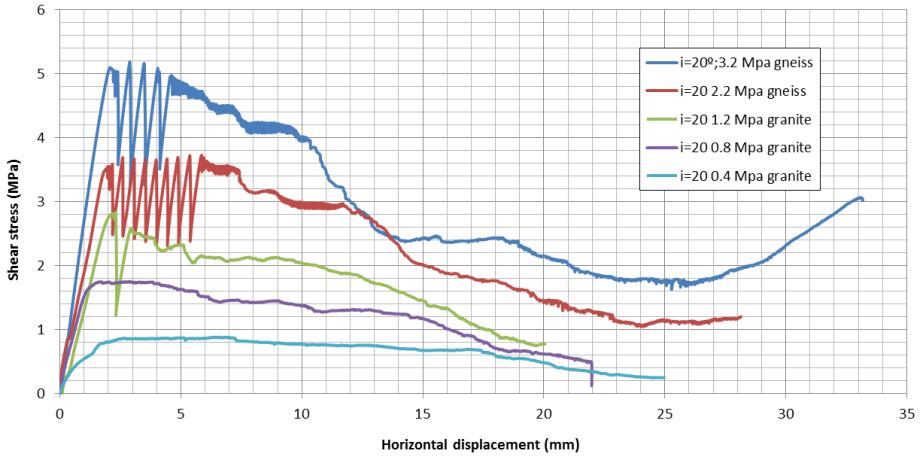

(b)

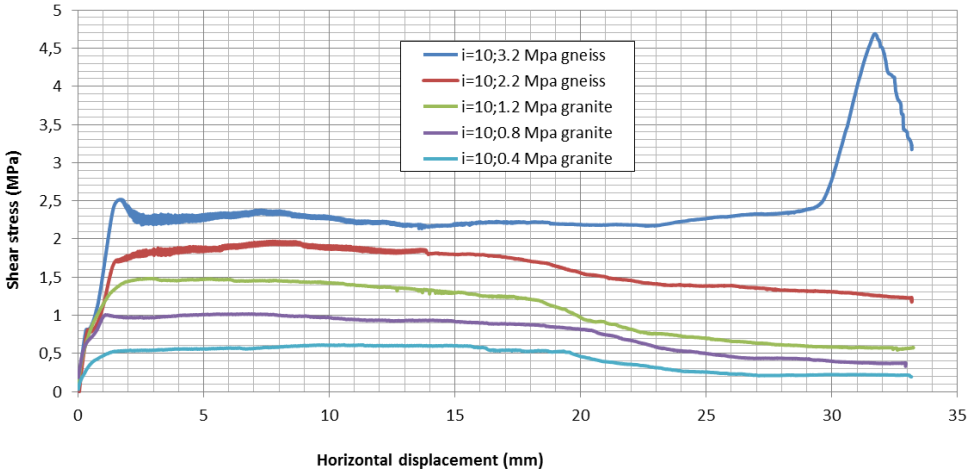

(c)

Figure 95. (a) Variation of the shear stress with horizontal displacement for i=40 from test 2012 and 2013 (b) Variation of the shear stress with horizontal displacement for i=40 from test 2012 and 2013 (c) Variation of the shear stress with horizontal displacement for i=40 from test 2012 and 2013.

As it can be seen from Figure 95, as the normal load increase, so it does the shear resistance between the concrete and the rock. The shape of the curves for i=40 degrees and i=10 degrees are very similar for both rock types used. This is because regardless the normal stress or the rock type used, the failure mode of the asperities was shearing and sliding for i=40 and i=10 respetively. For i=20 degrees, for low normal stress the curve is uniform because sliding is the failure mode occuring and for higher normal stresses, it can be seen that the shear response is more brittle with abrupt up and downs in the curve, this is because the failure mode changes to shearing off the asperities.

Figure 96 is showing the shear stress-horizontal displacement curve for the test with i=10 degrees and a normal stress applied of 1.2 MPa for the test carried out in 2012 with granite as rock type and for the test carried out this year with gneiss as rock type. Looking at the figure, it can be conclude that the shear stress response are very similar and therefore the rock type did not have much influence in the shear capacity between the concrete and the rock.

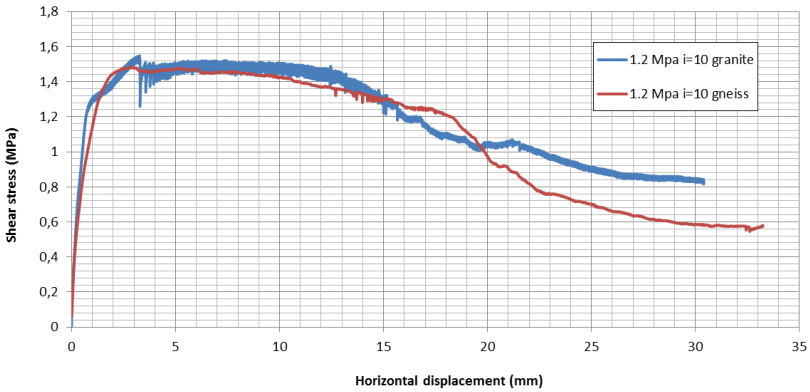

Figure 96. Comparison betwee the shear stress variation with horizontal displacement for i=10 degrees and 1.2 MPa for tests conducted in 2012 (granite) and 2013 (gneiss).

The basic friction angle varied from the tests carried out with granite, which was 35 degrees, and for the tests carried out this year with gneiss, which had a value of 30 degrees. Figure 97 shows the variation of the friction angle over the horizontal displacement for the tests carried out with granite and for the tests carried out with granite.

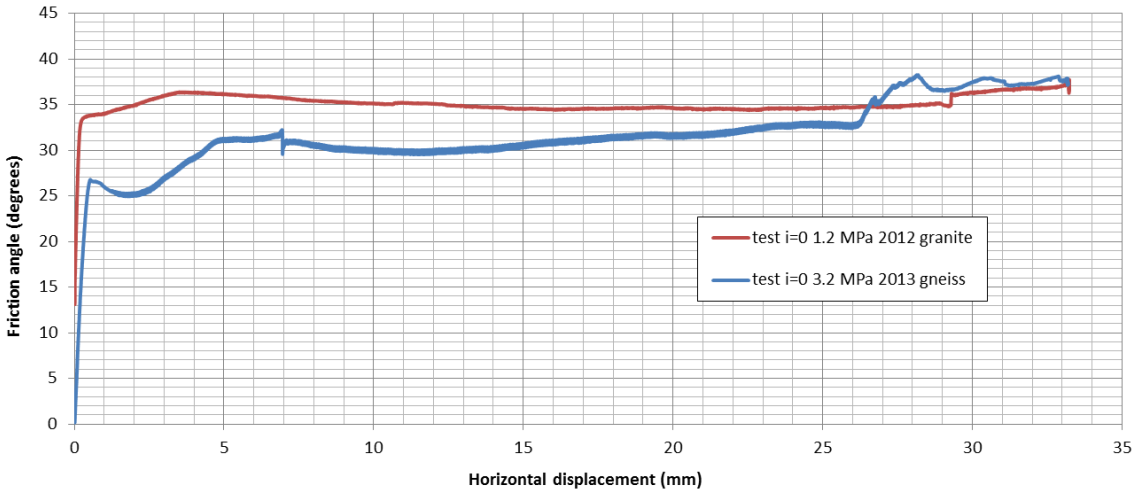

Figure 97. Variation of the friction angle over the horizontal displacement for 2012 and 2013 direct shear tests.

This also shows that the actual criterion used by the NVE guidelines to estimate does not reflect the reality of what is happening at the interface dam-rock, because the basic friction angle that is reccommended to use by the NVE when estimating the shear capacity is 45 degrees, and the basic frition angle found from the tests conducted by Liahagen (2012) was 35 degrees where the rock used was a sound granite. On the other hand, for the tests conducted this year where the rock type used was gneiss, the basic friction angle was found to be 30 degrees. Therefore, the Mohr-Coulomb criterion used in the NVE guidelines underestimates the shear strength between the dam and the rock due to the fact that it does not taken into consideration the roughness of the concrete-to-rock interface but also overestimates the friction factor $tan(\phi_b)$.

4.7.4 Comparison with NVE guidelines

As it was done in section 4.2.6, the test results are compared to the NVE guidelines for sliding stability of concrete dams. The maximum allowable horizontal load for a normal loading combination (safety factor = 1.5) is calculated by dividing the maximum horizontal load by the safety factor, as it has been done in section 4.2.6. Figure 97 shows the maximum allowable horizontal loads for each asperity angle and each normal load used in the tests. Above those lines the loads are considered as unstable against sliding a safety factor of 1.5. As we can see from the figure, as the roughness increases so it does the maximum horizontal loads considered as safe against sliding. It is interesting to remark that the envelop of maximum allowable horizontal loads for NVE is higher than the one calculated for i=10 degrees, the reason behind this is because the NVE guidelines uses a basic friction angle of 45 degrees and the basic friction angle calculated from the tests was 30 degrees.

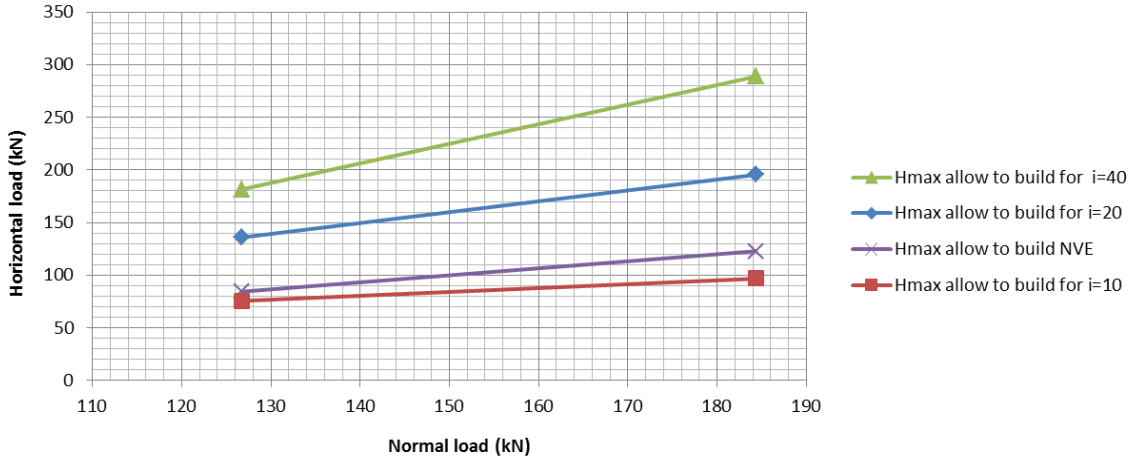

Figure 98. Variation of the maximum allowable horizontal loads envelopes for each asperity angle and for NVE guidelines.

Looking at the Figure 98, it becomes evident how conservative is the criterion used nowadays by the NVE guidelines to estimate the shear resistance between the dam and rock. It can be seen that if the effect of the roughness was incorporated to the shear capacity, a higher horizontal loads would be considered as safe against sliding and therefore it is clear that the actual NVE guidelines underestimates the and does not solve satisfactorily the problem. For example, if the case with a roughness of 40 degrees is considered for a horizontal load of 150 kN and a normal load of 126.72 kN (which is equivalent to the normal stress used in the tests 2.2 MPa), the dam would be stable against sliding. Since that load combination is below the green line att he Figure 98, but for that load combination, according to NVE the dam would be very far to be safe againt sliding. In order to show how the bonding between the concrete and the rock influences the maximum allowable horizontal loads, the Figure 99 shows a comparison between the maximum allowable loads obtained from the specimens tested with bonding and the ones obtained according to NVE guidelines. Looking at the figure below, it becomes obvious the bonding greatly increases the maximum allowable horizontal loads. For example, if we consider a dam subjeced to an horizontal laod of 200 kN and a normal load of

69.12 kN (equivalent to a normal stress fo 1.2 MPa used in one of the tests), according to the tests the dam would be safe against sliding but it would not be stable according to the NVE guidelines.

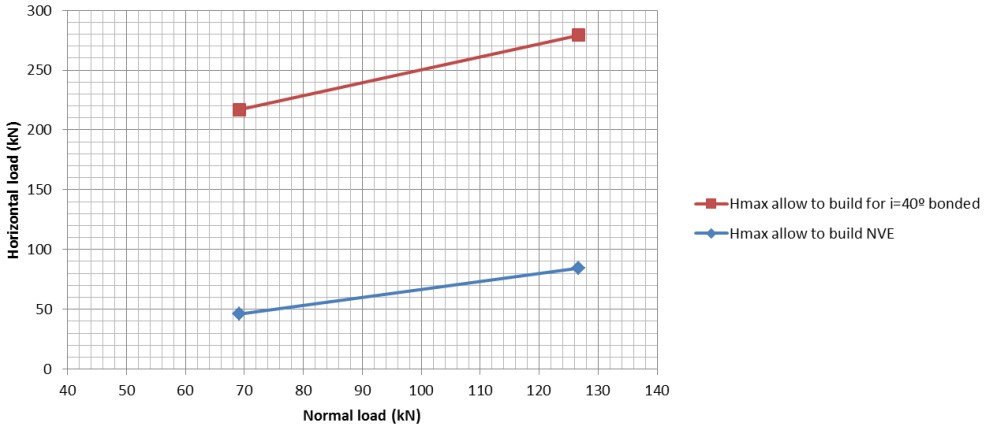

Figure 99. Comparison between the maximum allowable horizontal loads for bonded specimens and for NVE guidelines.

4.7.5 Validation of the proposed model

The model proposed in section 4.2.7 based on the test results conducted by Liahagen (2012) is validated in this section by using the test results obtained in the direct shear tests conducted within this thesis. The equation proposed to estimate the peak shear strength of concrete-to-rock joints with triangular aspertites on the interface can be expressed as:

$$\tau_p = \sigma_n \cdot \left(tan(\phi_b \cdot k_r)\right) \quad ;$$
$$k_r = -3.7141 \cdot i^2 + 4.2315 \cdot i + 0{,}8609; \qquad i = angle\ of\ asperities\ (radians)$$

The comparison between the peak shear stress values predicted by the proposed model and the actual peak shear stress values observed in the direct shear tests is shown in Figure 100. The proposed model seems to give a fair correlation between actual and predicrted values for an asperity angle of 20 degrees. For 10 degrees asperity angle, the correlation is good for a normal stress of 2.2 MPa but it does not seems to give that good correlation for a normal stress of 3.2 MPa. Finally, for the highest roughness tested, i=40 degrees, the comparison in figure below indicates that the correlation is not good. In general it could be concluded that in the range of low to medium asperity angles, the model gives a good correlation but for high roughnesses as for i=40 degrees, it does not give good correlation between predicted ans observed values.

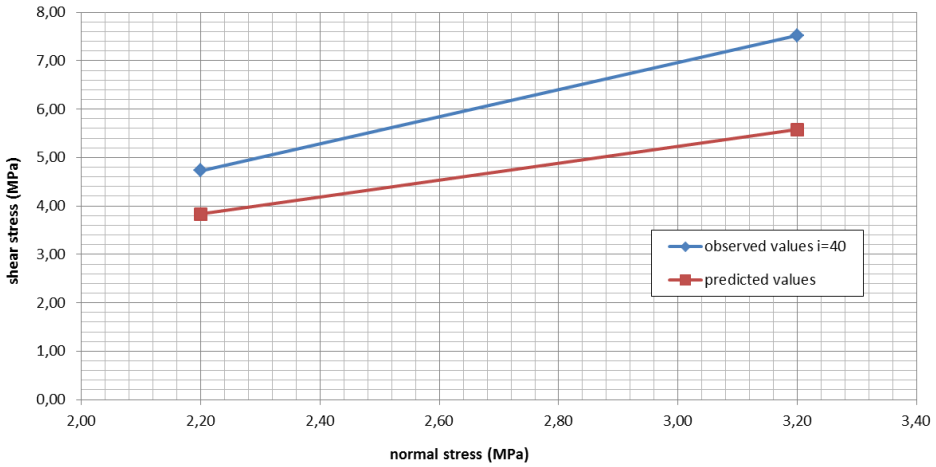

(a)

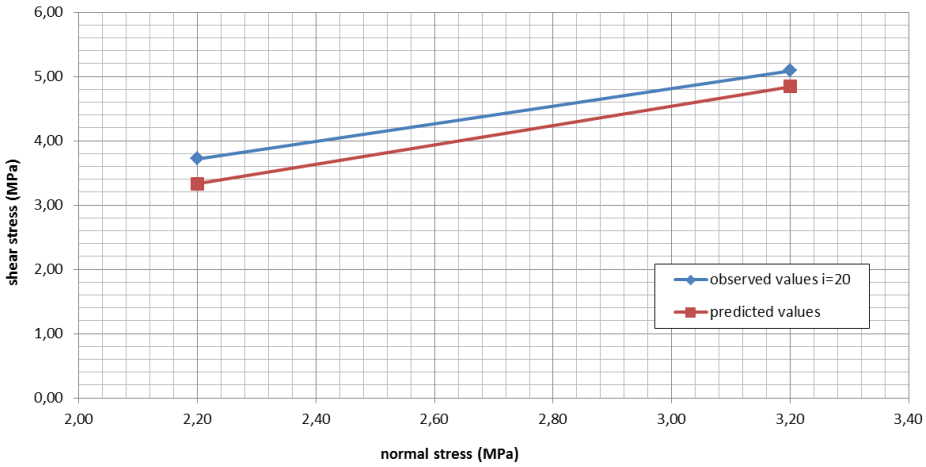

(b)

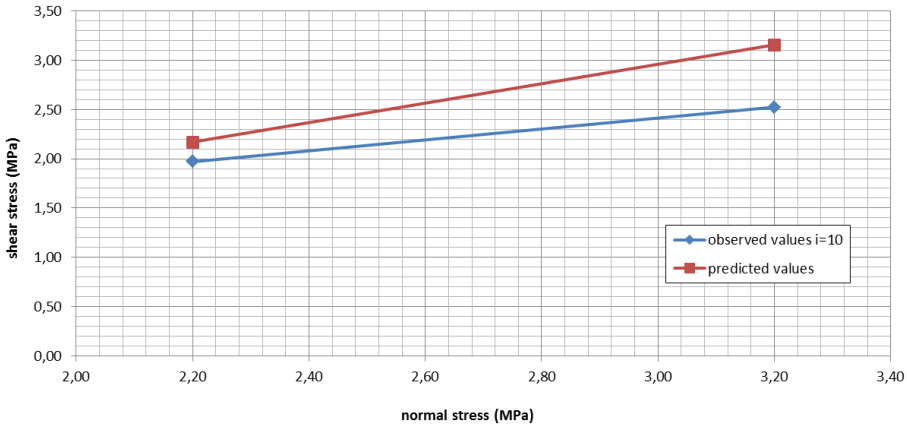

(c)

Figure 100. Validation of the proposed model. Comparison between predicted and observed peak shear stress values for (a) i=40 degrees (b) i=20 degrees and (c) i=10 degrees.

4.8 Summary

In this chapter the direct shear tests conducted at Luleå University of Technology (LTU) are introduced and the results from it are presented and analyzed. In order to study the influence of the roughness in the shear capacity between the dam and the rock, a series of direct shear tests were decided to implement in this thesis. In order to study the effect of the roughness the concrete-rock interface was artificially manipulated and shaped with triangular asperities, which have the same geometry over the whole surface of the interface. In total 12 tests were conducted at LTU and four different profiles were tested:

- 40 degrees asperity angle.
- 20 degrees asperity angle.
- 10 degrees asperity angle.
- 0 degrees asperity angle (flat surface).

The results from the shear tests conducted within this thesis are analyzed and discussed along with the tests carried out by Liahagen (2012). The rock type and the normal stress levels used in the tests are the only two differences between the two test series conducted in 2012 and in 2013. For the tests carried out last year, the rock type used was granite and this year it was decided to use gneiss. The normal stress level tested in 2012 were 0.4 MPa, 0.8 MPa and 1.2 MPa and for the 2013 tests the following were used; 2.2 MPa and 3.2 MPa.

For both test series, an increase of the angle of the asperites led to an increase of the shear capacity between the concrete and the rock. As the normal load applied increased, so it did the shear capacity of the concrete-to-rock joint. In both test series, several specimens were tested with bonding between the concrete and the rock in order to study how this affects the shear resistance. It can be concluded that for both rock types tested, the bonded specimens presented much higher shear capacity than the ones tested without bonding between the concrete and the rock. The governing failure mode of the asperities was sliding and shearing for the 10 degrees asperity angle and 40 degrees asperity angle, respectively in both test series. On the other hand, when the angle of the asperities was 20 degrees, sliding was the failure mode occuring for low normal stresses but for higher normal stresses, the concrete asperities were sheared off.

It remarkable that the for both test series the concrete asperities were sensitive both to the normal stress increment and to the aspertity angle, while the rock asperities failing seemed to be only depending on the angle of the asperities.

The results from the test series in 2012 and 2013 were tested into four different shear strength failure criterions in order to see which one gave the best fit with the actual shear capacity observed in the tests. The four failure criterions used in the analysis were the following; Mohr-Coulomb model, Patton model, Barton and Choubey model and Maksimovic model. The results from the analysis showed that for the test series carried out by Liahagen (2012) the model that gave the best fit with the observed shear resistance was the model proposed by

Maksimovic (1997), although the model proposed by Barton and Choubey gave also good correlation between the predicted and actual shear stress values. For the test series carried out within this thesis, both models, the one proposed by Maksimovic (1997) and the one developed by Barton and Choubey (1977), were the failure criterion that gave the best correlation with the observed shear capacity from the tests.

A comparison of the test results with the NVE guidelines has been also carried out within this chapter for both test series. The maximum allowable horizontal loads for each test were estimated to meet the requiriment of the safety factor for normal loading combination from NVE. It can be concluded that the NVE guidelines clearly underestimate the shear capacity between the dam and the rock by not taking into consideration the influence of the joint roughness. On the other hand, the NVE guidelines overestimate the friction factor used because it is recommended to use a basic friction angle of 45 degrees and the basic friction angle found for both test series was in the angle of 30-35 degrees.

Finally, an equation to estimate the peak shear stress of concrete-to-rock joint with surfaces shaped with triangular asperities is proposed based on the test results carried out by Liahagen (2012). The failure criterion proposed is based on the Mohr-Coulomb model but introducing a factor which incorporates the effect of the roughness into the shear capacity. The proposed model is tested into the test results carried out in this thesis, and the correlation seemed to be fairly good for 10 and 20 degrees asperity angle but not that good for the highest roughness tested, 40 degrees.

5. CONCLUSIONS AND FURTHER RESEARCH

The Mohr-Columb model is used nowadays to estimate the shear capacity between the dam and the rock by the NVE guidelines and this failure criterion to estimate the shear strength does not account the influence of the roughness in the shear resistance. In order to invetigate the effect of the roghness in the shear capacity, a dirct shear tests were conducted by testing concrete agaisnt rock specimens. The surface of the rock specimen was manipulated and shaped with triangular asperities.

The main conclusion that can be drawn of this research is the fact that the roughness strongly influences the shear capacity between the concrete and the rock. As the angle of the asperities of the concrete-to-rock joint increases, the shear capacity reached also experienced an increment. Another important conclusion that can be drawn is that the bonding between the concrete and the rock greatly influences the shear capacity, which was found a lot higher for the specimens tested with bonding than for the ones tested without bonding.

Therefore having proved that both bonding and roughness strongly increase the shear capacity between the dam and the rock, it is evident that the Mohr-Coulomb model used by NVE in their guidelines underestimates the maximum shear load that the dam-rock interface is able to withstand. On the other hand, the basic friction angle recommended using by NVE when assessing the sliding stability is 45 degrees and from the direct shear tests conducted in this thesis the basic friction angle obtained was 35 degrees for granite and 30 degrees for gneiss. This, along with the no consideration of the bonding and the roughness, shows that the actual guidelines given by NVE does not capture what is actually occuring between the concrete and the rock at the sliding plane at any ways.

It it the author believe that is an important need to develop a model that can estimates the shear capacity between the dam and the rock which incorporates the effect of the roughness and of the bonding, a failure criterion which can explain realistically the shear process between the dam and the rock. An attempt to develop a model has been done in this thesis, although only a few tests have been used to create it, the model seems to give a fair correlation for low asperity angles and not that good for higher asperity angles. It is therefore recommended by the author to carry out large amount of direct tests in order to improve the model that has been introduced in this work. An interesting thing would be to prepare the rock foundation by shaping it with triangular asperities in order to have a similar interface shape than in the tests.

Among the recommendations for further research, large amount of tests should be done to generate an equation that incorporates the effect of the roughness, the scale effect should be also considered and large in-situ tests should be carried out, further investigate the bonding effects on shear capacity, to conduct direct shear tests on more rock types to study how much the rock type influence the shear resistance and finally, it would be very interesting to carry out tests with irregular triangular asperities to analyze how this influence the shear capacity.

6. REFERENCES

B. Indraratna, A. Haque and N. Aziz (1997). *Laboratory modelling of shear behaviour of soft joints under constant normal stiffness conditions.*

Barton, N.; Bandis, S.C., (1982). *Effect of block size on the shear behaviour of jointed rock, 23rd U.S. Symp. on Rock Mech., pp. 739-760.*

Barton, N.; Choubey, V., (1977). *The shear strength of rock joints in theory and practice. Rock Mechanics, Vol. 10, pp. 1-54.*

Cai-Chu Xia, Zhi-Cheng Tang, Wei-Min Xiao and Ying-Long Song. *New Peak Shear Strength Criterion of Rock Joints Based on Quantified Surface Description,* (2013). Rock Mech Rock Eng.

CDA. (2007). *Technical bulletin: Structural considerations for dam safety.*

Eltervaag Ø. (2012). *Sliding Stability of Lightweight Concrete Dams. Contribution from Surface Roughness.* Specialization Project. NTNU, IVM, Trondheim, unpublished.

Energi Norge (2012*). Optimal og sikker rehabilitering av betongdammer: Glidestabilitet av betongdammer.* Preliminary unpublished, conducted by Norconsult.

EPRI. (1992). *Uplift pressures, shear strengths and tensile strengths for stability analysis of concrete gravity dams volum 1. Denver, Colorado: Stone and Webster Engineering Corp.*

FERC, The Federal Energy Regulatory Commission, (2002). *Engineering guidelines for the evaluation of hydropower projects,* Chapter III, Gravity dams.

Ghosh, A.K. (2010) *Shear Strength of Dam-Foundations Rock Interface- A Case of Study.* Indian Geothecnical Conference-2010.

Grasselli (2001). *Shear strength of rock joints based on quantified surface description*. Ph.D. Thesis. Ecole Polytechnique Federale de Lausanne.

Johansson, F., (2009). *Shear Strength of Unfilled and Rough Rock Joints in Sliding Stability Analyses of Concrete Dams*. Ph.D. Thesis. Royal Institute of Technology (KTH), Stockholm.

Johansson, F., Gustafsson, A., Rytters, K., Stille, H., (2012). *Proposal for new Swedish guidelines with respect to sliding stability of concrete dams founded on rock.* Workshop: Bærekraftig forvaltning av Betongdammer, Narvik 23.-24. October 2012. Norut. Conducted by KTH and Sweco.

Kodikara and Johnston (1994). *Shear Behaviour of Irregular Triangular Rock-Concrete Joints*. Int. J. Rock Mech. Min. Sci. & Geomech. Abstr. Vol. 31, No. 4, pp. 313-322

Ladanyi, B., Archambault, G. (1970). *Simulation of the shear behaviour of ajointed rock mass*, Proceedings of the 11th U.S. Symposium on Rock Mechanics,Vol. 7, pp.105-125.

Liahagen, S., (2012*) Stabilitet av betongdammer - Ruhetens påvirkning på skjærkapasiteten mellom betong og berg*. Master's Thesis. NTNU, IVM, Trondheim, unpublished.

Maksimovic (1996). *The Shear Strength Component of a rough Rock Joint.*

Negi R. (2012). *Shear and dilation behavior of rock-joints*. M.Sc. Thesis at Department of Civil and Environmental Engineering at Delhi Technological University, Delhi.

Nicholson, G. (1983). *Design of gravity dams on rock foundations: Sliding stability assessment by limit equilibrium and selection of shear strength parameters.* U.S. Army Engineer Waterways Experiment Station, Vicksburg.

Novak, P., Moffat, A.I.B., Nalluri, C. & Narayanan, R. (2007). *Hydraulic structures, fourth edition.* Taylor & Francis.

NVE, Norwegian Water Resources and Energy Directorate, (2005), *Retningslinje for betongdammer.*

Patton, F.D (1966). *Multiple modes of shear failure in rock*. 1st ISRM Congress, September 25 – October 1, 1966, Lisbon, Portugal.

Rocha M. (1964). *Mechanical behavior of rock foundations in concrete dams.*

Ruggeri, G. (2004). *Working group on sliding safety of existing gravity dams.* ICOLD European Club.

Xue F. Gu, Julian P. Seidelnand Chris M. Haberfield (2003). *Direct Shear Test of Sandstone-Concrete Joints.*

List of figures

Figure 1. Sliding resistance of a sliding plane with an inclination angle of α (taken from (NVE,2005)) 5
Figure 2. Plane sliding along a horizontal joint ending in the rock mass plus passive wedge resistance (taken from (Johansson,2009)) 6
Figure 3. Forces acting on a hypothetical dam with inclined sliding planes according to the shear friction method (taken from (Johansson, 2009)) 7
Figure 4. Bilinear failure envelop proposed by Patton (taken from (Johansson, 2009)) 23
Figure 5. (a) Definition of the degree of interlocking. (b) Results according to the bilinear model. (c) Results according to the proposed model. (taken from (Johansson, 2009)) 27
Figure 6. (a) Definition of the dilation rate and the shear area ratio. (b) expected failure enveloped for irregular rock surfaces, and rock mass, respectively. (c) Anticipated variation of dilation rate and shear area ratio with normal pressure. (taken from (Johansson, 2009)) 27
Figure 7. Geometrical identification of the apparent dip angles, in function of the shear direction. 28
Figure 8. Two dimensional idealized asperity used in the calculation (taken from (Johansson, 2009)) 30
Figure 9. Resistances fro different failure modes for an idealized asperity where the inclination angle of the asperity varies (sliding failure, equation 3.22; shear failure, equation 3.23; and tensile failure, equation 3.24 (taken from (Johansson, 2009)) 31
Figure 10. Total friction angle for an idealized asperity with a varying angle of inclinations i (taken from (Johansson, 2009)) 32
Figure 11. Conceptual behavior of the dilation angle at different scales and matedness (taken from (Johansson, 2009)) 33
Figure 12. Standard profiles used for visual estimation of the paramter JRC (taken from (Barton and Choubeu. 1977)) 35
Figure 13. Complete test setup at one of the locations (taken from (Ghosh, 2010)) 39
Figure 14. Forces applied in the test (taken from (Ghosh, 2010)) 39
Figure 15. Peak shear strength envelop (taken from (Ghosh, 2010)) 40
Figure 16. Constant normal stiffness condition (taken from (Xue F. Gu et Al, 2003)) 40
Figure 17. Laboratory model of socket interface (taken from (Xue F. Gu et Al, 2003)) 41
Figure 18, (a) Water-jet cut samples with regular profiles; (b) Sample ready for testing (taken from (Xue F. Gu et Al, 2003)) 41
Figure 19. Roughness profiles 41
Figure 20. (a) Shear responses for 5, 20, 30 and 45 regular asperity profiles under σ=400 kPa, K=0 kPa/mm; (b) Shear response for different mean angle of fractal profile under σ=400 kPa, K=800, 1600 and 3200 kPa/mm; (c) Shear responses for 5, 10 and 20 regular asperity profiles under σ=400 kPa, K=800 kPa/mm ; (d)) Shear response for 20 asperity profile under σ=400 kPa, K=800, 1600 and 3200 kPa/mm (taken from (Xu F. Gu et Al, 2003)) 42

Figure 21. Video still of direct shear test at 11 mm of shear displacement (taken from (Xue F. Gu et Al, 2003)) 42
Figure 22. Wear at 8 mm shear displacement with different asperity angles (taken from (Xue F. Gu et Al, 2003)) 42
Figure 23. Digitized surface profiles from before and after testing (taken from (Xue F. Gu et Al, 2003)) 43
Figure 24. Specimens tested with 15 asperity profile and 30 asperity profile (taken from Negi R. (,2012)) 44
Figure 25. Shear stress response for 15 asperity profile (taken from (Negi R. 2012)) 44
Figure 26. Shear stress response for 30 asperity profile (taken from (Negi R. 2012)) 44
Figure 27. Failure envelopes for the specimen with 15 and 30 asperity profile (taken from (Negi R. 2012)) 45
Figure 28. Joint profiles used in the direct shear tests (taken from (Kodikara and Johnston, 1993)) 46
Figure 29. Typical rock and concrete components of a joint (taken from (Kodikara and Johnston, 1993)) 46
Figure 30. Principle of the test technique (taken from (Kodikara and Johnston, 1993)) 46
Figure 31. Results obtained from the shear tests (taken from (Kodikara and Johnston, 1993)) 47
Figure 32. Asperity profiles tested (taken from (Indraratna et Al, 1997)) 48
Figure 33. Variation of shear stress and normal stress with horizontal displacment for 9.5 asperity profile (taken from (Indraratna et Al, 1997)) 49
Figure 34. Surface profile tested (40, 20, 10 and 0) (taken from (Liahagen, 2012)) 53
Figure 35. Formwork removed from rock sample and plastic wrap being removed (taken from (Liahagen, 2012)) 53
Figure 36. Location and setup for the LVDTs (taken from (Johansson, 2009)) 53
Figure 37. Specimen ready for testing (taken from (Liahagen, 2012)) 54
Figure 38. LVDTs glued to the specimens (taken from (Liahagen, 2012)) 54
Figure 39. (a) Results from the tests with 40º asperity profile and a normal stress of 0.4 MPa. (b) Results from the tests with 40º asperity profile and a normal stress of 0.8 MPa. (c) Results from the tests with 40 asperity profile and a normal stress of 1.2 MPa. (d) Results from the tests with 40º asperity profile and a normal stress of 1.2 MPa with cohesion. 55
Figure 40. (a) Results from the tests with 20º asperity profile and a normal stress of 0.4 MPa. (b) Results from the tests with 20º asperity profile and a normal stress of 0.8 MPa. (c) Results from the tests with 20º asperity profile and a normal stress of 1.2 MPa. 56
Figure 41. (a) Results from the tests with 10º asperity profile and a normal stress of 0.4 MPa. (b) Results from the tests with 10º asperity profile and a normal stress of 0.8 MPa. (c) Results from th tests with 10º asperity profile and a normal stress of 1.2 MPa. 57
Figure 42. (left) Results from the tests with 0º asperity profile and a normal stress of 1.2 MPa with bonding. (right) Results from the tests with 0º asperity profile and a normal stress of 1.2 MPa without bonding. 57
Figure 43. Shear stress response for the different asperity angles tested and a normal stress of 0.4 MPa. 58

Figure 44. Shear stress response for the different asperity angles tested and a normal stress of 0.8 MPa. 59
Figure 45. *Shear stress response for the different asperity angles tested and a normal stress of 1.2 MPa.* 59
Figure 46. Variation of the peak shear stress with asperity angle for a normal stress of 0.4, 0.8 and 1.2 MPa. 60
Figure 47. Shear stress response for different normal stresses and 40 asperity angle. 60
Figure 48. Shear stress response for tests with bonding and without bonding for i=40º and i=0º. 61
Figure 49. Failure for the specimens tested with bonding for i=40º and $\boldsymbol{\sigma n = 1.2\ MPa}$ 61
Figure 50. Failure for the specimens tested with bonding for i=0º and $\boldsymbol{\sigma n = 1.2\ MPa}$ 62
Figure 51. Test 3.1 Interface when peak shear stress is reached (taken from (Liahagen, 2012)). 62
Figure 52. Test 2.1 Interface when peak shear stress is reached (taken from (Liahagen, 2012)). 63
Figure 53. Test 1.1 Concrete-to-rock interface after the test is finished (taken from (Liahagen, 2012)). 63
Figure 54. Test 1.2 Concrete-to-rock interface when peak shear stress is reached (taken from (Liahagen, 2012)). 63
Figure 55. Test 1.4 Concrete-to-rock interface when peak shear stress is reached (taken from (Liahagen, 2012)). 63
Figure 56. Influence of the asperity angle in the friction angle. 64
Figure 57. Friction angle variation with the shear displacement for the different roughness. 64
Figure 58. Peak shear displacement variation with the normal stress and roughness. 65
Figure 59. Stiffnes variation with normal stress and roughness. 65
Figure 60. (a) Comparison between observed and predicted shear capacity envelopes for i=40º (b) Comparison between observed and predicted shear capacity envelopes for i=20º (c) Comparison between observed and predicted shear capacity envelopes for i=10º 67
Figure 61. (a) Comparison between observed values for i=20º and predicted envelop by Patton`s model for a basic friction angle of 50º and 35º. (b) Comparison between observed values for i=10º and predicted envelop by Patton`s model for a basic friction angle of 50º and 35º. 68
Figure 62. Variation of the safety factor with the asperity angle. 71
Figure 63. Variation of the maximum allowable horizontal loads envelopes for each asperity angle and for NVE guidelines. 72
Figure 64. Comparison between the maximum allowable horizontal loads for bonded specimens and for NVE guidelines. 72
Figure 65. Shear resistance enveloped for each asperity angle tested and for Mohr-Coulomb model. 73
Figure 66. Increment of gradient by incorporating a roughness factor into Mohr-Coulomb model. 74
Figure 67. Variation of the roughness factor with the asperity angle. 75
Figure 68. (a) Comparison between observed values and predicted values by using the proposed model for i=40º (b) Comparison between observed values and predicted values by

using the proposed model for i=20º (c) Comparison between observed values and predicted values by using the proposed model for i=10º. 76
Figure 69. Direct shear test machine used in the tests at LTU. 79
Figure 70. (0) stiff steel frame, (1) lower box, (2) upper box, (3) specimen holder, (4) hydrostatic bearing, (5) spherical bearing, (6) & (7) hydraulic actuators, (8) bucker up (taken from Saaiang et Al, 2005) 80
Figure 71. 12 rock samples used in the tests. 81
Figure 72. Four different profiles used. 81
Figure 73. Casting completed. 82
Figure 74. Samples ready for casting. 82
Figure 75. Plastic adhesive to avoid bonding (ii). 83
Figure 76. Plastic adhesive to avoid bonding (i). 83
Figure 77. Casting on the steel molds (i). 83
Figure 78. Casting on the steel molds (ii). 83
Figure 79. Test set-up for direct shear tests at LTU. 84
Figure 80. Sample ready for testing. 85
Figure 81. Shear stress response for the different asperity angles tested and a normal stress of 3.2 MPa. 86
Figure 82. Shear stress response for the different asperity angles tested and a normal stress of 2.2 MPa. 87
Figure 83. Test 2.3 asperities failing. 87
Figure 84. Shear stress response for different normal stresses and 40 asperity angle. 88
Figure 85. Shear stress response for different normal stresses and 20 asperity angle. 89
Figure 86. Shear stress response for different normal stresses and 10 asperity angle. 89
Figure 87. Variation of the peak shear stress with asperity angle for a normal stress of 2.2 and 3.2 MPa. 90
Figure 88. Variation of the shear capacity increment with the roughness. 90
Figure 89. Shear stress response for test 1.2 and 1.3 (bonded and unbonded specimens). 91
Figure 90. Shear stress response for tests 1.1, 2.1 and 4.1 (bonded specimens). 91
Figure 91. Shear stress response for tests with bonding and without bonding for i=40º and i=0º. 92
Figure 92. Variation of the friction angle with the asperity angle and normal stress applied. 93
Figure 93. Friction angle variation with horizontal displacement for each roughness tested. 93
Figure 94. (a) Comparison between observed and predicted shear capacity envelopes for i=40º (b) Comparison between observed and predicted shear capacity envelopes for i=20º (c) Comparison between observed and predicted shear capacity envelopes for i=10º 95
Figure 95. (a) Variation of the shear stress with horizontal displacement for i=40 from test 2012 and 2013 (b) Variation of the shear stress with horizontal displacement for i=40 from test 2012 and 2013 (c) Variation of the shear stress with horizontal displacement for i=40 from test 2012 and 2013. 97
Figure 96. Comparison betwee the shear stress variation with horizontal displacement for i=10 degrees and 1.2 MPa for tests conducted in 2012 (granite) and 2013 (gneiss). 97

Figure 97. Variation of the friction angle over the horizontal displacement for 2012 and 2013 direct shear tests. 98
Figure 98. Variation of the maximum allowable horizontal loads envelopes for each asperity angle and for NVE guidelines. 99
Figure 99. Comparison between the maximum allowable horizontal loads for bonded specimens and for NVE guidelines. 100
Figure 100. Validation of the proposed model. Comparison between predicted and observed peak shear stress values for (a) i=40 degrees (b) i=20 degrees and (c) i=10 degrees. 101
Figure 101. Test 1.1 Concrete interface after the test. 118
Figure 102. Test 1.1 Rock interface after the test. 118
Figure 103. Test 1.1 before starting the test. 119
Figure 104. Test 1.1 after the test is finished. 119
Figure 105. Test 1.1 Concrete asperities profile after the test. 119
Figure 106. Test 1.1 Rock asperities profile after the test. 119
Figure 107. Test 1.2 Concrete interface after the test. 120
Figure 108. Test 1.2 Rock interface after the test. 120
Figure 109. Test 1.2 before starting the test. 121
Figure 110. Test 1.2 after the bond breaking. 121
Figure 111. Test 1.2 Concrete asperities profile after the test. 121
Figure 112. Test 1.2 Rock asperities profile after the test. 121
Figure 113. Test 1.3 Concrete interface after the test. 122
Figure 114. Test 1.3 Rock interface after the test. 122
Figure 115. Test 1.3 Rock asperities profile after the test. 123
Figure 116. Test 1.3 Concrete asperities profile after the test. 123
Figure 117. Test 1.3 before the test. 123
Figure 118. Test 1.3 after the test. 123
Figure 119. Test 1.4 Rock interface after the test. 124
Figure 120. Test 1.4 Concrete interface after the test. 124
Figure 121. Test 1.4 Rock asperities after the test. 125
Figure 122. Test 1.4 after the test. 125
Figure 123. Test 1.4 before the test. 125
Figure 124. Test 1.4 Concrete asperities after the test. 125
Figure 125. Test 2.1 Concrete interface after the test. 126
Figure 126. Test 2.1 Rock interface after the test. 126
Figure 127. Test 2.1 before the test. 127
Figure 128. Test 2.1 after the test. 127
Figure 129. Test 2.2 Concrete interface after the test. 128
Figure 130. Test 2.2 Rock interface after the test. 128
Figure 131. Test 2.2 before the test. 129
Figure 132. Test 2.2 after the test. 129
Figure 133. Test 2.3 Rock interface after the test. 130
Figure 134. Test 2.3 Concrete interface after the test. 130
Figure 135. Test 2.3 Rock asperities profile after the test. 131
Figure 136. Test 2.3 Concrete asperities profile after the test. 131

Figure 137. Test 2.3 after the test. 131
Figure 138. Test 2.3 before the test. 131
Figure 139. Test 3.1 Concrete interface after the test. 132
Figure 140. Test 3.1 Rock interface after the test. 132
Figure 141. Test 3.2 Concrete interface after the test is finished. 133
Figure 142. Test 3.2 Rock interface after the test is finished. 133
Figure 143. Test 3.2 before starting the test. 134
Figure 144. Test 3.2 after the test is finished. 134
Figure 145. Test 3.2 Concrete asperities profile after the test. 134
Figure 146. Test 3.2 Rock asperities after the test. 134
Figure 147. Test 3.3 Concrete interface after the test is finished. 134
Figure 148. Test 3.3 Rock interface after the test is finished. 134
Figure 149. Test 3.3 Concrete interface after the test. 135
Figure 150. Test 3.3 Rock interface after the test. 135
Figure 151. Test 3.3 Rock asperities after the test. 136
Figure 152. Test 3.3 Concrete asperities profile after the test. 136
Figure 153. Test 3.3 after the test is finished. 136
Figure 154. Test 3.3 before starting the test. 136
Figure 155. Test 4.1 Concrete interface after the test. 137
Figure 156. Test 4.1 Rock interface after the test. 137
Figure 157. Test 4.1 after the test is finished. 138
Figure 158. Test 4.1 before starting the test. 138
Figure 159. Test 4.2 Rock interface after the test. 139
Figure 160. Test 4.2 Concrete interface after the test. 139
Figure 161. Test 4.2 after the test is finished. 140
Figure 162. Test 4.2 before starting the test. 140

List of tables

Table 1. Results from the direct shear tests at LTU. viii
Table 2. Recommended shear friction safety factors in USBR guidelines (taken from (Novak,2007)) 8
Table 3. Minimum safety factors against sliding stability (taken from (NVE. 2005)) 11
Table 4. Classification of the load combinations (taken from (CDA,2010)) 12
Table 5. Minimum acceptable safety factors against sliding (taken from (CDA, 2007)) 15
Table 6. Minimum recommended safety factors for high and low risk dams (taken from (FERC,2002)) 16
Table 7. Minimum recommended safety factors against sliding if cohesion is not considered. 16
Table 8. Minimum requirements for safety factors against sliding for different loading cases (taken from (USBR, 1974)) 16
Table 9. Recommended coefficients of friction according to RIDAS for dams founded on rock of good quality (Johansson, 2009). 17
Table 10. Factors of safety according to RIDAS for reduction of the failure value of tan(ϕ) (taken from (Johansson,2009)) 18
Table 11. Minimum requirements for safety factors against sliding for each type of failure (taken from (Johansson et Al, 2012)) 19
Table 12. Results from the in-situ shear tests conducted (taken from (Rocha M. , 1964)) 38
Table 13. Peak shear strength obatined (taken from (Ruggeri, 2004)) 39
Table 14. Residual shear strength obtained (taken from (Ruggeri, 2004)) 39
Table 15. Results from the direct shear tests conducted by Simen Liahagen at LTU in 2012 54
Table 16. JRC and JCS used in Barton`s and Maksimovic's model. 69
Table 17. Results from the uniaxial compressive strength tests carried out at LTU. 82
Table 18. Values of the concrete strength. 84
Table 19. Results from the direct shear tests conducted at LTU. 85
Table 20. Table 21. JRC and JCS used in Barton`s and Maksimovic's model equation. 95

APPENDIX A

Derivation of equation 2.3

When the sliding plane of the dam is inclined an angle α (see Figure 33) the vertical and horizontal forces shall be decomposed over the sliding plane according to figure 34.

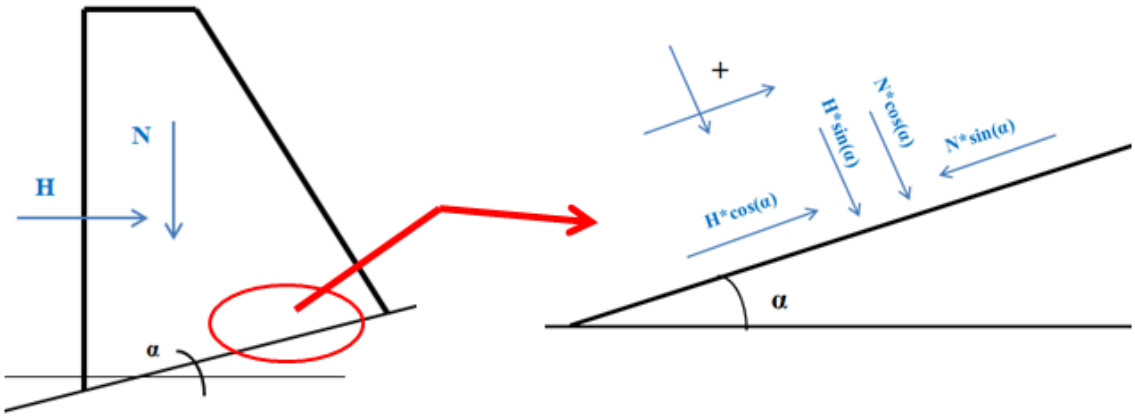

The shear friction method estimates the safety factor as follows:

$$SF = \frac{\sum H_f}{\sum H}$$

Where $\sum H_f$ is the maximal horizontal sliding resistance and $\sum H$ is the sum of horizontal forces acting on the dam. When an the sliding plane is inclined then the maximal horizontal sliding resistance is calculated as follows:

$$\sum H_f = \sum N \cdot tan(\varphi) = \left(\sum H_f \cdot sin(\alpha) + \sum N \cdot cos(\alpha)\right) \cdot tan(\varphi) + c \cdot A$$

Where; $\sum H_f$ is the horizontal sliding resistance (defined positive upwards), $\sum N$ is the sum of vertical forces (defined positive downwards), α is the inclination angle of the sliding plane, φ is the basic friction angle of the sliding plane, c is the cohesion of the sliding plane, A is the area of the sliding plane.

If we divide by $cos(\alpha)$ on both sides of the equation:

$$\sum H_f = \sum N \cdot tan(\varphi) + \left(\sum N + \sum H_f \cdot tan(\varphi)\right) \cdot tan(\alpha) + \frac{c \cdot A}{cos(\alpha)}$$

If we place the friction parameter to the left side of the equation:

$$\sum H_f - \left(\sum H_f \cdot tan(\varphi) + \sum N\right) \cdot tan(\alpha) = \sum N \cdot tan(\alpha) + \frac{c \cdot A}{cos(\alpha)}$$

Organizing the equation:

$$\sum H_f - \left(\sum H_f \cdot tan(\varphi) \cdot tan(\alpha) + \sum N \cdot tan(\alpha)\right) = \sum N \cdot tan(\alpha) + \frac{c \cdot A}{cos(\alpha)}$$

Sacando factor comun de Hf:

$$\sum H_f \cdot \left(1 - tan(\alpha) \cdot tan(\varphi)\right) - \sum N \cdot tan(\varphi) = \sum N \cdot tan(\alpha) + \frac{c \cdot A}{cos(\alpha)}$$

Placing the $\sum N \cdot tan(\varphi)$ to the right side of the equation:

$$\sum H_f \cdot \left(1 - tan(\alpha) \cdot tan(\varphi)\right) = \sum N \cdot tan(\varphi) + \sum N \cdot tan(\alpha) + \frac{c \cdot A}{cos(\alpha)}$$

Sacando factor comun de N

$$\sum H_f \cdot \left(1 - tan(\alpha) \cdot tan(\varphi)\right) = \sum N \cdot \left(tan(\varphi) + tan(\alpha)\right) + \frac{c \cdot A}{cos(\alpha)}$$

Organizing the equation, we have:

$$\sum H_f = \sum N \cdot \frac{\left(tan(\varphi) + tan(\alpha)\right)}{\left(1 - tan(\alpha) \cdot tan(\varphi)\right)} + \frac{c \cdot A}{cos(\alpha) \cdot \left(1 - tan(\alpha) \cdot tan(\varphi)\right)}$$

Knowing that:

$$\frac{\left(tan(\alpha) + tan(\varphi)\right)}{\left(1 - tan(\alpha) \cdot tan(\varphi)\right)} = tan(\alpha + \varphi)$$

Then, the equation can be written as:

$$\sum H_f = \sum N \cdot tan(\alpha + \varphi) + \frac{c \cdot A}{cos(\alpha) \cdot \left(1 - tan(\alpha) \cdot tan(\varphi)\right)}$$

If equation 6.4 is inserted into the equation to calculate the SF with the shear friction factor:

$$SF = \frac{\sum N \cdot tan(\alpha + \varphi) + \frac{c \cdot A}{cos(\alpha) \cdot \left(1 - tan(\alpha) \cdot tan(\varphi)\right)}}{\sum H}$$

APPENDIX B

Derivation of the equation 3.25 (according to Johansson, 2009):

The true contact area, $A_{c,x}$ can be expressed, according to the adhesion theory, as the quotient between effective normal stress, σ'_n, and yielding stress of the joint surface, σ_{ci} :

$$A_{c,x} = \frac{\sigma'_n}{\sigma_{ci}} \qquad (B.1)$$

The potential contact area, $A_{c,p}$, for rough joint surfaces, can be expresses by an empirical formulation according to Grasselli (2001):

$$A_{c,p} = A_o \cdot \left(\frac{\theta^*_{max} - \theta^*}{\theta^*_{max}}\right)^C \qquad (B.2)$$

Where A_o is the maximum possible contact area ratio against the shear direction. θ^*_{max} is the maximum measured dip angle measured on the sample and θ^* is the measured dip angle defined as the inclination of the asperities against the shear direction. C is a roughness parameter which governs the concavity of the curve.

The relation between the asperities heights, h_{asp} and the base lengths of different asperity orders, L_{asp} , can be expresses with the following function:

$$h_{asp} = a \cdot {L_{asp}}^H \qquad (B.3)$$

Where a is the amplitude constant and H is the Hurst exponent, both based on the base lengths of different asperity orders. Under a constant normal stress, the variation of the area of average contacting asperities is depending on the change in the number of contact points with an increased size of the joints. This change can be expressed as follows:

$$L_{asp,n} = L_{asp,g} \cdot \left(\frac{L_n}{L_g}\right)^k \qquad (B.4)$$

where L is the length of the sample and L_{asp} is the base length of the asperity. The subscript (g) corresponds to grain size and (n) to full sized joints. k is an empirical constant which range between zero and one, depending on the degree of matedness.

Combining equation (B.1) and (B.2), the dilation angle, i, for a perfectly mated joint could be expresses as:

$$i = \theta^*_{max} - 10^{\frac{log \cdot \frac{\grave{\sigma_n}}{\sigma_{ci}} - log \cdot A_o}{C}} \cdot \theta^*_{max} \qquad (B.5)$$

The dilation angle is by geometry expresses as:

$$i = arctan\left(\frac{h_{asp}}{0.5 \cdot L_{asp}}\right) \qquad (B.6)$$

If we use the scaling relation expresses in equation (B.4), together with the equation (B.5) and (B.6), the length of the contacting asperities at grain size could also be expresses as:

$$L_{asp,g} = \left[0.5 \cdot a^{-1}\left[tan\left(\theta^*_{max} - 10^{\frac{log\cdot\frac{\grave{\sigma_n}}{\sigma_{ci}} - log\cdot A_o}{C}} \cdot \theta^*_{max}\right)\right]\right]^{\frac{1}{H-1}} \qquad (B.7)$$

Combining equation (B.3), (B.4), (B.5) and (B.6), the dilation angle for full sized joints can be expresses as follows:

$$i = arctan\left(2a \cdot \left(\left[0.5 \cdot a^{-1}\left[tan\left(\theta^*_{max} - 10^{\frac{log\cdot\frac{\grave{\sigma_n}}{\sigma_{ci}} - log\cdot A_o}{C}} \cdot \theta^*_{max}\right)\right]\right]^{\frac{1}{H-1}}\right)\right) \qquad (B.8)$$

Equation (B.8) may be rewritten as:

$$i = \left(\theta^*_{max} - 10^{\frac{log\cdot\frac{\grave{\sigma_n}}{\sigma_{ci}} - log\cdot A_o}{C}} \cdot \theta^*_{max}\right) \cdot \left(\frac{L_n}{L_g}\right)^{kH-k} \qquad (B.9)$$

APPENDIX C

Pictures from the direct shear tests conducted at LTU.

Figure 101. Test 1.1 Concrete interface after the test.

Figure 102. Test 1.1 Rock interface after the test.

Figure 103. Test 1.1 before starting the test.

Figure 104. Test 1.1 after the test is finished.

Figure 105. Test 1.1 Concrete asperities profile after the test.

Figure 106. Test 1.1 Rock asperities profile after the test.

Figure 107. Test 1.2 Concrete interface after the test.

Figure 108. Test 1.2 Rock interface after the test.

Figure 109. Test 1.2 before starting the test.

Figure 110. Test 1.2 after the bond breaking.

Figure 111. Test 1.2 Concrete asperities profile after the test.

Figure 112. Test 1.2 Rock asperities profile after the test.

Figure 113. Test 1.3 Concrete interface after the test.

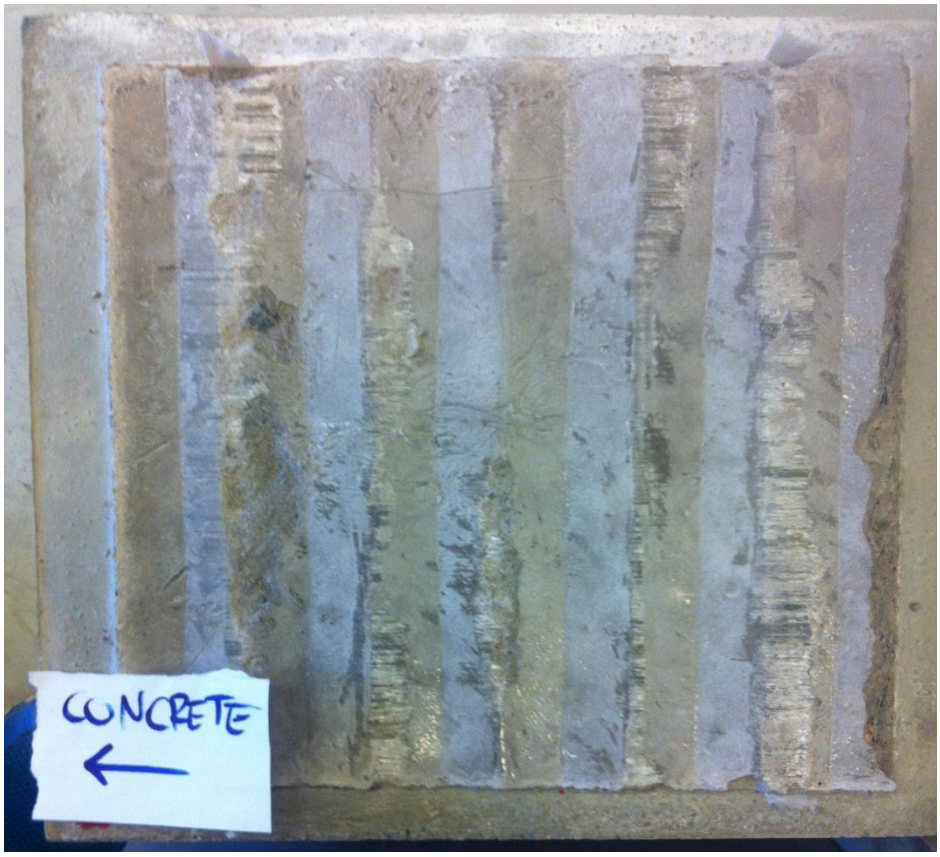

Figure 114. Test 1.3 Rock interface after the test.

Figure 117. Test 1.3 before the test.

Figure 118. Test 1.3 after the test.

Figure 116. Test 1.3 Concrete asperities profile after the test.

Figure 115. Test 1.3 Rock asperities profile after the test.

Figure 120. Test 1.4 Concrete interface after the test.

Figure 119. Test 1.4 Rock interface after the test.

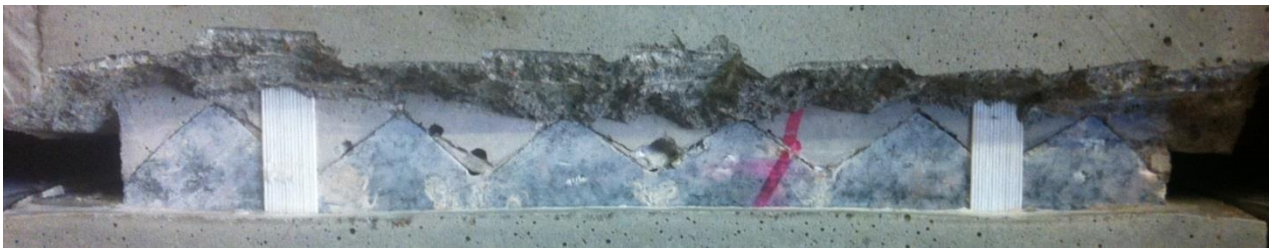

Figure 123. Test 1.4 before the test.

Figure 122. Test 1.4 after the test.

Figure 124. Test 1.4 Concrete asperities after the test.

Figure 121. Test 1.4 Rock asperities after the test.

Figure 125. Test 2.1 Concrete interface after the test.

Figure 126. Test 2.1 Rock interface after the test.

Figure 127. Test 2.1 before the test.

Figure 128. Test 2.1 after the test.

Figure 129. Test 2.2 Concrete interface after the test.

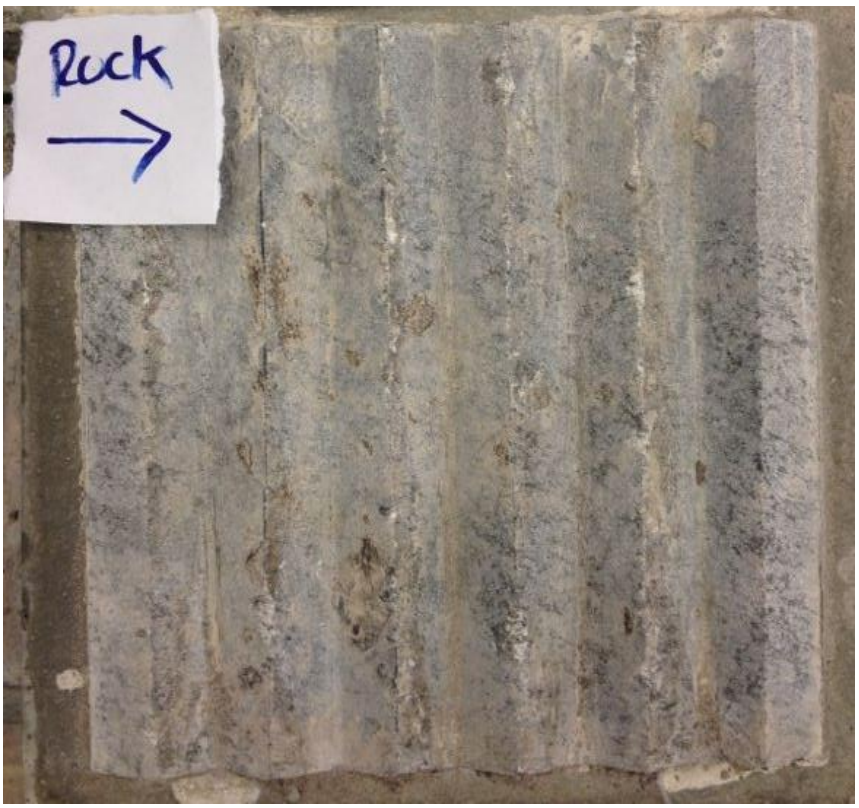

Figure 130. Test 2.2 Rock interface after the test.

Figure 131. Test 2.2 before the test.

Figure 132. Test 2.2 after the test.

Figure 134. Test 2.3 Concrete interface after the test.

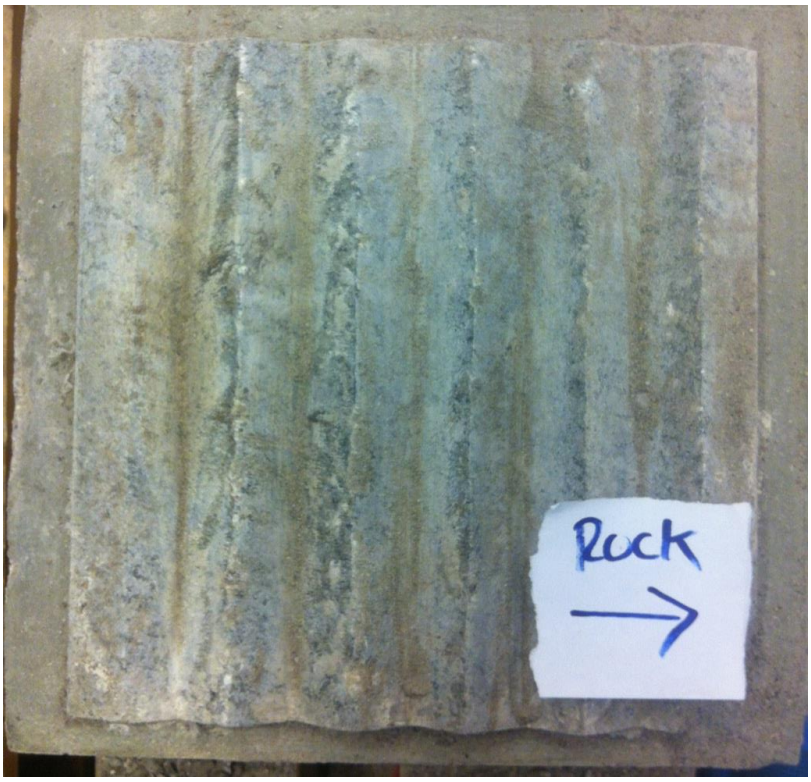

Figure 133. Test 2.3 Rock interface after the test.

Figure 138. Test 2.3 before the test.

Figure 137. Test 2.3 after the test.

Figure 136. Test 2.3 Concrete asperities profile after the test.

Figure 135. Test 2.3 Rock asperities profile after the test.

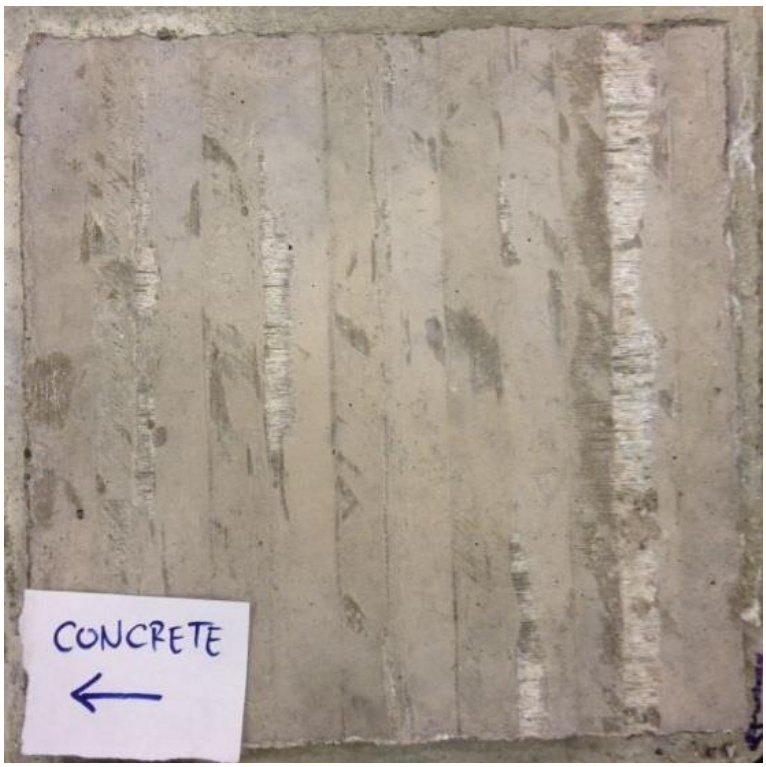

Figure 139. Test 3.1 Concrete interface after the test.

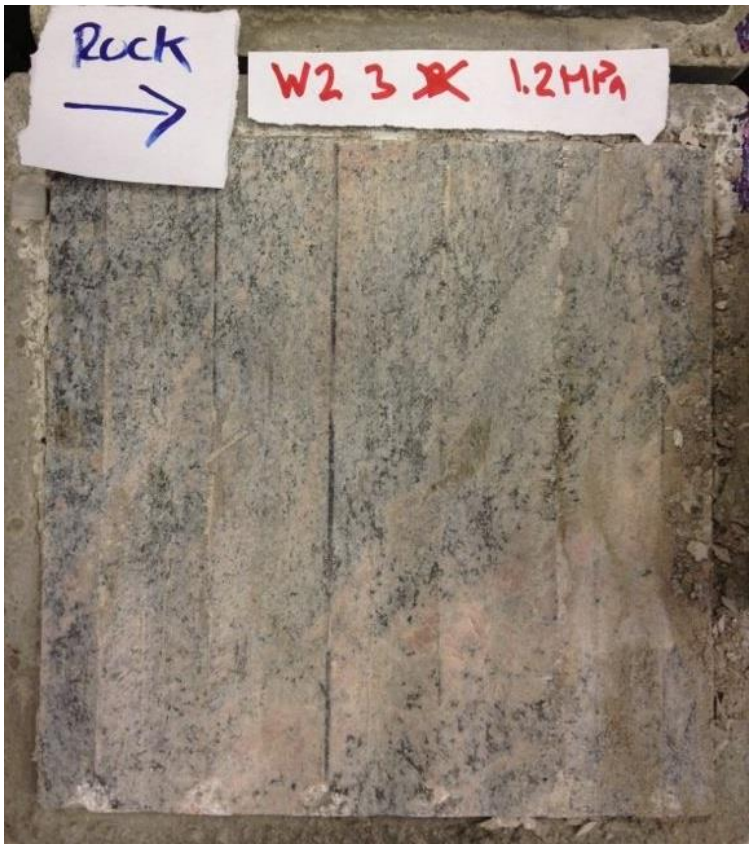

Figure 140. Test 3.1 Rock interface after the test.

Figure 141. Test 3.2 Concrete interface after the test is finished.

Figure 142. Test 3.2 Rock interface after the test is finished.

Figure 143. Test 3.2 before starting the test.

Figure 144. Test 3.2 after the test is finished.

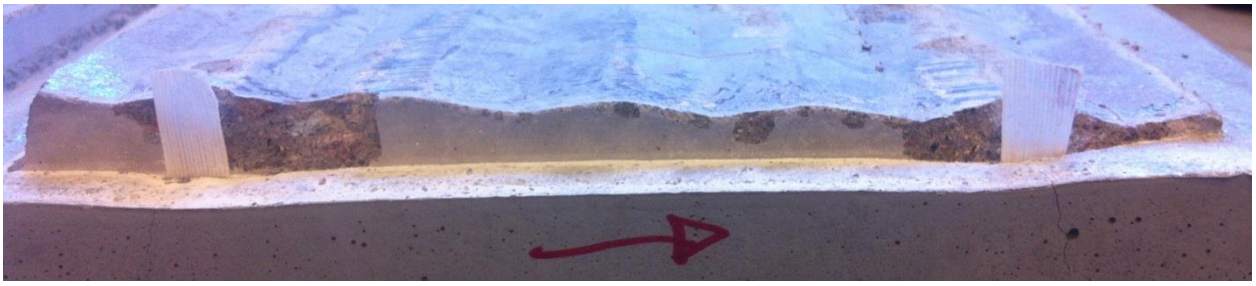

Figure 145. Test 3.2 Concrete asperities profile after the test.

Figure 146. Test 3.2 Rock asperities after the test.

Figure 149. Test 3.3 Concrete interface after the test.

Figure 150. Test 3.3 Rock interface after the test.

Figure 154. Test 3.3 before starting the test.

Figure 153. Test 3.3 after the test is finished.

Figure 152. Test 3.3 Concrete asperities profile after the test.

Figure 151. Test 3.3 Rock asperities after the test.

Figure 155. Test 4.1 Concrete interface after the test.

Figure 156. Test 4.1 Rock interface after the test.

Figure 158. Test 4.1 before starting the test.

Figure 157. Test 4.1 after the test is finished.

Figure 160. Test 4.2 Concrete interface after the test.

Figure 159. Test 4.2 Rock interface after the test.

Figure 162. Test 4.2 before starting the test.

Figure 161. Test 4.2 after the test is finished.

APPENDIX D

Results from the direct shear tests conducted at LTU.

Test 1.1:

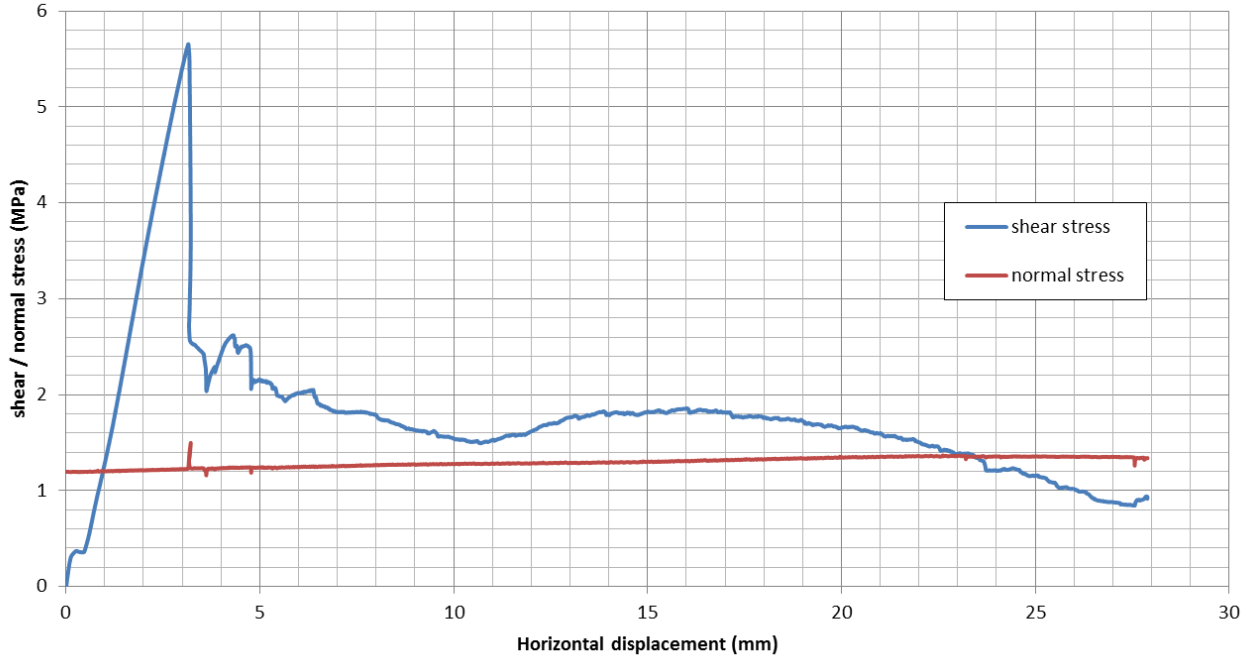

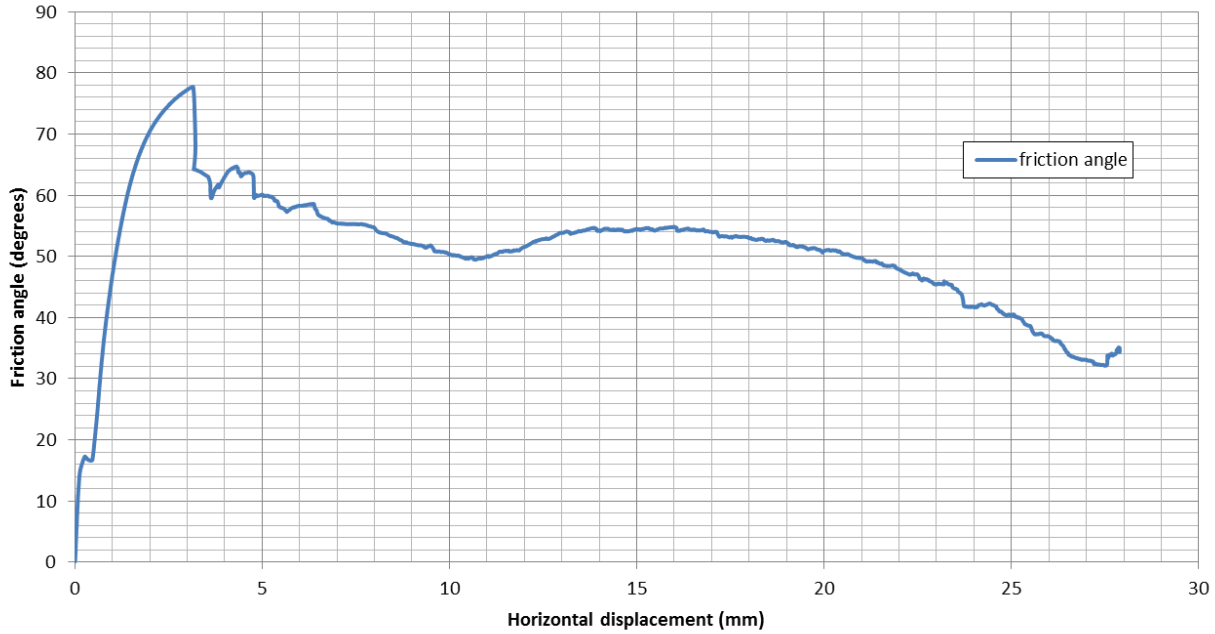

Test 1.2:

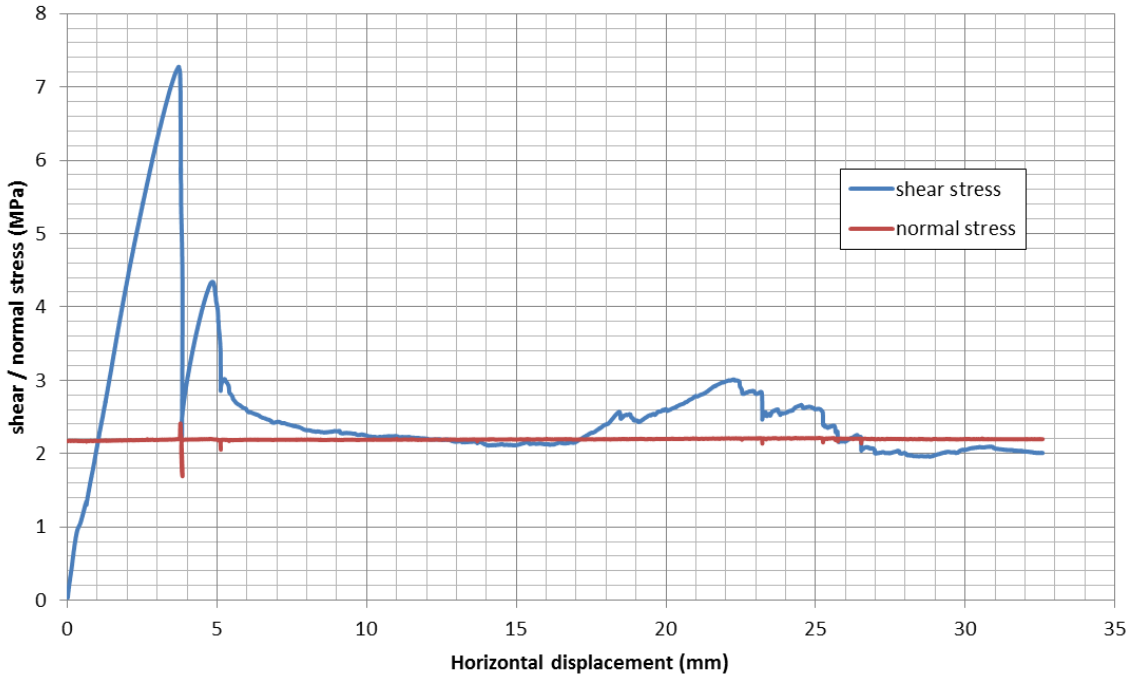
shear / normal stress (MPa)
Horizontal displacement (mm)
shear stress
normal stress
0
1
2
3
4
5
6
7
8
0
5
10
15
20
25
30
35

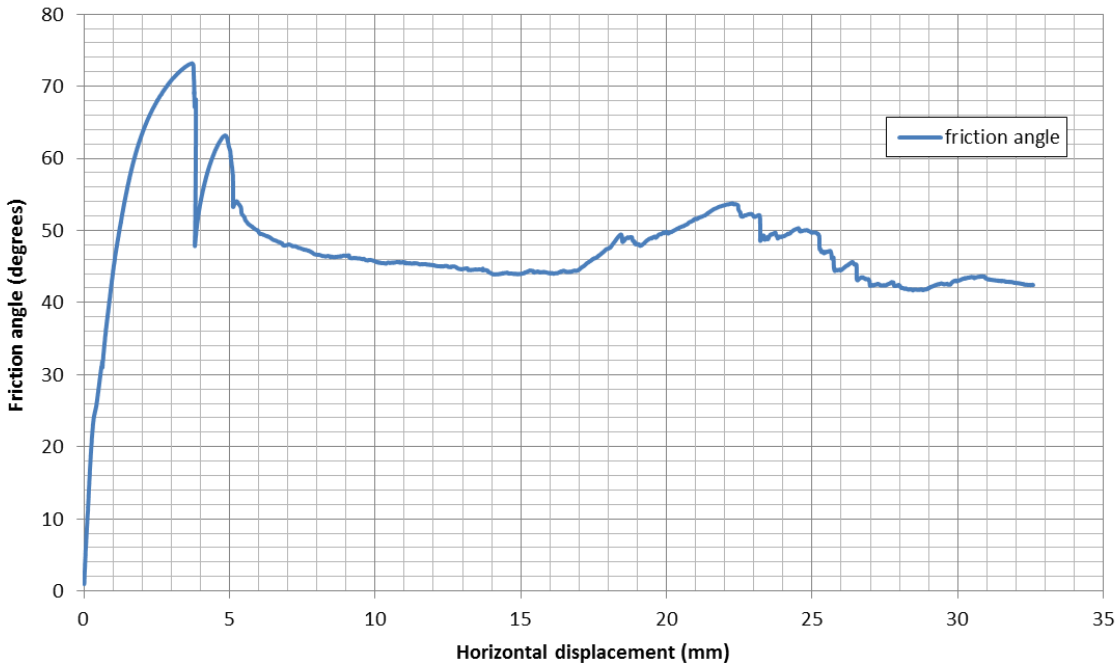
Friction angle (degrees)
Horizontal displacement (mm)
friction angle
0
10
20
30
40
50
60
70
80
0
5
10
15
20
25
30
35

Test 1.3:

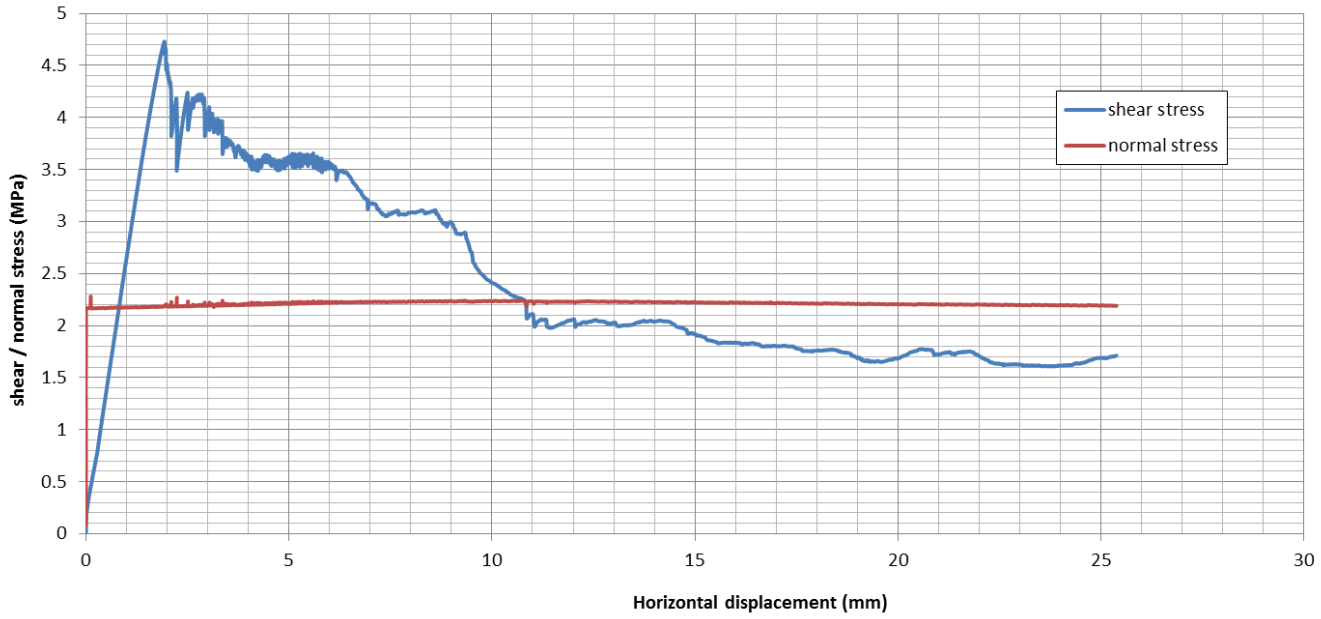
shear / normal stress (MPa)
Horizontal displacement (mm)
shear stress
normal stress
0
0.5
1
1.5
2
2.5
3
3.5
4
4.5
5
0
5
10
15
20
25
30

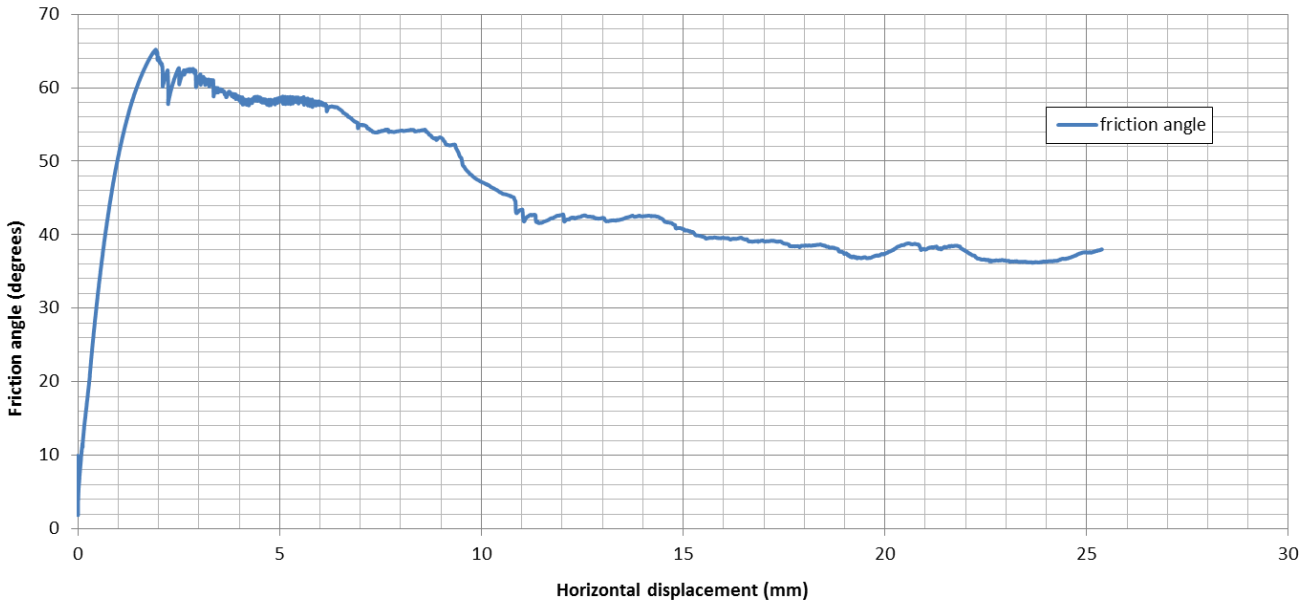
Friction angle (degrees)
Horizontal displacement (mm)
friction angle
0
10
20
30
40
50
60
70
0
5
10
15
20
25
30

Test 1.4:

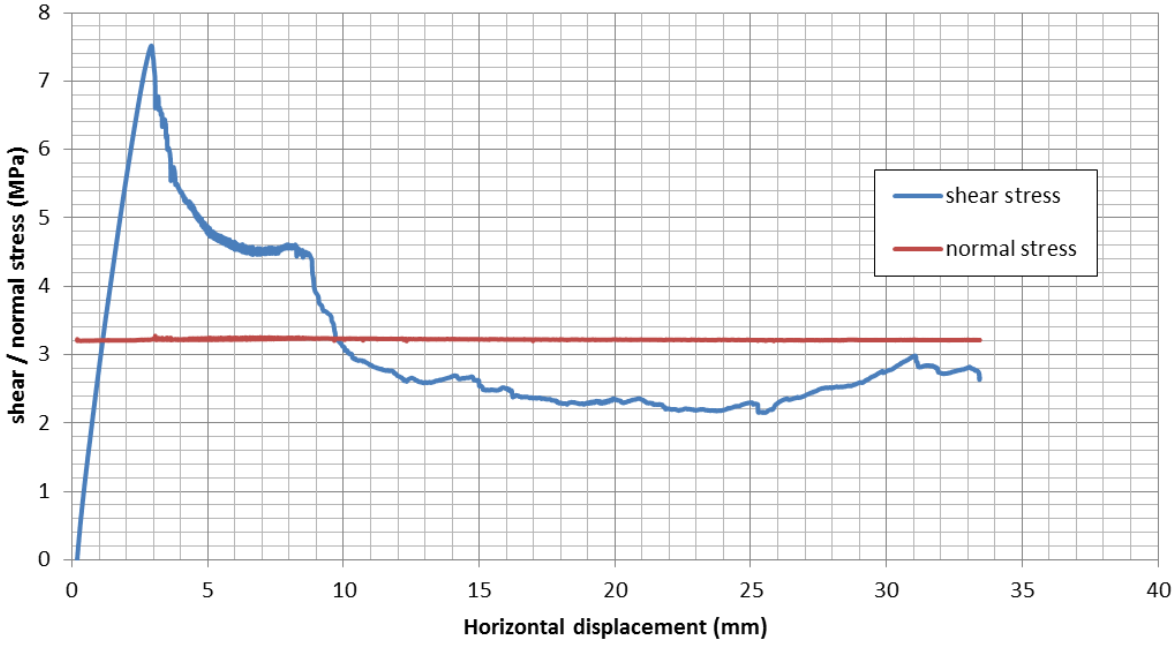
shear / normal stress (MPa)
Horizontal displacement (mm)
shear stress
normal stress
0
1
2
3
4
5
6
7
8
0
5
10
15
20
25
30
35
40

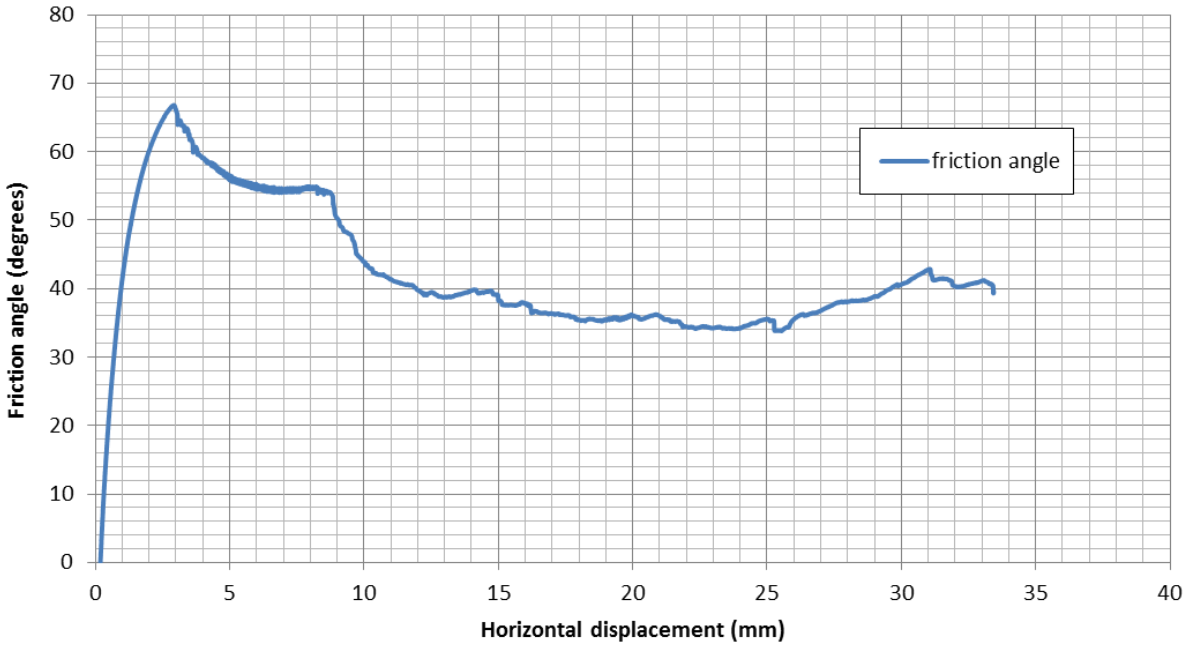
Friction angle (degrees)
Horizontal displacement (mm)
friction angle
0
10
20
30
40
50
60
70
80
0
5
10
15
20
25
30
35
40

Test 2.1:

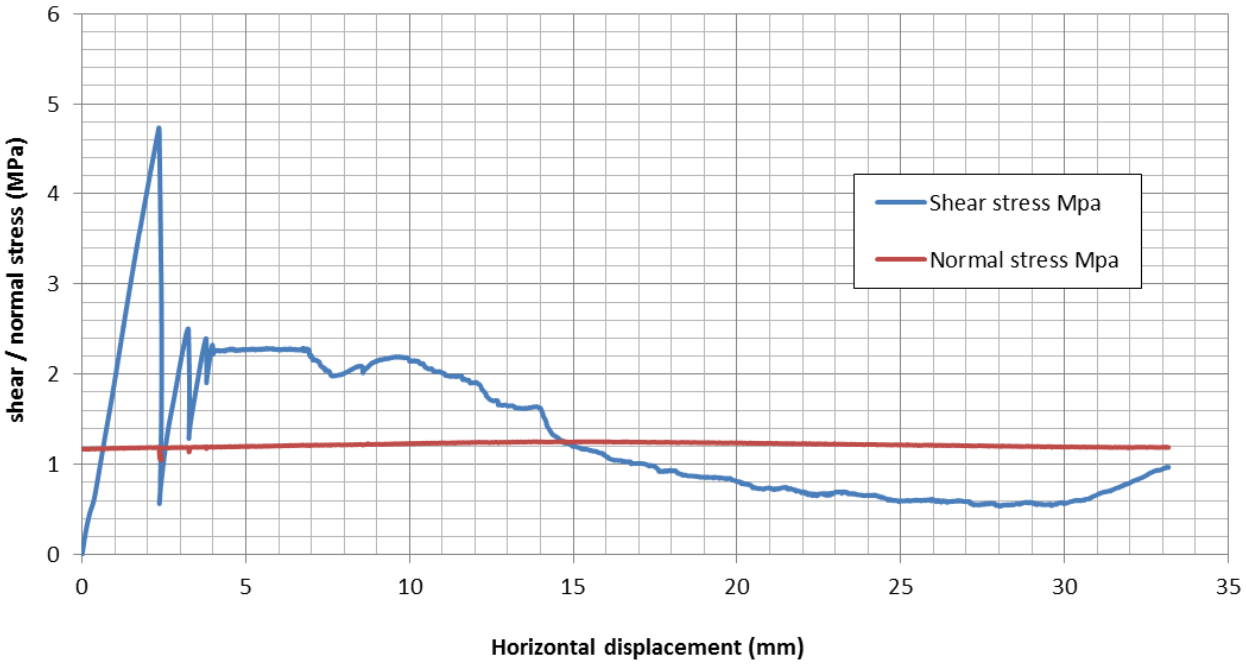
shear / normal stress (MPa)
Horizontal displacement (mm)
Shear stress Mpa
Normal stress Mpa
0
1
2
3
4
5
6
0
5
10
15
20
25
30
35

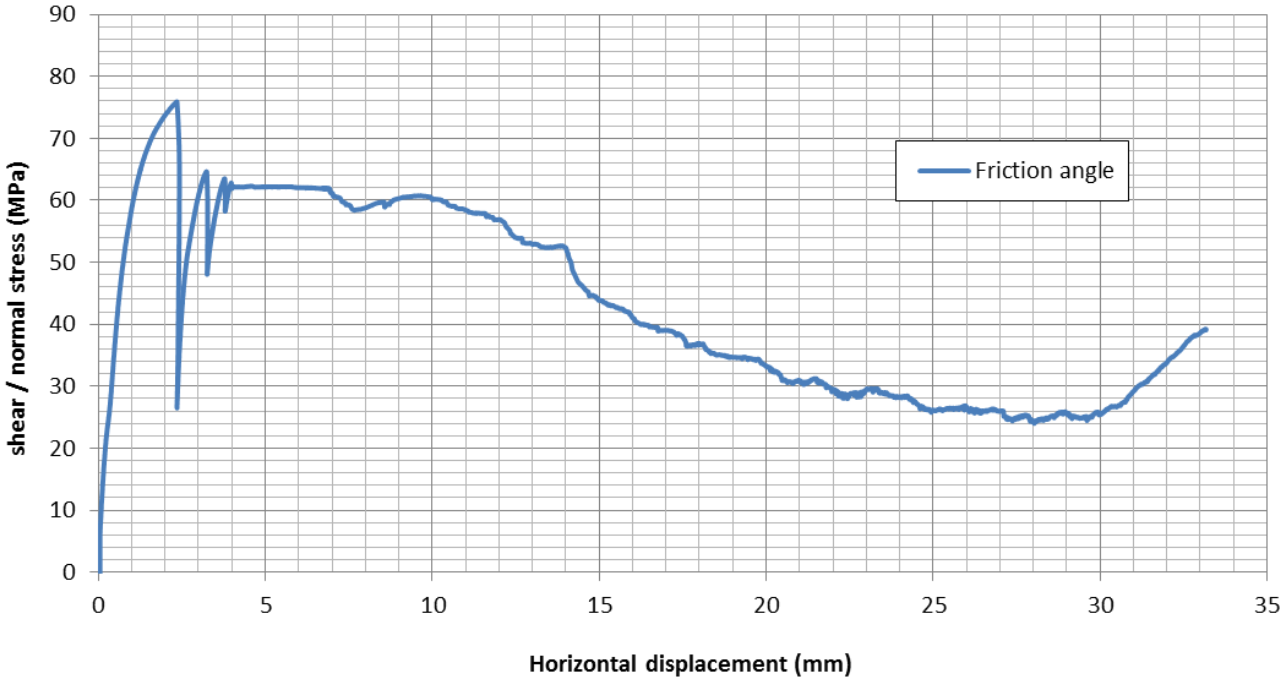
shear / normal stress (MPa)
Horizontal displacement (mm)
Friction angle
0
10
20
30
40
50
60
70
80
90
0
5
10
15
20
25
30
35

Test 2.2:

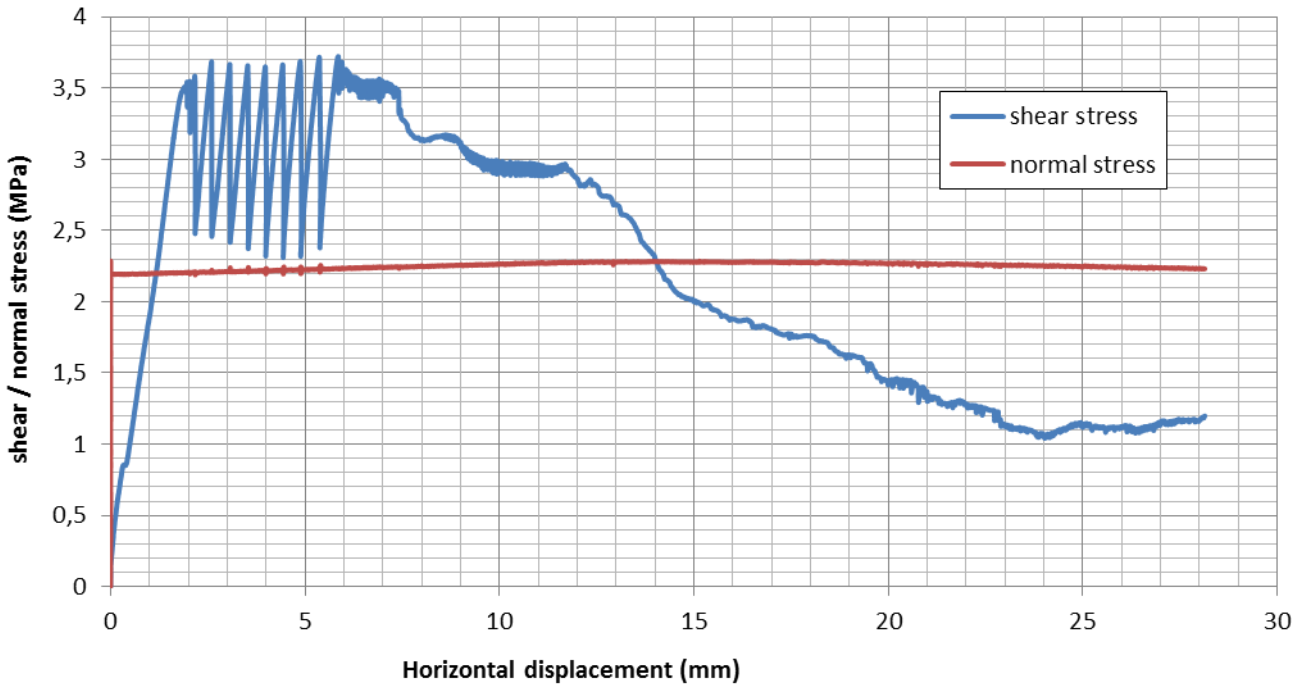
shear / normal stress (MPa)
4
3,5
3
2,5
2
1,5
1
0,5
0
0
5
10
15
20
25
30
Horizontal displacement (mm)
shear stress
normal stress

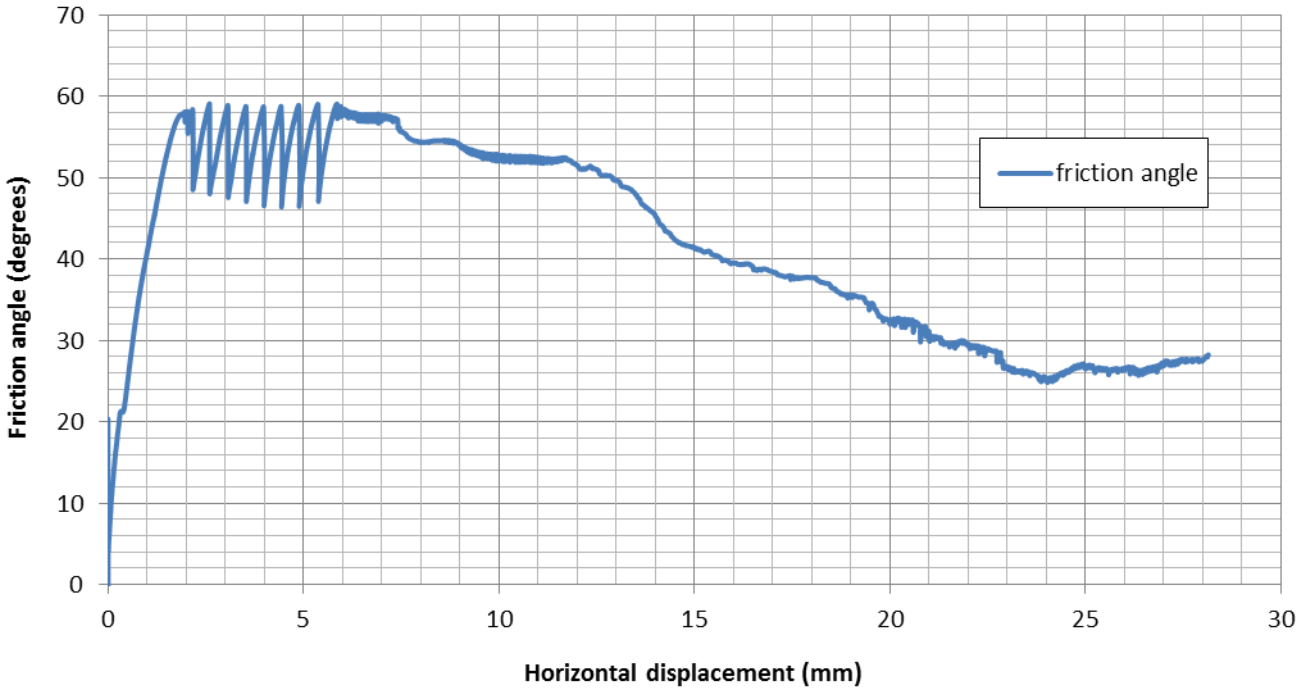
Friction angle (degrees)
70
60
50
40
30
20
10
0
0
5
10
15
20
25
30
Horizontal displacement (mm)
friction angle

Test 2.3:

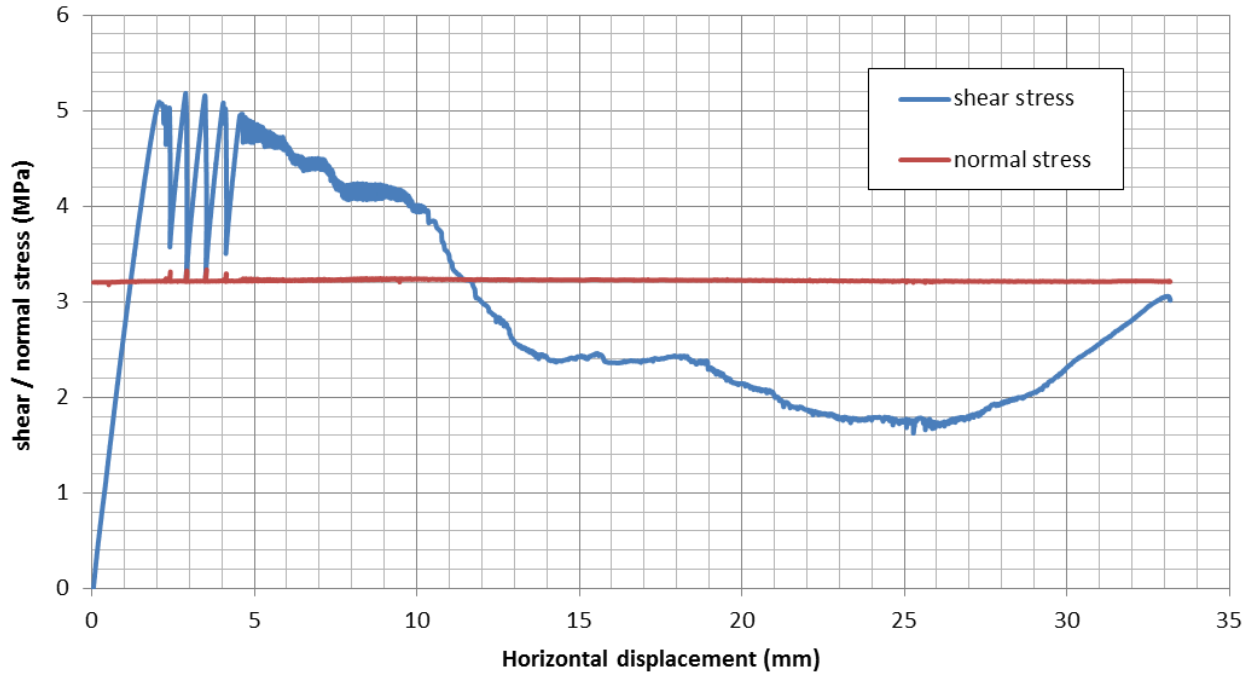
shear stress
normal stress
shear / normal stress (MPa)
Horizontal displacement (mm)
0
1
2
3
4
5
6
0
5
10
15
20
25
30
35

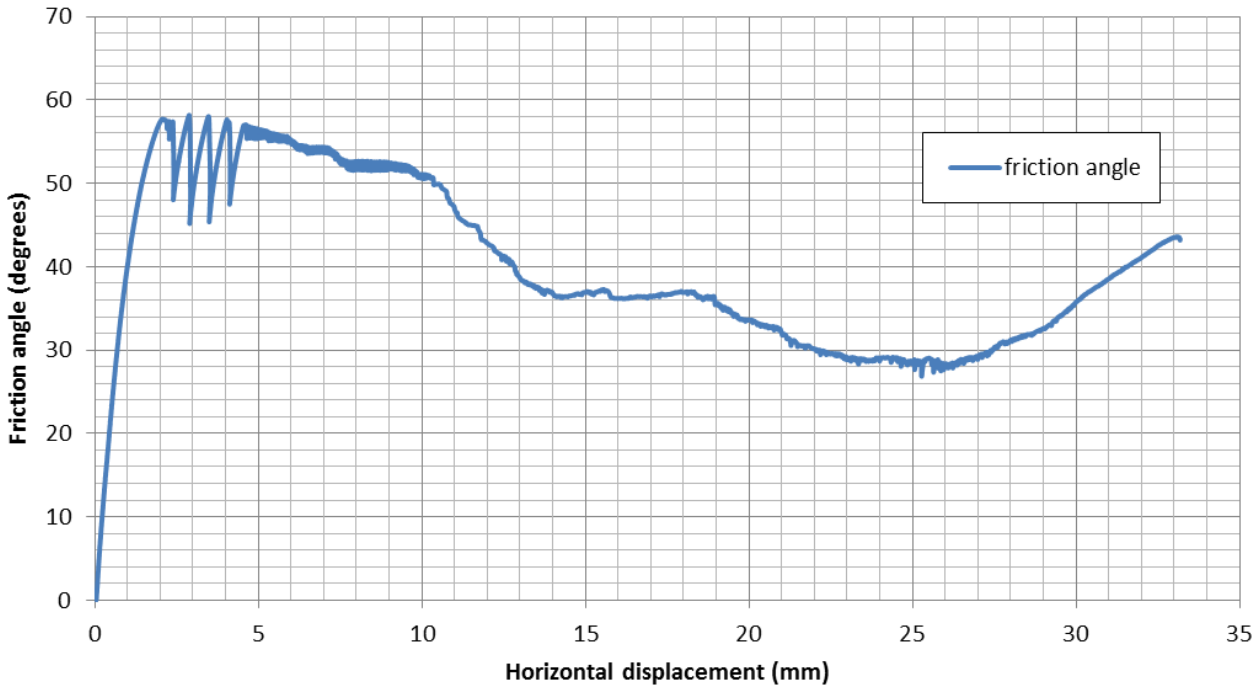
friction angle
Friction angle (degrees)
Horizontal displacement (mm)
0
10
20
30
40
50
60
70
0
5
10
15
20
25
30
35

Test 3.1:

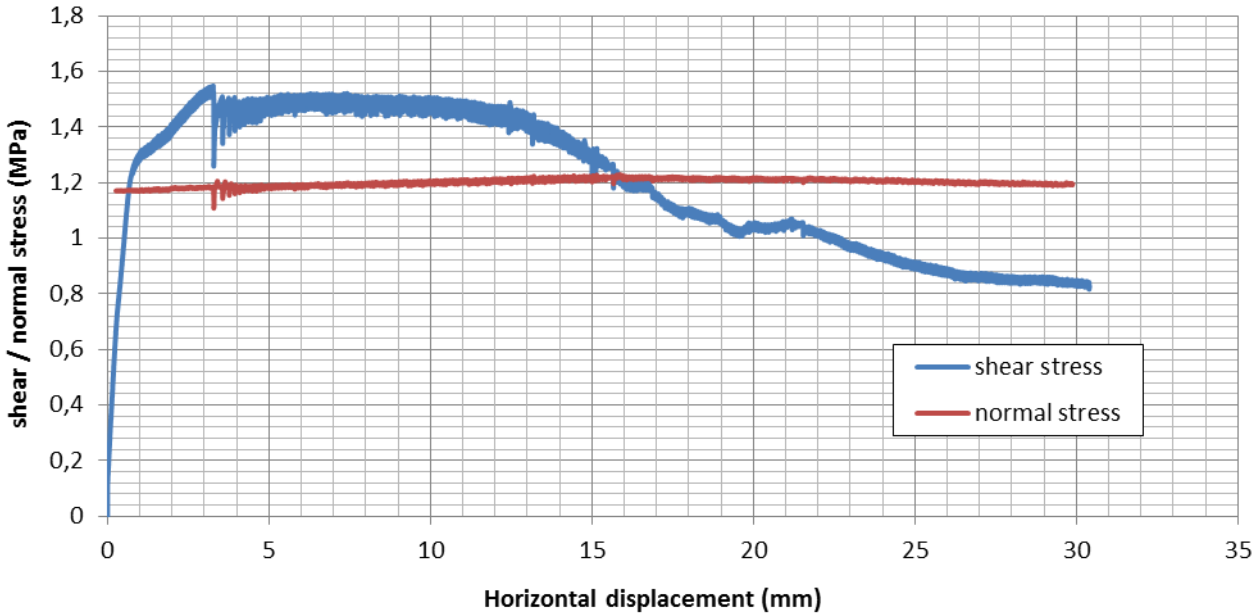
shear / normal stress (MPa)
1,8
1,6
1,4
1,2
1
0,8
0,6
0,4
0,2
0
0
5
10
15
20
25
30
35
Horizontal displacement (mm)
shear stress
normal stress

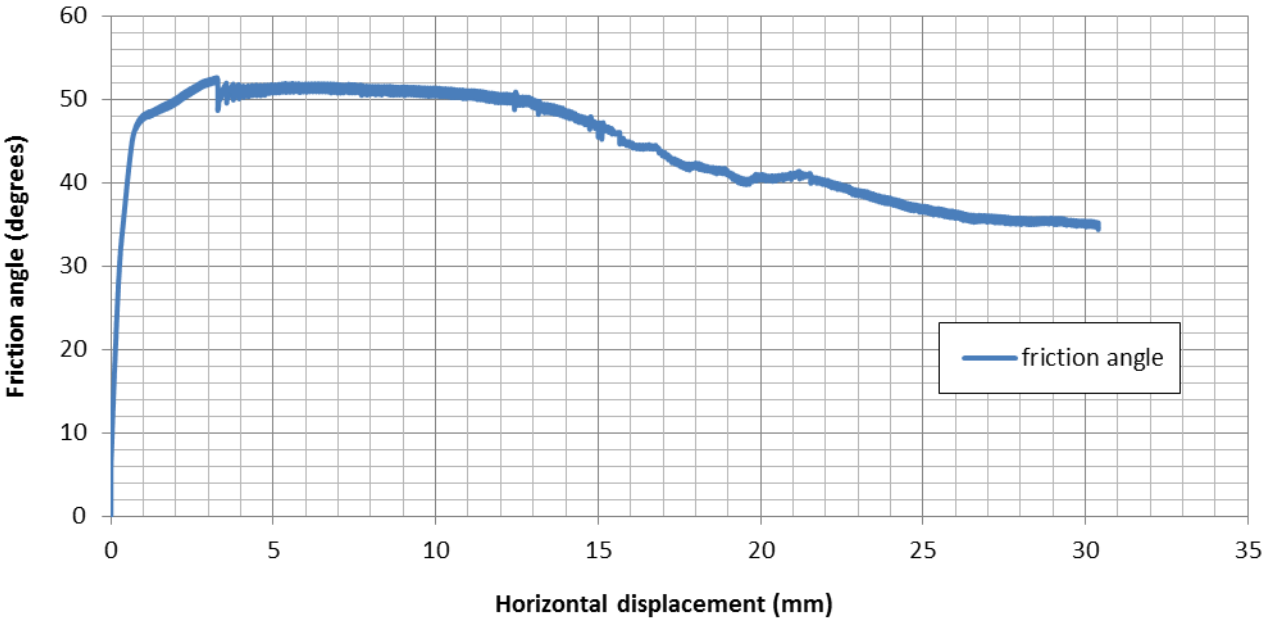
Friction angle (degrees)
60
50
40
30
20
10
0
0
5
10
15
20
25
30
35
Horizontal displacement (mm)
friction angle

Test 3.2:

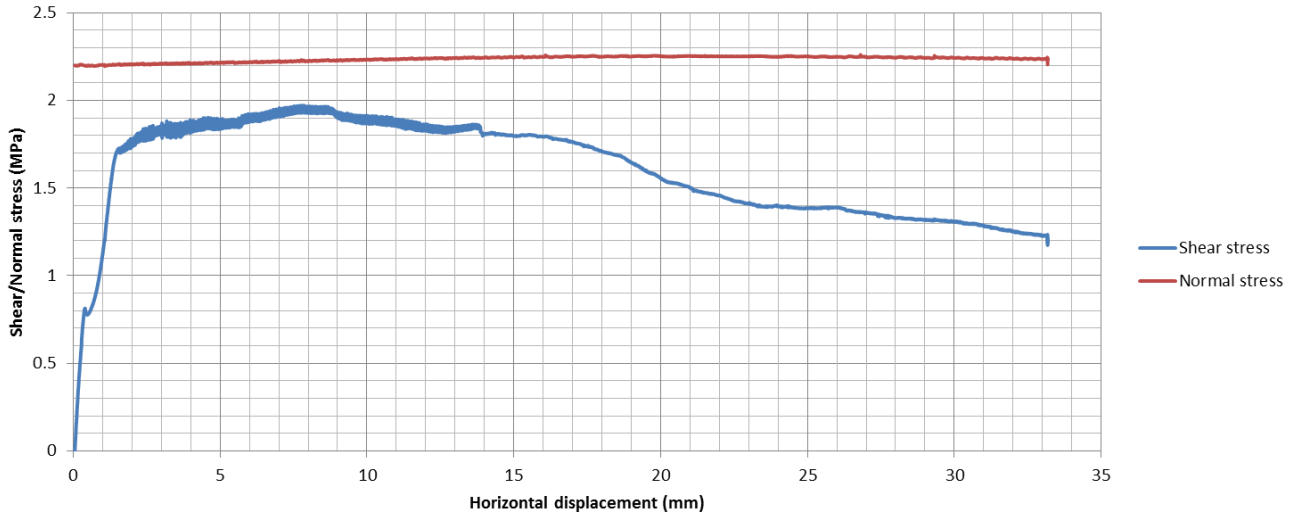
2.5
2
1.5
1
0.5
0
Shear/Normal stress (MPa)
0
5
10
15
20
25
30
35
Horizontal displacement (mm)
Shear stress
Normal stress

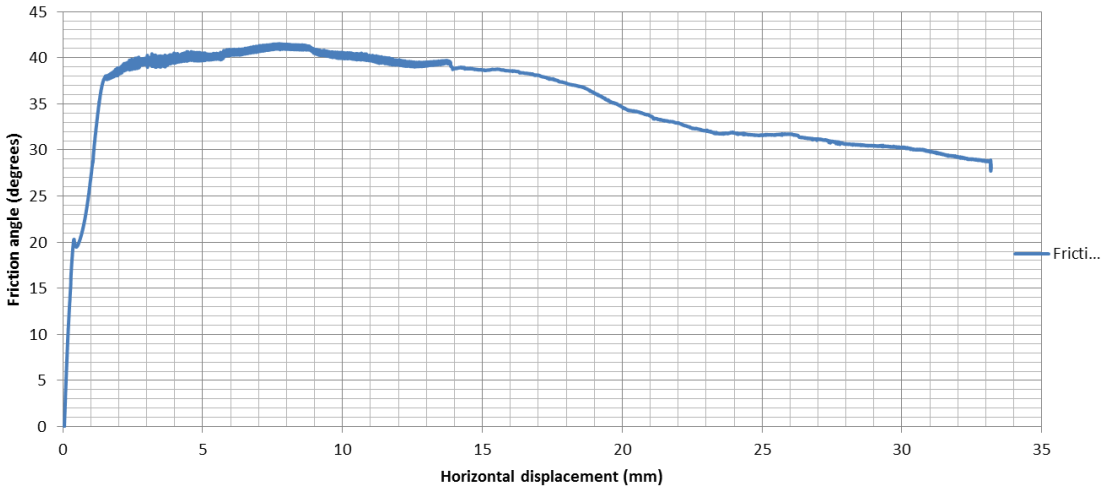
45
40
35
30
25
20
15
10
5
0
Friction angle (degrees)
0
5
10
15
20
25
30
35
Horizontal displacement (mm)
Fricti...

Test 3.3:

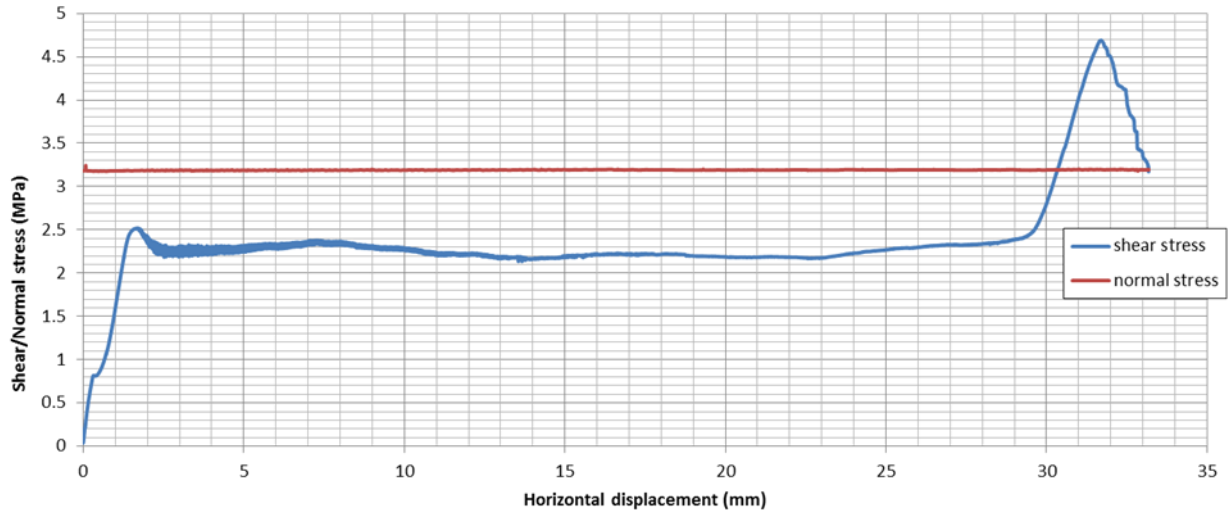
Shear/Normal stress (MPa)
Horizontal displacement (mm)
shear stress
normal stress

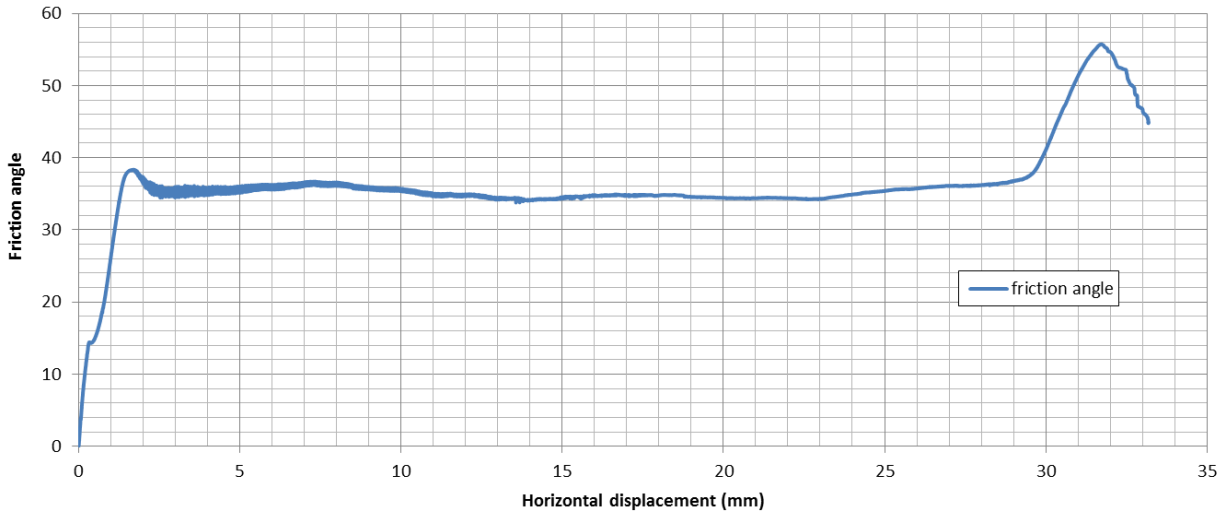
Friction angle
Horizontal displacement (mm)
friction angle

Test 4.1:

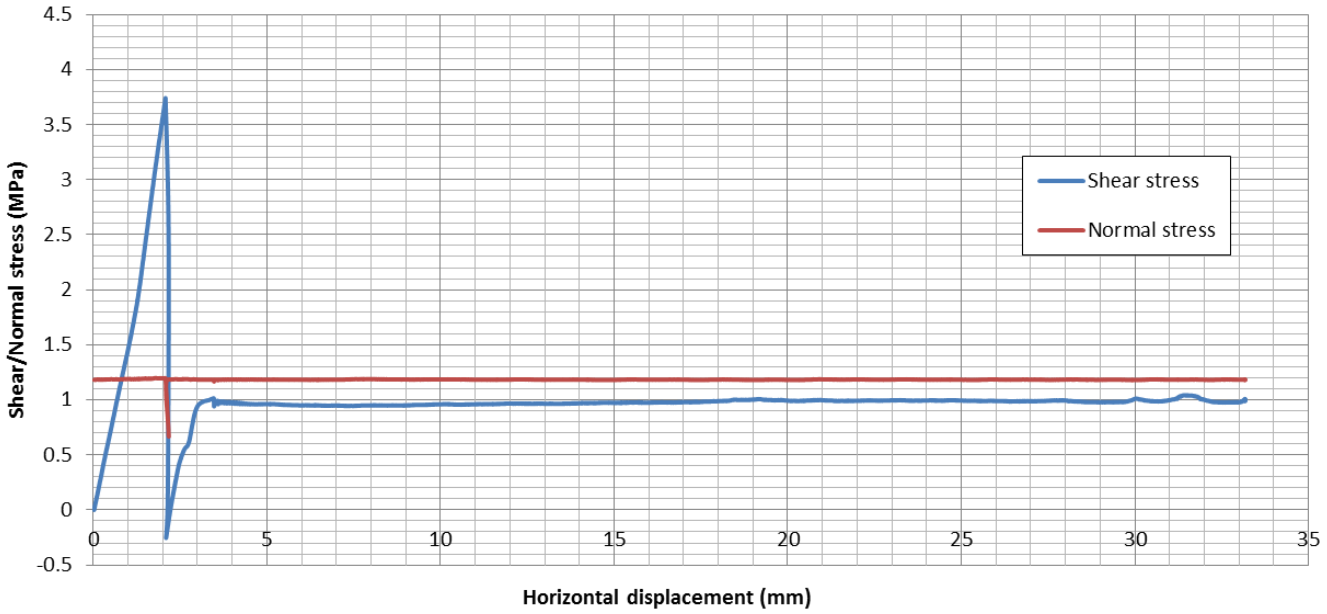
4.5
4
3.5
3
2.5
2
1.5
1
0.5
0
-0.5
0
5
10
15
20
25
30
35
Shear/Normal stress (MPa)
Horizontal displacement (mm)
Shear stress
Normal stress

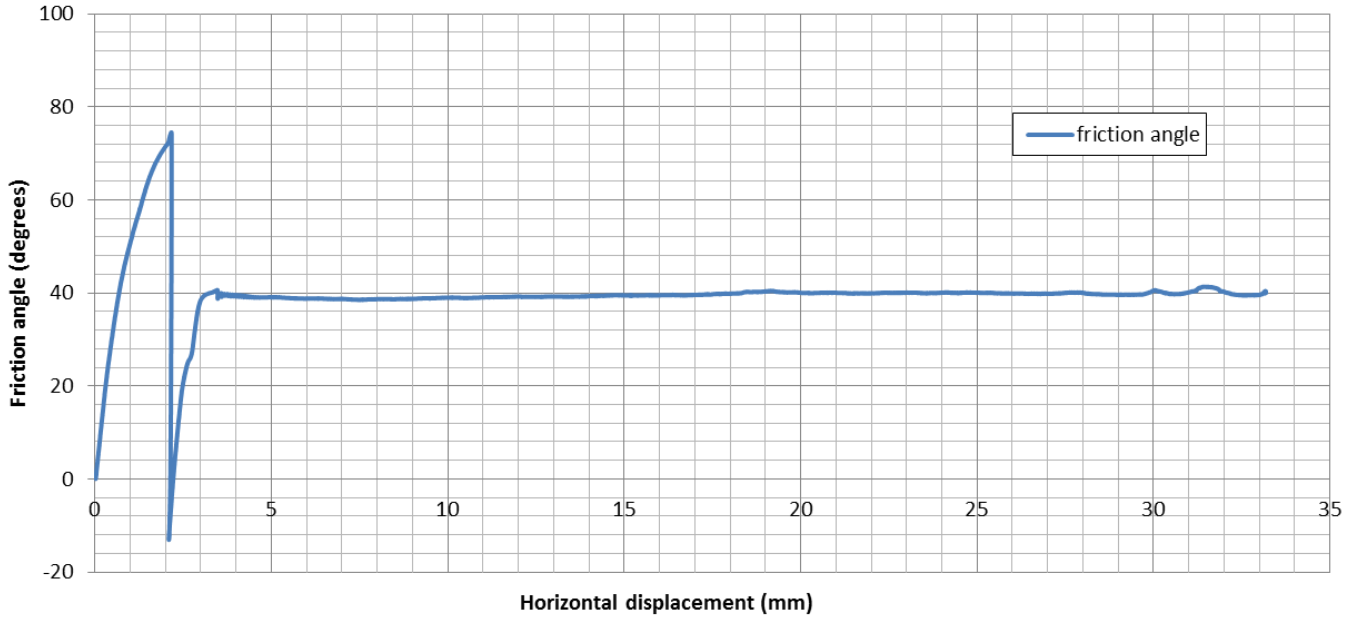
100
80
60
40
20
0
-20
0
5
10
15
20
25
30
35
Friction angle (degrees)
Horizontal displacement (mm)
friction angle

Test 4.2:

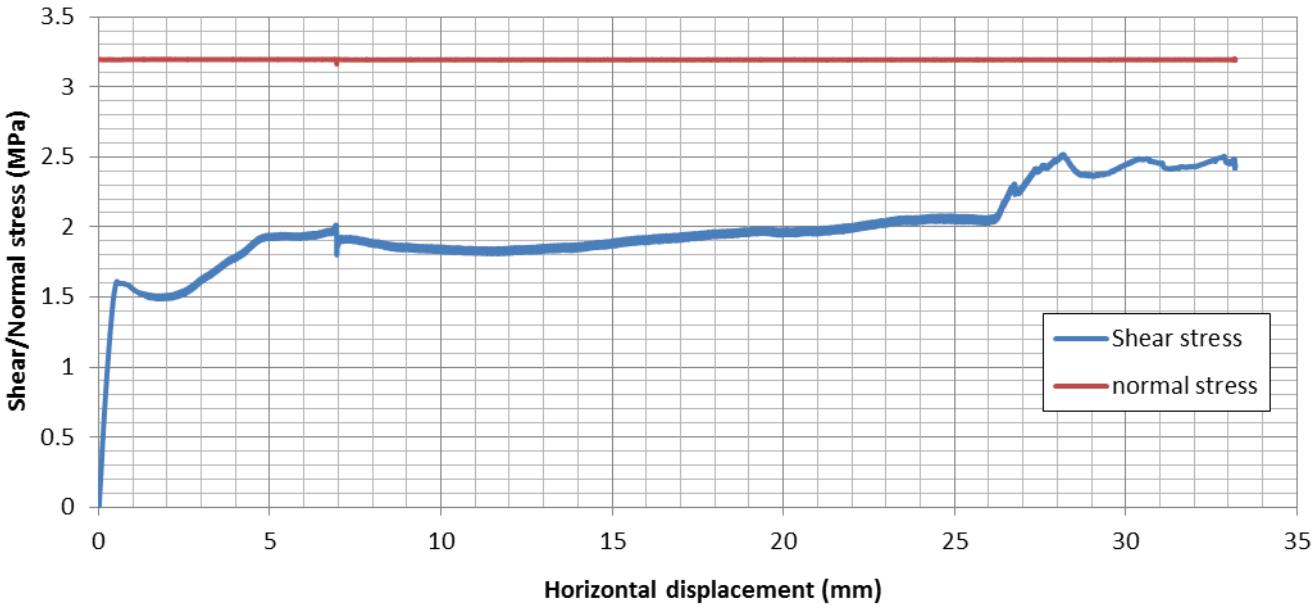
Shear/Normal stress (MPa)
3.5
3
2.5
2
1.5
1
0.5
0
0
5
10
15
20
25
30
35
Horizontal displacement (mm)
Shear stress
normal stress

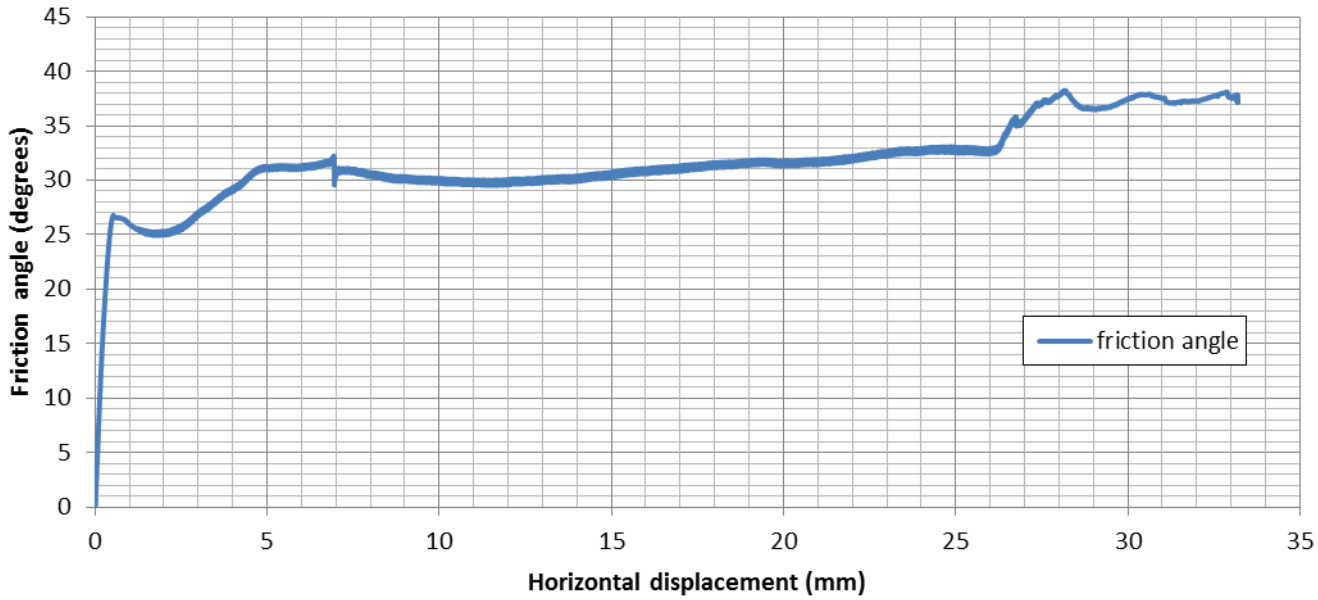
Friction angle (degrees)
45
40
35
30
25
20
15
10
5
0
0
5
10
15
20
25
30
35
Horizontal displacement (mm)
friction angle